

The sensitivity of $\mu \rightarrow e$ processes to τ flavour change

Marco Ardu^{1*}, Sacha Davidson^{1†}, and Martin Gorbahn^{2‡}

¹*LUPM, CNRS, Université Montpellier Place Eugene Bataillon, F-34095 Montpellier, Cedex 5, France*

²*Department of Mathematical Sciences, University of Liverpool, Liverpool L69 3BX, United Kingdom*

Abstract

Transforming a μ to a τ , then the τ to to an e , results in $\mu \rightarrow e$. In an EFT framework, we explore the sensitivity of $\mu \rightarrow e$ observables to products of $(\mu \rightarrow \tau) \times (\tau \rightarrow e)$ interactions, and show that the exceptional sensitivity of upcoming $\mu \leftrightarrow e$ experiments could allow to probe parameter space beyond the reach of upcoming $\tau \leftrightarrow l$ searches in Higgs, τ and B decays. We describe the $\tau \leftrightarrow l$ interactions as dimension six operators in the SM EFT, identify pairs of them giving interesting contributions to $\mu \leftrightarrow e$ processes, and obtain the anomalous dimensions mixing those pairs into dimension eight $\mu \rightarrow e$ operators. We find that $\mu \rightarrow e$ processes are sensitive to τ flavour-changing B decays at rates comparable to current B anomalies, but cannot reduce rates — as appropriate in many current B anomalies — because they do not interfere with the SM.

1 Introduction

The three lepton flavours are accidentally conserved in the Standard Model, if it is defined with massless neutrinos. But the non-zero neutrino masses and mixing angles established by the observation of neutrino oscillations clearly demonstrate that leptons change flavour. Extending the Standard Model (SM) with Dirac neutrino masses generically predicts flavour-changing contact interactions among the charged leptons (LFV or CLFV— for reviews, see, eg, [1, 2]), but the branching ratios are GIM-suppressed by small neutrino masses $Br \sim G_F^2 m_\nu^4 \sim 10^{-50}$ [3, 4], so beyond any foreseeable experimental reach. Searches for CLFV are thus of great interest, as an observation would be an unambiguous signature of New Physics (NP) that could shed light on the neutrino mass mechanism. In addition, null results generally limit the parameter space of Beyond the SM theories, many of which predict sizable LFV rates. In Table 1 a subset of LFV processes is listed with the current experimental bounds on their branching ratios, and the expected sensitivities of upcoming searches.

Process	Current bound on BR	Future Sensitivity
$\mu \rightarrow e\gamma$	$< 4.2 \times 10^{-13}$ [5]	10^{-14} [6]
$\mu \rightarrow \bar{e}ee$	$< 1.0 \times 10^{-12}$ [7]	10^{-16} [8]
$\mu A \rightarrow eA$	$< 7 \times 10^{-13}$ [9]	10^{-16} [10]
$\tau \rightarrow l\gamma$	$< 3.3 \times 10^{-8}$ [11]	$3 \times 10^{-9}(e), 10^{-9}(\mu)$
$\tau \rightarrow e\bar{e}e$	$< 2.7 \times 10^{-8}$ [12]	5×10^{-9} [13]
$\tau \rightarrow \mu\bar{\mu}\mu$	$< 2.1 \times 10^{-8}$ [12]	4×10^{-9} [13]
$\tau \rightarrow \mu\bar{e}e, e\bar{\mu}\mu$	$< 1.8, 2.7 \times 10^{-8}$ [12]	$3, 5 \times 10^{-9}$ [13]
...
$\tau \rightarrow \ell\pi^0$	$< 8.0 \times 10^{-8}$ [14]	4×10^{-9} [13]
$\tau \rightarrow \ell\eta$	$< 6.5 \times 10^{-8}$ [14]	7×10^{-9} [13]
$\tau \rightarrow \ell\rho$	$< 1.2 \times 10^{-8}$ [14]	10^{-9} [13]
$h \rightarrow e^\pm\mu^\mp$	$< 6.1 \times 10^{-5}$ [15]	2.1×10^{-5} [16]
$h \rightarrow e^\pm\tau^\mp$	$< 2.2 \times 10^{-3}$ [17]	2.4×10^{-4} [16]
$h \rightarrow \tau^\pm\mu^\mp$	$< 1.5 \times 10^{-3}$ [17]	2.3×10^{-4} [16]

Table 1: Some $\mu \leftrightarrow e$ and $\tau \leftrightarrow l$ processes ($l \in \{e, \mu\}$), with the current experimental bound on the branching ratios. The last column lists the future sensitivities used in our projections, which correspond to the expected reach of upcoming or planned experiments (except for $\mu \rightarrow e\gamma$, where the MEGII experiment at PSI, which starts taking data in 2022, aims to reach $BR \sim 6 \times 10^{-14}$). Additional $\tau \leftrightarrow l$ processes involving b quarks are listed in table 14.

The current limits on $\mu \rightarrow e$ flavour change are more retractive than those on $\tau \rightarrow l$, where $l \in \{e, \mu\}$, due to the possibility of making intense muon beams. Furthermore, a significant gain in sensitivity is expected at

*E-mail address: marco.ardu@umontpellier.fr

†E-mail address: s.davidson@lupm.in2p3.fr

‡E-mail address: martin.gorbahn@liverpool.ac.uk

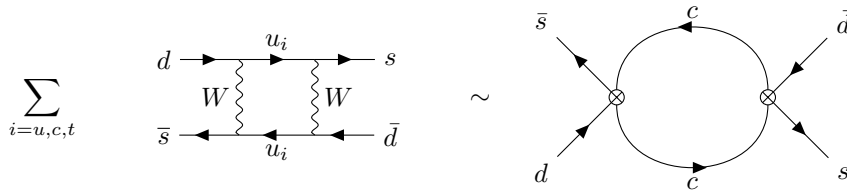


Figure 1: The GIM mechanism in $K - \bar{K}$ mixing: the mass-independent dimension six contribution from the box cancels in the flavour sum because of CKM unitarity. Then at $\mathcal{O}(G_F^2)$, the top contribution is not dominant due to small mixing with the down quark, whereas the dimension eight term $\sim G_F^2 m_c^2$ is relevant, and can be calculated in the low-energy EFT (Fermi theory) as the loop contribution with two dimension six operators inserted, as illustrated on the right.

upcoming $\mu \rightarrow e$ experiments (see table 1), sometimes allowing:

$$Br(\mu \rightarrow e \dots) \lesssim Br(\tau \rightarrow e \dots) Br(\tau \rightarrow \mu \dots) \quad (1)$$

This is interesting, as the three $\Delta F = 1$ lepton flavour changes are related:

$$\begin{array}{ccc} & \tau & \\ \nearrow & & \searrow \\ e & \longrightarrow & \mu \end{array}$$

If two lepton flavours are unconserved, then no symmetry forbids the third to happen, so it could be generated from the first two at some order in the perturbative expansion. Eq. (1) tells us that $\mu \rightarrow e$ searches are potentially sensitive to the product of $\mu \rightarrow \tau$ and $\tau \rightarrow e$ interactions respecting τ LFV constraints. So the aim of this manuscript, is to explore what can be learned about $\tau \leftrightarrow l$ interactions, using $\mu \rightarrow e$ observables. We are interested in the model-independent aspects of this question, so we assume that the NP responsible for LFV is heavy, and use Effective Field Theory (EFT) [18–20] to parametrise low energy LFV.

In this EFT approach, lepton flavour violation is mediated by contact interactions among Standard Model particles, which correspond in the Lagrangian to higher dimensional operators respecting the appropriate gauge symmetries (Our EFT formalism is presented in more detail in section 2). We will suppose a New Physics scale $\Lambda_{\text{NP}} \geq 4 \text{ TeV}$ (“beyond the LHC”), describe $\tau \rightarrow l$ interactions via dimension six operators, and calculate the log-enhanced contributions to dimension eight $\mu \rightarrow e$ operator coefficients, which appear in their Renormalization Group evolution between Λ_{NP} and m_W . These contributions arise from the insertion in loop diagrams of both a $\mu \rightarrow \tau$ and a $\tau \rightarrow e$ operator, and can be reliably computed in EFT — although they may not be the dominant contributions to $\mu \rightarrow e$ processes coming from $\tau \leftrightarrow l$ interactions (see section 2.1). We will find that upcoming $\mu \leftrightarrow e$ searches could be sensitive to $\tau \leftrightarrow l$ interactions beyond the reach of upcoming τ experiments.

The paper is organized as follows. In Section 2 we introduce the formalism for the EFT calculation (notation and operators), and we make several estimates to focus the calculations on contributions within future $\mu \rightarrow e$ experimental sensitivity. Our results are illustrated in Section 3, where the Renormalization Group Equations (RGEs) for dimension eight operators are reviewed, we discuss examples of anomalous dimensions calculated from double insertions of dimension six operators, and give the weak scale matching of $\mu \rightarrow \tau \times \tau \rightarrow e$ onto low energy $\mu \rightarrow e$ operators. The complete results for (dimension 6) $^2 \rightarrow$ dimension 8 mixing can be found in appendix B. In Section 4 we discuss some phenomenological implications : $\mu \rightarrow e$ observables are sensitive to products of $\tau \leftrightarrow l$ operator coefficients and we compare this sensitivity to the limits coming from searches for $\tau \leftrightarrow l$ processes.

2 EFT, operators and notation

In this section, we start by comparing our calculation to the expectations of a few models in subsection 2.1, then review the EFT framework in sections 2.2 to 2.4. Finally in subsection 2.5, we estimate which $(\mu \rightarrow \tau) \times (\tau \rightarrow e)$ loop diagrams could be accessible to future $\mu \rightarrow e$ experiments, making them interesting to calculate.

2.1 A few models

In this subsection, we discuss two models—one being the SM— in order to illustrate the relationships between $\tau \leftrightarrow l$ and $\mu \leftrightarrow e$ observables, and to compare our EFT calculation with the expectations of UV complete models.

First, consider a model where two heavy bosons, $M \gg m_W$, are added to the SM, with flavour diagonal, and respectively $\tau \leftrightarrow \mu$ and $\tau \leftrightarrow e$ renormalizable interactions. A first source of $\mu \leftrightarrow e$ flavour change could be

additional renormalizable $\mu \leftrightarrow e$ interactions of the heavy bosons — not forbidden by symmetry — but these do not interest us, because their magnitude depends on the model and is independent of the $\tau \leftrightarrow l$ interactions. We are interested in $\mu \rightarrow e$ processes which occur due to diagrams involving both the $\mu \rightarrow \tau$ and $\tau \rightarrow e$ interactions. The part of these amplitudes which is reproduced by our EFT calculation, can be identified by matching the model onto EFT at the heavy boson mass scale M . The model generates $\tau \leftrightarrow l$ four-fermion amplitudes at tree level, and could induce $\mu \leftrightarrow e$ amplitudes at one loop. These all are expected to match onto dimension six operators in the EFT, with coefficients of $\mathcal{O}(\lambda_{\tau l}/M^2)$ and $\mathcal{O}(\frac{\lambda_{\mu\tau}^* \lambda_{\tau e}}{16\pi^2 M^2})$. Our EFT calculation cannot reproduce these model dependent coefficients¹. Instead, the EFT below the heavy boson scale allows to combine the dimension six $\tau \leftrightarrow e$ and $\tau \leftrightarrow \mu$ operators into a dimension eight $\mu \leftrightarrow e$ operator, giving a contribution to the $\mu \leftrightarrow e$ amplitude $\lesssim \mathcal{O}(\frac{\lambda_{\mu\tau}^* \lambda_{\tau e} v^2}{16\pi^2 M^4})$ (v is the vacuum expectation value of the SM Higgs). By power-counting, this is subdominant compared to the model-dependent matching contribution discussed above. So this model illustrates that $\tau \leftrightarrow e$ and $\tau \leftrightarrow \mu$ interactions could generically combine into larger $\mu \leftrightarrow e$ rates than the EFT allows to compute.

As a second example, consider $K - \bar{K}$ mixing in the SM, where the dominant contribution is computable in the EFT (Fermi theory). The box diagram in the full SM is illustrated on the left in figure 1; evaluated with only massless u quarks in the loop, it gives an amplitude $\propto (V_{us}^* V_{ud})^2 / (16\pi^2 m_W^2)$, where V is the CKM matrix. This would match at m_W onto a dimension six $\Delta F = 2$ operator in the low-energy theory Fermi theory. However, due to CKM unitarity, this $\mathcal{O}(\frac{1}{16\pi^2 m_W^2})$ amplitude vanishes when summing over all up-type quark flavours and neglecting their masses. Instead, the amplitude in the full SM has a GIM dependence on the quark masses $\propto (V_{cs}^* V_{cd})^2 m_c^2 / 16\pi^2 m_W^4 + (V_{ts}^* V_{td})^2 m_t^2 / 16\pi^2 m_W^4$. In matching this to the low-energy EFT, the $m_t^2 / 16\pi^2 m_W^4$ piece would match onto a dimension six operator, but is negligible due to the small mixing between the third and first generation. And the log-enhanced part of the amplitude $\propto m_c^2$ is reproduced in the EFT by calculating the diagram with two insertions of dimension six operators, illustrated on the right of Figure 1. So in the Standard Model, our calculation can sometimes reproduce the observed flavour changing rates.

2.2 EFT for LFV

If the new particles with lepton flavour changing interactions are heavy, LFV at lower energies can be parametrised via contact interactions, which appear as non-renormalisable operators in the Lagrangian of an EFT (see eg [19, 20] for a review). In this subsection, we sketch the EFT background of our calculation, and introduce some notation.

Above the weak scale, we use the Lagrangian of the SMEFT, in which the SM Lagrangian is augmented by operators of higher dimension that respect the $SU(3) \times SU(2) \times U(1)$ gauge symmetry of the SM, and are constructed out of SM fields. We are interested in LFV operators of dimension 6 or 8, so we write

$$\mathcal{L}_{\text{SMEFT}} = \mathcal{L}_{\text{SM}} + \left(\sum_{A,\zeta} \frac{C_A^{[6]\zeta} \mathcal{O}_A^{[6]\zeta}}{v^2} + \sum_{B,\xi} \frac{C_B^{[8]\xi} \mathcal{O}_B^{[8]\xi}}{v^4} + \text{h.c.} \right) \quad (2)$$

where $v = 174$ GeV, the operator subscripts indicate the gauge structure and particle content, and the superscripts contain the operator dimension in brackets [suppressed when unnecessary], additional information about the operator structure in parentheses (see section 2.3 for examples), and the flavour indices. The LFV operators of interest here are listed in section 2.3. In the flavour sums of eq. (2), each index runs over all three generations. The doublet and singlet lepton generations are the charged lepton mass eigenstates $\{e, \mu, \tau\}$, the singlet quarks are also labelled by their flavour, and the quark doublets are in the u -type mass basis, with generation indices that run $1 \rightarrow 3$.

The SM Lagrangian is in the notation of [22], so the covariant derivative on doublet leptons is

$$(D_\mu \ell)_i^I = \left(\delta_{IJ} \partial_\mu + i \frac{g}{2} \tau_{IJ}^a W_\mu^a + i \delta_{IJ} g' Y(\ell) B_\mu \right) \ell_i^J, \quad (3)$$

where τ^a are Pauli matrices, I, J are $SU(2)$ doublet indices and i is a flavour index. At all scales, the doublet and singlet leptons are in the low energy mass eigenstate basis, so the lepton Yukawa matrix $[y_e]$ can have off-diagonal entries, in the presence of the operator \mathcal{O}_{eH} (see equations 17 and 70). We follow [23] in choosing this basis, because it defines lepton flavour in the presence of LFV, so it simplifies our calculations (as mentioned at the end of section 2.4). The Yukawa matrix eigenvalue of fermion f is written y_f .

The dimension six operators in eq. (2) are in the “on-shell” basis of [24] as pruned in [25], where “on-shell” means that the equations of motion were used to reduce the basis. Complete bases of on-shell dimension eight operators have appeared recently [26, 27], and our dimension eight operators are in these lists. However in

¹Despite that the UV dependence is also apparent in the loop integrals performed in the EFT, which are power divergent [21].

reality, we are only interested in the subset of dimension eight $\mu \leftrightarrow e$ operators to which experiments could be sensitive, which was given in [23]. Finally, some operators in eq. (2) are hermitian in flavour space (*ie* $[\mathcal{O}_A^{ij\bar{k}l}]^\dagger = \mathcal{O}_A^{\bar{j}ilk}$); we include these operators multiplied by an extra 1/2, as the Hermitian conjugate is included in (2) and summing over flavour indices would otherwise lead to double counting with respect to the conventions of [22].

We assume LFV heavy particles are beyond the reach of the LHC in the next decade, because we are interested in combining observables from upcoming experiments at low-energy. Concretely, this means that the operator coefficients, or Wilson coefficients (WCs), satisfy

$$C_A^{[n]\zeta} \leq \left(\frac{v}{\Lambda_{\text{NP}}} \right)^{n-4}, \quad \Lambda_{\text{NP}} = 4 \text{ TeV}, (v = 174 \text{ GeV})$$

and that we calculate Renormalisation Group running of LFV operators in SMEFT from $\Lambda_{\text{NP}} \rightarrow m_W$. Should new particles with LFV interactions and masses $m_W < M_{\text{NP}} < 4 \text{ TeV}$ induce larger coefficients, our results would still apply, but might be incomplete because additional operators and diagrams could contribute.

The WCs $\{C_A^{[n]\zeta}\}$ function as coupling constants for LFV interactions. Their numerical value can be obtained by matching the EFT onto a model, for instance by equating the Greens functions of the model and the EFT at the new particle mass scale $\sim \Lambda_{\text{NP}}$. The Renormalisation the Group Equations (RGEs) govern the scale dependence of the WCs below Λ_{NP} . The solution of these equations resums the logarithms that are generated by the light particle, which propagate as dynamical particles in the EFT. So in SMEFT, the one-loop RGEs of dimension six SMEFT operators arise from decorating a dimension six operator with a loop involving renormalisable interactions [22, 28, 29], and from loops involving two dimension 5 operators [30]. The mixing of a product of dimension five and six operators into dimension seven has also been calculated in SMEFT [31], as have some anomalous dimensions for some operators of dimension eight [32–34].

Upon reaching a particle mass scale, the high scale EFT can be matched onto another EFT, where the now-heavy particles are removed. For instance, in crossing the electroweak scale, SMEFT Greens functions are calculated in the broken SM, with the Higgs doublet written

$$H = \left(v + \frac{1}{\sqrt{2}}(h + iG^0) \right) \quad (4)$$

where the G s are the Goldstones and h is the SM Higgs boson. These Greens functions are then matched to those of a QED and QCD invariant EFT (we refer to it as low energy EFT) in which the non-renormalisable operators are built out of SM fields lighter than the W boson [35].

The running and matching continues from the weak scale down to the experimental scale, where rates can be calculated in terms of the WCs and matrix elements of the operators. For three or four-legged $\mu \rightarrow e$ processes which are otherwise flavour diagonal (*ie* $\mu \rightarrow e\gamma$ and $\mu \rightarrow e\gamma\gamma$, but not including $K \rightarrow \mu^\pm e^\mp$), the “leading” evolution between the experimental scale and the weak scale has been obtained [36]. This includes the one-loop RGEs for dimension five and six operators, and some large two-loop anomalous dimensions where the one loop mixing vanishes [37]. Several branching ratio calculations in the low energy EFT are given in the $\mu \rightarrow e$ review [1], and $\mu A \rightarrow e A$ conversion rates can be calculated from [38]. These results can be combined to calculate the current and upcoming sensitivity of $\mu \leftrightarrow e$ experiments to WCs at the weak scale, and also extrapolated to give the sensitivities to the $\tau \leftrightarrow l$ WCs considered in this manuscript [39].

The aim of this manuscript is to calculate the contributions to $\mu \rightarrow e$ observables that arise from combining $\tau \rightarrow e$ and $\mu \rightarrow \tau$ operators. This could occur in SMEFT running, in matching at the weak scale, and in running below the weak scale. In SMEFT, loop diagrams containing pairs of dimension six operators renormalize the Wilson coefficients of dimension eight operators, such that the RGEs for the latter take the schematic form [40]

$$(16\pi^2) \frac{d\vec{C}_A^{[8]}}{d \log M} = \vec{C}_B^{[8]} \gamma_{BA} + \vec{C}_X^{[6]} \hat{\gamma}_{XY,A} \vec{C}_Y^{[6]}, \quad (5)$$

having aligned the operator coefficients in the row vectors $\vec{C}^{[8]}$, $\vec{C}^{[6]}$, and where γ is the anomalous dimension matrix of dimension eight coefficients while $\hat{\gamma}$ mixes pairs of dimension six into dimension eight. The RGEs of dimension eight operators are currently unknown and only partial calculations have been performed [32, 33]. This manuscript fits into this ongoing effort.

We define the anomalous dimensions with a $1/(16\pi^2)$ prefactor, while we unconventionally do not factor out SM couplings. Two insertion of dimension six operators renormalize the dimension eight coefficients as

$$\Delta \vec{C}_A^{[8]} = \vec{C}_X^{[6]} \hat{Z}_{XY,A} \vec{C}_Y^{[6]}, \quad (6)$$

where \hat{Z} is the divergent renormalization factor and may contain renormalizable couplings. In dimensional regularization, the independence of bare Wilson coefficients from the arbitrary renormalization scale gives the

anomalous dimension matrix of eq. (5), which at one-loop and with our conventions takes the following form

$$\hat{\gamma} \propto 16\pi^2 \epsilon \hat{Z}. \quad (7)$$

Note that $\hat{Z} \propto 1/\epsilon$ and the product above is finite as expected. A more detailed derivation of $\hat{\gamma}$ can be found in section 3.1.

Pairs of $\tau \leftrightarrow l$ operators also contribute to $\mu \rightarrow e$ amplitudes in matching SMEFT onto the low energy EFT at m_W . In “integrating out” the heavy bosons h, Z and replacing the Higgs doublet with its vacuum expectation value, it is possible to draw diagrams built out of $\tau \leftrightarrow l$ operators that match onto three or four-legged $\mu \rightarrow e$ operators in the low energy EFT. We calculate these matching conditions, which are meant to complete the tree-level $\mathcal{O}(v^4/\Lambda_{\text{NP}}^4)$ matching performed in [23].

Finally, combining two $\tau \leftrightarrow l$ operators contributes to the RGEs of Wilson coefficients in the EFT below m_W . We neglect these running contributions because they carry a suppression factor with respect to dimension six anomalous dimensions which is $\lesssim m_b^2/\Lambda_{\text{NP}}^2$, given that the bottom quark is the heaviest dynamical particle in the EFT. Such suppression is absent in SMEFT, where the top quark, the Higgs and gauge bosons are present, allowing Higgs legs to be attached with order one couplings to heavier particles running in loops. SMEFT has also the advantage of having two-fermion “penguin” operators that are efficiently generated in mixing and which match onto vector operators in the low energy EFT. For the above reasons we focus on SMEFT RGEs and matching, while we neglect the running below m_W .

Equation (5) has a straightforward solution if the anomalous dimension matrices are constant, which occurs when the running of all-but-one of the SM renormalisable couplings can be neglected. We take all SM couplings constant between $m_W \rightarrow \Lambda_{\text{NP}} = 4$ TeV, in solving eq. (5). It is augmented by the RGEs of dimension six coefficients:

$$\frac{d\vec{C}^{[6]}}{dt} = -\vec{C}^{[6]}\hat{\gamma} \quad (8)$$

so the solution is

$$\vec{C}^{[6]}(t) = \vec{C}^{[6]}(0) \exp(-\hat{\gamma}t) \quad (9)$$

$$\vec{C}^{[8]}(t) = \left[\vec{C}^{[8]}(0) - \int_0^t d\tau \vec{C}^{[6]}(0) \exp(-\hat{\gamma}\tau) \hat{\gamma} \exp(-\hat{\gamma}^T \tau) \vec{C}^{[6]}(0) \exp(\gamma\tau) \right] \exp(-\gamma t). \quad (10)$$

Expanding the exponential at leading log, the dimension eight coefficients at the electroweak scale take the following form

$$\vec{C}^{[8]}(m_W) = \vec{C}^{[8]}(\Lambda_{\text{NP}}) \left(1 - \frac{\gamma}{16\pi^2} \log\left(\frac{\Lambda_{\text{NP}}}{m_W}\right) \right) - \vec{C}^{[6]}(\Lambda_{\text{NP}}) \frac{\hat{\gamma}}{16\pi^2} \vec{C}^{[6]}(\Lambda_{\text{NP}}) \log\left(\frac{\Lambda_{\text{NP}}}{m_W}\right) + \dots \quad (11)$$

2.3 Operators

This subsection lists the operators included in the SMEFT Lagrangian of eq. (2). They are classified into subgroups ($D_6, 4f_6, \dots$), in order to facilitate the estimates of section 2.5.

The SMEFT dimension six operators that are $\tau \rightarrow e$ or $\mu \rightarrow \tau$ flavour changing are the following, where the indices ij take the values $e\tau$ or $\tau\mu$ (except for the $4l_6$ operators).

- Dipole operators $\equiv D_6$:

$$\mathcal{O}_{eB}^{ij} = y_\tau (\bar{\ell}_i H \sigma^{\alpha\beta} e_j) B_{\alpha\beta} \quad \mathcal{O}_{eW}^{ij} = y_\tau (\bar{\ell}_i \tau^a H \sigma^{\alpha\beta} e_j) W_{\alpha\beta}^a \quad (12)$$

The Hermitian conjugates with exchanged $i \leftrightarrow j$ match onto the dipole operator with opposite chirality.

- Penguin operators $\equiv P_6$:

$$\mathcal{O}_{He}^{ij} = i(\bar{e}_i \gamma^\alpha e_j)(H^\dagger \overleftrightarrow{D}_\alpha H) \quad \mathcal{O}_{H\ell(1)}^{ij} = i(\bar{\ell}_i \gamma^\alpha \ell_j)(H^\dagger \overleftrightarrow{D}_\alpha H) \quad (13)$$

$$\mathcal{O}_{H\ell(3)}^{ij} = i(\bar{\ell}_i \tau^a \gamma^\alpha \ell_j)(H^\dagger \overleftrightarrow{D}_\alpha^a H) \quad (14)$$

where we have defined

$$iH^\dagger \overleftrightarrow{D}_\mu H \equiv iH^\dagger (D_\mu H) - i(D_\mu H^\dagger) H \quad (15)$$

$$iH^\dagger \overleftrightarrow{D}_\mu^a H \equiv iH^\dagger \tau^a (D_\mu H) - i(D_\mu H^\dagger) \tau^a H. \quad (16)$$

- Yukawa operators $\equiv Y_6$:

$$\mathcal{O}_{eH}^{ij} = (\bar{\ell}_i H e_j)(H^\dagger H) \quad (17)$$

and their Hermitian conjugates.

- Four lepton operators $\equiv 4l_6$:

$$\mathcal{O}_{ee}^{ijkl} = (\bar{e}_i \gamma^\alpha e_j)(\bar{e}_k \gamma_\alpha e_l) \quad \mathcal{O}_{\ell e}^{ijkl} = (\bar{\ell}_i \gamma^\alpha \ell_j)(\bar{e}_k \gamma_\alpha e_l) \quad (18)$$

$$\mathcal{O}_{\ell\ell}^{ijkl} = (\bar{\ell}_i \gamma^\alpha \ell_j)(\bar{\ell}_k \gamma_\alpha \ell_l) \quad (19)$$

where the pairs ij, kl, kj, il can be $e\tau$ or $\tau\mu$, while the remaining pair is diagonal and can be $\{e, \mu, \tau\}$.

- Two-lepton two-quark operators $\equiv 4f_6$:

$$\mathcal{O}_{\ell q}^{(1)ijnm} = (\bar{\ell}_i \gamma^\alpha \ell_j)(\bar{q}_n \gamma_\alpha q_m) \quad \mathcal{O}_{\ell q}^{(3)ijnm} = (\bar{\ell}_i \tau^a \gamma^\alpha \ell_j)(\bar{q}_n \tau^a \gamma_\alpha q_m) \quad (20)$$

$$\mathcal{O}_{\ell u}^{ijnm} = (\bar{\ell}_i \gamma^\alpha \ell_j)(\bar{u}_n \gamma_\mu u_m) \quad \mathcal{O}_{\ell d}^{ijnm} = (\bar{\ell}_i \gamma^\alpha \ell_j)(\bar{d}_n \gamma_\alpha d_m) \quad (21)$$

$$\mathcal{O}_{eq}^{ijnm} = (\bar{e}_i \gamma^\alpha e_j)(\bar{q}_n \gamma_\alpha q_m) \quad \mathcal{O}_{eu}^{ijnm} = (\bar{e}_i \gamma^\alpha e_j)(\bar{u}_n \gamma_\alpha u_m) \quad (22)$$

$$\mathcal{O}_{ed}^{ijnm} = (\bar{e}_i \gamma^\alpha e_j)(\bar{d}_n \gamma_\alpha d_m) \quad (23)$$

$$\mathcal{O}_{\ell edq}^{ijnm} = (\bar{\ell}_i e_j)(\bar{d}_n q_m) \quad \mathcal{O}_{\ell equ}^{ijnm} = (\bar{\ell}_i e_j)\epsilon(\bar{q}_n u_m) \quad (24)$$

with $n, m \in \{1, 2, 3\}$ running over the three quark families.

At dimension eight, there are thousands of operators, but here are listed only the subset relevant for our calculations, where relevant means that their contribution could be detectable in the upcoming $\mu \rightarrow e$ experimental searches, assuming a NP scale $\Lambda_{\text{NP}} \gtrsim 4 \text{ TeV}$. A list of such operators was identified in [23], and is given below.

These include dipole operators $\equiv D_8$

$$\begin{aligned} \mathcal{O}_{\ell e W H^3}^{(1)e\mu} &= y_\mu (\bar{\ell}_e \tau^a H \sigma^{\alpha\beta} e_\mu) W_{\alpha\beta}^a (H^\dagger H) \\ \mathcal{O}_{\ell e W H^3}^{(2)e\mu} &= y_\mu (\bar{\ell}_e H \sigma^{\alpha\beta} e_\mu) W_{\alpha\beta}^a (H^\dagger \tau^a H) \\ \mathcal{O}_{\ell e B H^3}^{e\mu} &= y_\mu (\bar{\ell}_e H \sigma^{\alpha\beta} e_\mu) B_{\alpha\beta} (H^\dagger H) \end{aligned} \quad (25)$$

and their Hermitian conjugates with the lepton indices exchanged. Two-lepton two-quark vector $\equiv 4f_8$

$$\mathcal{O}_{\ell^2 q^2 H^2}^{(1)e\mu nn} = (\bar{\ell}_e \gamma^\alpha \ell_\mu)(\bar{q}_n \gamma_\alpha q_n)(H^\dagger H) \quad \mathcal{O}_{\ell^2 q^2 H^2}^{(2)e\mu nn} = (\bar{\ell}_e \tau^a \gamma^\alpha \ell_\mu)(\bar{q}_n \gamma_\alpha q_n)(H^\dagger \tau^a H) \quad (26)$$

$$\mathcal{O}_{\ell^2 q^2 H^2}^{(3)e\mu nn} = (\bar{\ell}_e \tau^a \gamma^\alpha \ell_\mu)(\bar{q}_n \tau^a \gamma_\alpha q_n)(H^\dagger H) \quad \mathcal{O}_{\ell^2 q^2 H^2}^{(4)e\mu nn} = (\bar{\ell}_e \gamma^\mu \ell_\mu)(\bar{q}_n \tau^a \gamma_\mu q_n)(H^\dagger \tau^a H) \quad (27)$$

$$\mathcal{O}_{\ell^2 u^2 H^2}^{(1)e\mu nn} = (\bar{\ell}_e \gamma^\alpha \ell_\mu)(\bar{u}_n \gamma_\mu u_n)(H^\dagger H) \quad \mathcal{O}_{\ell^2 u^2 H^2}^{(2)e\mu nn} = (\bar{\ell}_e \tau^a \gamma^\alpha \ell_\mu)(\bar{u}_n \gamma_\alpha u_n)(H^\dagger \tau^a H) \quad (28)$$

$$\mathcal{O}_{\ell^2 d^2 H^2}^{(1)e\mu nn} = (\bar{\ell}_e \gamma^\alpha \ell_\mu)(\bar{d}_n \gamma_\alpha d_n)(H^\dagger H) \quad \mathcal{O}_{\ell^2 d^2 H^2}^{(2)e\mu nn} = (\bar{\ell}_e \tau^a \gamma^\alpha \ell_\mu)(\bar{d}_n \gamma_\alpha d_n)(H^\dagger \tau^a H) \quad (29)$$

$$\mathcal{O}_{e^2 q^2 H^2}^{(1)e\mu nn} = (\bar{e}_e \gamma^\alpha e_\mu)(\bar{q}_n \gamma_\alpha q_n)(H^\dagger H) \quad \mathcal{O}_{e^2 q^2 H^2}^{(2)e\mu nn} = (\bar{e}_e \tau^a \gamma^\alpha e_\mu)(\bar{q}_n \tau^a \gamma_\alpha q_n)(H^\dagger \tau^a H) \quad (30)$$

$$\mathcal{O}_{e^2 u^2 H^2}^{e\mu nn} = (\bar{e}_e \gamma^\alpha e_\mu)(\bar{u}_n \gamma_\alpha u_n)(H^\dagger H) \quad \mathcal{O}_{e^2 d^2 H^2}^{e\mu nn} = (\bar{e}_e \gamma^\alpha e_\mu)(\bar{d}_n \gamma_\alpha d_n)(H^\dagger H) \quad (31)$$

with in most cases $n = u, d$ belonging to the first generation quarks. There are also penguin operators $\equiv P_8$

$$\begin{aligned} \mathcal{O}_{\ell^2 H^4 D}^{(1)e\mu} &= i(\bar{\ell}_e \gamma^\alpha \ell_\mu)(H^\dagger \overleftrightarrow{D}_\alpha H)(H^\dagger H) \quad \mathcal{O}_{\ell^2 H^4 D}^{(2)e\mu} = i(\bar{\ell}_e \tau^a \gamma^\alpha \ell_\mu)[(H^\dagger \overleftrightarrow{D}_\alpha^a H)(H^\dagger H) + (H^\dagger \overleftrightarrow{D}_\alpha H)(H^\dagger \tau^a H)] \\ \mathcal{O}_{e^2 H^4 D}^{e\mu} &= i(\bar{e}_e \gamma^\alpha e_\mu)(H^\dagger \overleftrightarrow{D}_\alpha H)(H^\dagger H). \end{aligned} \quad (32)$$

Furthermore, the following two-fermion two-lepton scalar and tensor operators are also relevant

$$\mathcal{O}_{\ell edq H^2}^{(1)e\mu nn} = (\bar{\ell}_e e_\mu)(\bar{d}_n q_n)(H^\dagger H) \quad \mathcal{O}_{\ell edq H^2}^{(2)e\mu nn} = (\bar{\ell}_e e_\mu) \tau^a (\bar{d}_n q_n)(H^\dagger \tau^a H) \quad (33)$$

$$\mathcal{O}_{\ell equ H^2}^{(1)e\mu nn} = (\bar{\ell}_e e_\mu) \epsilon(\bar{q}_n u_n)(H^\dagger H) \quad \mathcal{O}_{\ell equ H^2}^{(2)e\mu nn} = (\bar{\ell}_e e_\mu) \tau^a \epsilon(\bar{q}_n u_n)(H^\dagger \tau^a H) \quad (34)$$

$$\mathcal{O}_{\ell equ H^2}^{(3)e\mu nn} = (\bar{\ell}_e \sigma^{\alpha\beta} e_\mu) \epsilon(\bar{q}_n \sigma_{\alpha\beta} u_n)(H^\dagger H) \quad \mathcal{O}_{\ell equ H^2}^{(4)e\mu nn} = (\bar{\ell}_e \sigma^{\alpha\beta} e_j) \tau^a \epsilon(\bar{q}_n \sigma_{\alpha\beta} u_n)(H^\dagger \tau^a H) \quad (35)$$

$$\mathcal{O}_{\ell edq H^2}^{(3)e\mu nn} = (\bar{\ell}_e H e_\mu)(\bar{q}_n H d_n) \quad \mathcal{O}_{\ell edq H^2}^{(4)e\mu nn} = (\bar{\ell}_e \sigma^{\alpha\beta} H e_\mu)(\bar{q}_n \sigma_{\alpha\beta} H d_n) \quad (36)$$

$$\mathcal{O}_{\ell equ H^2}^{(5)e\mu nn} = (\bar{\ell}_e H e_\mu)(\bar{u}_n \tilde{H}^\dagger q_n), \quad (37)$$

with $n = u, c, t, d, s, b$ running over all quark flavours. Finally the four-lepton operators $\equiv 4l_8$ read

$$\mathcal{O}_{\ell^2 e^2 H^2}^{(4)e\mu\tau\tau} = (\bar{\ell}_e H \sigma^{\alpha\beta} e_\mu)(\bar{\ell}_\tau H \sigma_{\alpha\beta} e_\tau) \quad \mathcal{O}_{\ell^2 e^2 H^2}^{(3)e\mu ee} = (\bar{\ell}_e H e_\mu)(\bar{\ell}_e H e_e) \quad (38)$$

$$\mathcal{O}_{\ell^4 H^2}^{(1)e\mu ee} = (\bar{\ell}_e \gamma^\alpha \ell_\mu)(\bar{\ell}_e \gamma_\alpha \ell_e)(H^\dagger H) \quad \mathcal{O}_{\ell^4 H^2}^{(2)e\mu ee} = (\bar{\ell}_e \gamma^\alpha \ell_\mu)(\bar{\ell}_e \tau^a \gamma_\alpha \ell_e)(H^\dagger \tau^a H) \quad (39)$$

$$\mathcal{O}_{\ell^2 e^2 H^2}^{(1)e\mu ee} = (\bar{\ell}_e \gamma^\alpha \ell_\mu)(\bar{e}_e \gamma_\alpha e_e)(H^\dagger H) \quad \mathcal{O}_{\ell^2 e^2 H^2}^{(2)e\mu ee} = (\bar{\ell}_e \tau^a \gamma^\alpha \ell_\mu)(\bar{e}_e \gamma_\alpha e_e)(H^\dagger \tau^a H) \quad (40)$$

$$\mathcal{O}_{e^4 H^2}^{e\mu ee} = (\bar{e}_e \gamma^\alpha e_\mu)(\bar{e}_e \gamma_\alpha e_e)(H^\dagger H). \quad (41)$$

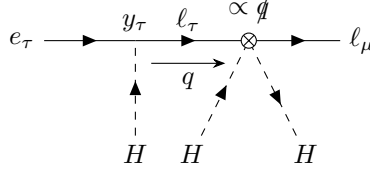


Figure 2: The diagram shows that the operator $i(\bar{\ell}_\mu \not{D} \ell_\tau)(H^\dagger H)$ leads to the same S -matrix elements as $y_\tau(\bar{\ell}_\mu H e_\tau)(H^\dagger H)$. The non-local momentum dependence of the internal line propagator cancels with the inverse propagator present in the Equation of Motion.

Note that in the Lagrangian of eq. (2) we sum over all possible generation indices, and more flavour structures are relevant for low energy LFV interactions. For instance, $\mathcal{O}_{\ell^4 H^2}^{e\mu ee}$, $\mathcal{O}_{\ell^4 H^2}^{ee e\mu}$ match onto the same vector operator in the EFT below m_W . Similarly, in the case of $e\mu\tau\tau$ tensor operator, the permutations $\tau\tau e\mu$, $\tau\mu e\tau$, $e\tau\tau\mu$ must be considered.

2.4 Equations of Motion

In this section, we discuss some of the technical subtleties that occur when two dimension six operators mix into dimension eight operators. In our calculations of anomalous dimensions we consider two different approaches: we can systematically apply the equations of motions onto the amplitudes of our loop calculations in order to arrive at expressions that are proportional to tree-level amplitudes of the on-shell, or “physical” operators. Alternatively, we could use a complete set of off-shell operators and project our loop amplitudes onto the on-shell operator basis. The situation is slightly complicated by the facts that the dimension six operators will contribute themselves to the equations of motion, and that there are a huge number of dimension eight operators. In the following we will show how both approaches are equivalent in our calculation, where we determine the mixing into the subset of dimension eight operators that contribute to LFV at low energy experiments.

Working with a on-shell (or physical) operator basis implies the choice of a set of operators that vanish when the Equation of Motions (EOM) are satisfied. Take two operators \mathcal{O}_1 , \mathcal{O}_2 which differ by an operator \mathcal{O}_{EOM} that is EOM vanishing, i.e

$$\mathcal{O}_1 - \mathcal{O}_2 = \mathcal{O}_{EOM} \propto \frac{\delta S}{\delta \phi} \quad (42)$$

where S is the action and ϕ labels a generic field. \mathcal{O}_{EOM} can be dropped in physical processes because it leads to vanishing S -matrix elements, so that the operators \mathcal{O}_1 , \mathcal{O}_2 are physically equivalent and only one of them is retained in the basis.

For instance, at dimension six, the operators

$$i(\bar{\ell}_\mu \not{D} \ell_\tau)(H^\dagger H), \quad (D^2 \bar{\ell}_\tau H \mu) \quad (43)$$

can be generated at one-loop from a penguin operator (see Figure 4). The first is relevant here, because it is on-shell equivalent to $(\bar{\ell}_\mu H e_\tau)(H^\dagger H)$ by means of the dimension four EOM of the lepton field $i(\not{D} \ell_\tau) = y_\tau H e_\tau$. (The second operator will be relevant for the $C_{Hl} \times C_{He}$ mixing into dipoles, which is discussed in section 3.1.1.)

Therefore, we can project an amplitude that is proportional to the left hand side of the previous equation of motion

$$i(\bar{\ell}_\mu \not{D} \ell_\tau)(H^\dagger H) \rightarrow [i(\bar{\ell}_\mu \not{D} \ell_\tau)(H^\dagger H) - y_\tau(\bar{\ell}_\mu H e_\tau)(H^\dagger H)] + y_\tau(\bar{\ell}_\mu H e_\tau)(H^\dagger H) \quad (44)$$

onto physical and EOM vanishing – in brackets – operators. In Figure 2 we show how the equivalence can be understood diagrammatically: the \not{D} operator Feynman rule is proportional to the \not{q} momentum of the virtual ℓ_τ line coming out of a renormalizable Yukawa coupling; the momentum dependence cancels with the ℓ_τ propagator, yielding an S -matrix element reproduced by the local operator $y_\tau(\bar{\ell}_\mu H e_\tau)(H^\dagger H)$.

Once a reduced physical basis is identified, the theory can be consistently renormalized among on-shell operators, as redundant counterterms $A\mathcal{O}_2/\epsilon$ are equivalent to $A(\mathcal{O}_1 - \mathcal{O}_{EOM})/\epsilon$ and EOM vanishing operators mix exclusively among themselves in the RGEs [41]².

However, in order to consistently renormalize an EFT in a given basis up to dimension eight ($1/\Lambda_{\text{NP}}^4$), the dimension six ($1/\Lambda_{\text{NP}}^2$) terms in the EOM must be included when removing redundant operators. Concretely, if a divergent contribution to a redundant dimension six operator, $\mathcal{O}_2^{[6]}/(\Lambda_{\text{NP}}^2 \epsilon)$ is generated via loops, then it can be rewritten

$$\frac{A}{\Lambda_{\text{NP}}^2 \epsilon} \left(\mathcal{O}_1^{[6]} + \frac{\mathcal{O}^{[8]}}{\Lambda_{\text{NP}}^2} - \mathcal{O}_{EOM} \right) \quad (45)$$

²Gauge fixing and ghost terms that appear in the EOM are found to have no physical effects in operator mixing and S -matrix elements [41].

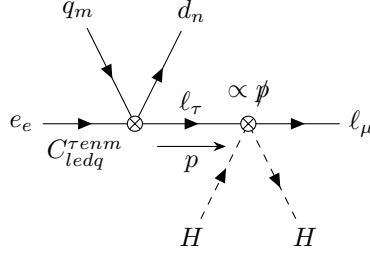


Figure 3: Correction to the Equation of Motion due to dimension six operators. At $1/\Lambda_{\text{NP}}^4$ order, the operator $i(\bar{\ell}_\mu \not{D} \ell_\tau)(H^\dagger H)$ is on-shell equivalent to a combination of dimension six and dimension eight operators. The dimension eight contribution can be understood by attaching dimension six interactions to the operator, where the internal line propagator cancels against the vertex Feynman rule. The diagram shows an example with the insertion $\mathcal{O}_{ledq}^{\tau enm} = (\bar{\ell}_\tau e_e)(\bar{d}_n q_m)$, which reproduces the EOM reduction of eq. (46).

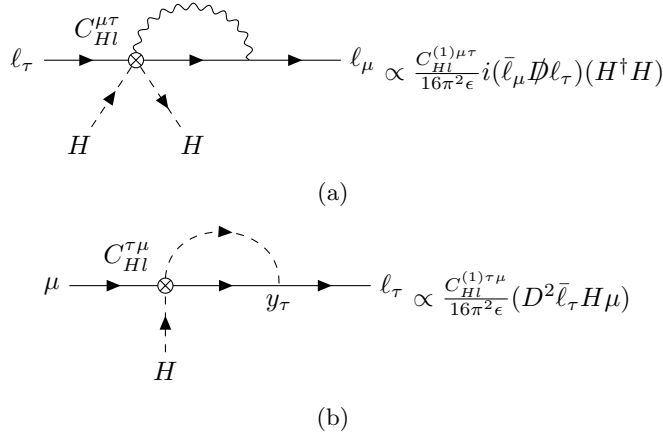


Figure 4: One-loop diagrams with the penguin operators of eq. (13). Matching the divergences off-shell, the redundant operators $i(\bar{\ell}_\mu \not{D} \ell_\tau)(H^\dagger H)$, $(D^2 \bar{\ell}_\tau H \mu)$ are generated.

where $\mathcal{O}_1^{[6]}$ is equivalent to $\mathcal{O}_2^{[6]}$ via the renormalizable EOM $\delta S^{d=4}/\delta\phi = 0$ of eq. (42), and the dimension eight $\mathcal{O}^{[8]}$ is generated by the dimension six corrections $\delta S^{d=6}/\delta\phi$. The dimension eight contribution is proportional to the product of two dimension six operator coefficients, which is the kind of contribution that we are interested in.

As an example of the impact of dimension six terms in the EOM, suppose that the only $\tau \leftrightarrow e$ operator at dimension six is $\mathcal{O}_{ledq}^{\tau enm} = (\bar{\ell}_\tau e_e)(\bar{d}_n q_m)$, and that the operator $i(\bar{\ell}_\mu \not{D} \ell_\tau)(H^\dagger H)$ is generated via loop corrections. Then eq. (44), up to dimension 8, becomes

$$i(\bar{\ell}_\mu \not{D} \ell_\tau)(H^\dagger H) = \left[i(\bar{\ell}_\mu \not{D} \ell_\tau)(H^\dagger H) - y_\tau (\bar{\ell}_\mu H e_\tau)(H^\dagger H) + \frac{C_{ledq}^{\tau enm}}{\Lambda_{\text{NP}}^2} (\bar{\ell}_\mu e_e)(\bar{d}_n q_m)(H^\dagger H) \right] + y_\tau (\bar{\ell}_\mu H e_\tau)(H^\dagger H) - \frac{C_{ledq}^{\tau enm}}{\Lambda_{\text{NP}}^2} (\bar{\ell}_\mu e_e)(\bar{d}_n q_m)(H^\dagger H) \quad (46)$$

where the EOM vanishing operator in square brackets now contains the dimension eight $\mathcal{O}_{ledqH^2}^{(1)iknm} = (\bar{\ell}_\mu e_e)(\bar{d}_n q_m)(H^\dagger H)$. Similarly to the renormalizable case, the on-shell equivalence is apparent diagrammatically, by dressing the redundant operator with dimension six contact interactions as shown in Figure 3. Once again the inverse propagator that is present in the EOM, and appears in the operator Feynman rule, cancels the momentum dependence of the internal line, such that the amplitude is local and equivalent to a dimension eight operator. Its coefficient will be proportional to the product of two dimension six WC. For instance, $i(\bar{\ell}_\mu \not{D} \ell_\tau)(H^\dagger H)$ is generated in matching off-shell the divergence of the one-loop diagram of Figure 4 that involves the penguin operators of eq (13). Eq. (46) allows to project the divergence onto the on-shell basis, giving a contribution to the renormalisation of the dimension eight $\mu \leftrightarrow e$ operator $\mathcal{O}_{ledqH^2}^{(1)\mu enm} = (\bar{\ell}_\mu e_e)(\bar{d}_n q_m)(H^\dagger H)$ from the product $\mathcal{O}_{H\ell}^{(1)} \times \mathcal{O}_{ledq}$. This contribution from the EOM projection must be included in calculating the mixing from (dimension 6) $^2 \rightarrow$ dimension 8, together with one particle irreducible (1PI) diagrams $\propto C_{H\ell}^{(1)} \times C_{ledq}$. (Indeed, the anomalous dimension is only gauge invariant if one includes both the IP1 vertex and the non-1PI “wavefunction” contributions.)

The EOM contribution can be reproduced by calculating non-1PI divergent diagrams, as shown in figure 3. In working with a subspace of dimension eight operators (as we do here), proceeding diagrammatically can be particularly convenient. Our subspace is phenomenologically selected to contribute to the low energy $\mu \rightarrow e$ processes. When using the EOM to project the off-shell divergences, the redundant terms must be written in terms of operators in the full basis (which can include operators outside the subspace) and the EOM vanishing operators that the basis choice implies. In the end, only the interesting operators in the subspace are retained but it required working with the full basis as an intermediate step. On the other hand, in the approach of calculating one-particle -reducible diagrams, it is often easier to restrict to diagrams that directly give dimension eight operators of the subspace. In this manuscript, we calculate the one-particle-reducible diagrams that generate the relevant dimension eight operators. We cross-checked our diagrammatic results by calculating the dimension eight LFV operators obtained from the list of EOM-vanishing operators in [25], by using Equations of Motion up to dimension six.

Finally, recall that we work in the low-energy mass eigenstate basis of the leptons, where the lepton mass matrix is:

$$m_{e_i} \delta_{ij} = v \left([y_e]_{ij} - C_{eH}^{ij} \right) . \quad (47)$$

So in the above diagrammatic and EOM-based arguments, the Yukawa matrix element y_τ is replaced by the matrix element of the parenthesis on the right side of (47), which is also flavour-diagonal³. Therefore we do not include non-1PI diagrams involving a loop on the external leg of \mathcal{O}_{eH}^{ij} .

2.5 Estimates

The goal of this section is to better identify the dimension eight contributions that are interesting to calculate in the context of $\mu \rightarrow e$ LFV, that is, those that will be within the reach of future experiments. The Wilson coefficients of the dimension eight operators presented in the previous section were estimated in [23] to be within upcoming experimental sensitivity if they have values $\gtrsim v^4/\Lambda^4$, for $\Lambda \gtrsim 4$ TeV. We estimate in this section the additional loop and small couplings suppression that could be encountered in generating these coefficients in running and matching. This will allow to narrow-down the list of diagrams that should be calculated.

In estimating diagrams built out of $\mu \rightarrow \tau \times \tau \rightarrow e$ operators, we take into account the constraints on $\tau \leftrightarrow l$ processes coming from the bounds reported in the lower part of Table 1. Employing the acronyms introduced in the previous section for sets of τ LFV operators, current and upcoming one-at-a-time-limits on their coefficients are written in Table 2. These estimates assume that the Branching Ratio sensitivities on τ decays will improve of an order of magnitude at BelleII [13], and use the future sensitivities to $h \rightarrow \tau^\pm l^\mp$ decays at the ILC [16]. It is understood that the limits do not apply exactly to all operators identified by the collective label, but rather provide the order of magnitude of the one-at-a-time-limit, or sensitivity, to most of them. In the case where the operators are not (loosely) bounded, we assume

$$C^{[6]l\tau\dots} \lesssim (v/4 \text{ TeV})^2 \sim 2 \times 10^{-3} \quad (48)$$

corresponding to an $\mathcal{O}(1)$ coefficient at a New Physics scale of 4 TeV.

Operator coefficient	Current sensitivity	Future sensitivity	Process
$C_{D_6}^{l\tau}$	$\lesssim 7 \times 10^{-6}$	$\lesssim 2 \times 10^{-6}$	$\tau \rightarrow l\gamma$
$C_{Y_6}^{l\tau}$	$\lesssim 10^{-3}$	$\lesssim 3 \times 10^{-4}$	$h \rightarrow l\tau$
$C_{F_6}^{l\tau}$	$\lesssim 4 \times 10^{-4}$	$\lesssim 10^{-4}$	$\tau \rightarrow \bar{l}l$
$C_{4l_6}^{l\tau ll}$	$\lesssim 3 \times 10^{-4}$	$\lesssim 10^{-4}$	$\tau \rightarrow \bar{l}l$
$C_{4f_6}^{l\tau qq}$	$\lesssim 3 \times 10^{-4}$	$\lesssim 10^{-4}$	$\tau \rightarrow l\pi(\eta)$

Table 2: Sensitivities to $\tau \leftrightarrow l$ dimension six operator coefficients, normalized as in eq. (2). Current limits come from the Branching ratio bounds of Table 1, while the third column assumes that the experimental sensitivity to $\tau \leftrightarrow l$ decays will improve by an order of magnitude.

Diagrams that can generate the dimension eight $\mu \leftrightarrow e$ operators of section 2.3, in matching or in running, are drawn with a pair of $\tau \leftrightarrow l$ operators. The contribution to the coefficients are estimated as

$$\Delta C^{[8]e\mu} \simeq C_1^{[6]e\tau} C_2^{[6]\tau\mu} \left(\frac{1}{16\pi^2} \right)^n \times \{y^k g^l \lambda^m \dots\} \times \log \quad (49)$$

where n is the number of loops, SM couplings are factored out into the curly brackets, and the $\log(4 \text{ TeV}/m_W)$ factor is present in running, while absent in matching. In running, we restrict the number of loops to $n = 1$, while up to two loop diagrams contribute in “tree-level”(in the low-energy EFT) matching.

³However, in this basis, the h retains LFV interactions — see eq. (71).

Operator coefficient	Current sensitivity	Future sensitivity	Process
$C_{D_8}^{e\mu}$	$\lesssim 10^{-8}$	$\lesssim 1.5 \times 10^{-9}$	$\mu \rightarrow e\gamma$
$C_{4f_8,T}^{e\mu tt}$	$\lesssim 3 \times 10^{-11}$	$\lesssim 5 \times 10^{-12}$	$\mu \rightarrow e\gamma$
$C_{4l_8,T}^{e\mu\tau\tau}, C_{4f_8,T}^{e\mu cc}$	$\lesssim 10^{-8}$	$\lesssim 1.5 \times 10^{-9}$	$\mu \rightarrow e\gamma$
$C_{4f_8,T}^{e\mu bb}$	$\lesssim 8 \times 10^{-9}$	$\lesssim 10^{-9}$	$\mu \rightarrow e\gamma$
$C_{P_8}^{e\mu}$	$\lesssim 10^{-7}$	$\lesssim 10^{-9}$	$\mu A \rightarrow eA$
$C_{4l_8}^{e\mu ee}$	$\lesssim 8 \times 10^{-7}$	$\lesssim 8 \times 10^{-9}$	$\mu \rightarrow \bar{e}ee$
$C_{4f_8,S}^{e\mu uu, e\mu dd}$	$\lesssim 10^{-8}$	$\lesssim 10^{-10}$	$\mu A \rightarrow eA$

Table 3: Sensitivities to $\mu \rightarrow e$ dimension eight operator coefficients, normalized as in eq. (2). Current and future limits correspond to the experimental sensitivities of Table 1. T, S label the Lorentz structure of the operator for tensor and scalar respectively. For instance, $C_{4f_8,T}^{e\mu tt}$ is the coefficient of the dimension eight tensor in eq. (35) with top quarks.

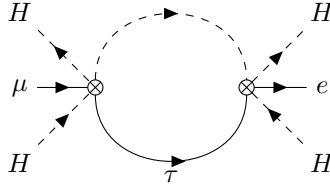


Figure 5: Mixing to the dimension eight $\mu \rightarrow e$ penguin operator from double insertion of dimension six Yukawas $Y_6 \times Y_6 \rightarrow P_8$.

An example of a diagram contributing to the RGEs is shown in the diagram of Figure 5, where two Yukawa operators $\mathcal{O}_{eH}^{e\tau} \times \mathcal{O}_{eH}^{\tau\mu} \sim Y_6 \times Y_6$ mix into dimension eight $\mu \rightarrow e$ penguin operators $\mathcal{O}_{e^2 H^2 D}^{e\mu}, \mathcal{O}_{l^2 H^2 D}^{e\mu} \sim P_8$ by exchanging the τ and closing the loop with a Higgs line. The estimated contribution to the penguin coefficients is then

$$\Delta C_{P_8} \sim (C_{Y_6})^2 \frac{\log(4 \text{ TeV}/m_W)}{16\pi^2} \sim 3 \times 10^{-9}. \quad (50)$$

Future $\mu A \rightarrow eA$ experiments will be sensitive to penguin coefficients larger than $\sim 10^{-9}$, hence our estimate lies within experimental reach and $Y_6 \times Y_6 \rightarrow P_8$ mixing is calculated in section 3.

As another example, $\tau \leftrightarrow l$ dipoles D_6 are defined with a built-in τ Yukawa suppression — see eq. (12)— so $y_\tau \sim 10^{-2}$ multiplies any dipole insertion. For instance, if $D_6 \times \mathcal{O}_6$ mix into a dimension eight operator \mathcal{O}_8 , its coefficient is estimated to be

$$\Delta C_8 \sim y_\tau C_{D_6} C_6 \frac{\log(4 \text{ TeV}/m_W)}{16\pi^2} \lesssim 10^{-12}, \quad (51)$$

where we took $C_6 \lesssim v^2/\Lambda^2$, for $\Lambda \sim 4 \text{ TeV}$. Equation (51) is smaller than any future $\mu \rightarrow e$ sensitivity to operator coefficients, so we disregard mixing that involves τ dipoles in our calculations.

The results of our estimates are summarized in Tables 4 and 5, referring respectively to RGEs and matching contributions. There, we report the potentially detectable dimension eight operators generated by a given pair of dimension six operators.

	P_6	Y_6	$4l_6$	$4f_6$
P_6	$D_8 \equiv 0$	$D_8 \equiv 0$	\times	$4f_8$
Y_6	$D_8 \equiv 0$	P_8	\times	\times
$4l_6$	\times	\times	\times	\times
$4f_6$	$4f_8$	\times	\times	$4f_8$

Table 4: We present the dimension eight operators that we estimate to be generated within experimental sensitivity through (dimension six)² mixing in the RGEs. The \times means that the contributions is too small or that there is no one-loop diagram that can generate the desired dimension eight operators with the given pair. $P_6 \times P_6 \rightarrow D_8$, $Y_6 \times P_6 \rightarrow D_8$ mixing diagrams exist and appear to be interesting, however we find that the anomalous dimension vanishes (see section 3.1.1).

	P_6	Y_6	$4l_6$	$4f_6$
P_6	\times	D_8	\times	\times
Y_6	\times	$D_8, 4l_8$	\times	\times
$4l_6$	\times	\times	\times	\times
$4f_6$	\times	\times	\times	\times

Table 5: We present the dimension eight operators that we estimate to be generated within experimental sensitivity through (dimension six)² in matching. The \times means that the contributions is too small or that there is no tree-level matching that can generate the desired dimension eight operators with the given pair.

3 Calculation

The contributions that were estimated in the previous section to be within experimental sensitivity are calculated here. Section 3.1 determines the divergences of the relevant one-loop diagrams and relates them to the anomalous dimensions of the dimension eight Wilson coefficients in SMEFT, and in Section 3.2, pairs of $\tau \leftrightarrow l$ dimension six operators are tree-level-matched at m_W onto the low energy $\mu \rightarrow e$ EFT.

3.1 SMEFT Running

In this section, we outline the calculation of the anomalous dimension matrix $\hat{\gamma}_{XY,A}$, that mixes the dimension six $\tau \leftrightarrow l$ operators $\mathcal{O}_X^{[6]}, \mathcal{O}_Y^{[6]}$ into the $\mu \rightarrow e$ dimension eight $\mathcal{O}_A^{[8]}$. We work in dimensional regularization in $4 - 2\epsilon$ dimensions and renormalize in the $\overline{\text{MS}}$ scheme, where we label the renormalization scale with M (rather than the usual μ). Double insertions of dimension six operators renormalize dimension eight coefficients as

$$\Delta \vec{C}_A^{[8]} = \vec{C}_X^{[6]} \hat{Z}_{XY,A} \vec{C}_Y^{[6]}, \quad (52)$$

where the Wilson coefficients of dimension eight and six are respectively aligned in the row vectors $\vec{C}^{[8]}, \vec{C}^{[6]}$, dimension eight and six operator labels are respectively capitals from the beginning and end of the alphabet, and flavour indices are suppressed. The bare dimension eight coefficients can be written as

$$\vec{C}_{A,bare}^{[8]} = M^{a_A \epsilon} (\vec{C}_B^{[8]} Z_{BA} + \vec{C}_X^{[6]} \hat{Z}_{XY,A} \vec{C}_Y^{[6]}) \quad (53)$$

where we have factored out the sliding scale power $M^{a_A \epsilon}$ to assure that the renormalized WC stay dimensionless in $d = 4 - 2\epsilon$ dimensions. The RGEs can be obtained from the independence of the bare Lagrangian from the arbitrary renormalization scale M

$$(16\pi^2) \frac{d\vec{C}_{A,bare}^{[8]}}{d\log M} = 0, \quad (54)$$

which implies the following differential equation for the renormalized Wilson coefficients

$$(16\pi^2) \frac{d\vec{C}_A^{[8]}}{d\log M} = (16\pi^2) \left[-a_A \epsilon (\vec{C}_A^{[8]} + \vec{C}_X^{[6]} \vec{C}_Y^{[6]} \hat{Z}_{XY,B} Z_{BA}^{-1}) - \vec{C}_B^{[8]} \frac{dZ_{BC}}{d\log M} Z_{CA}^{-1} + \right. \\ \left. - \frac{d\vec{C}_X^{[6]}}{d\log M} \hat{Z}_{XY,B} \vec{C}_Y^{[6]} Z_{BA}^{-1} - \vec{C}_X^{[6]} \hat{Z}_{XY,B} \frac{d\vec{C}_Y^{[6]}}{d\log M} Z_{BA}^{-1} - \vec{C}_X^{[6]} \frac{d\hat{Z}_{XY,B}}{d\log M} \vec{C}_Y^{[6]} Z_{BA}^{-1} \right]. \quad (55)$$

The RGEs of dimension six Wilson coefficients are the following

$$(16\pi^2) \frac{d\vec{C}_X^{[6]}}{d\log M} = -(16\pi^2) a_X \epsilon \vec{C}_X^{[6]} + \vec{C}_Y^{[6]} \tilde{\gamma}_{YX} + \dots \quad (56)$$

where $a_X \epsilon$ is the mass dimension of the bare coefficient of \mathcal{O}_X and $\tilde{\gamma}$ is the anomalous dimension matrix for dimension six operators. In the limit $\epsilon \rightarrow 0$, the term proportional to ϵ is irrelevant for the dimension six renormalization, while it plays a crucial role in (dimension6)² to dimension eight mixing. Upon substitution, eq. (55) becomes

$$(16\pi^2) \frac{d\vec{C}_A^{[8]}}{d\log M} = (16\pi^2) \left[-a_A \epsilon \vec{C}_A^{[8]} + \vec{C}_B^{[8]} \gamma_{BA} - (a_A - a_X - a_Y) \epsilon (\vec{C}_X^{[6]} \vec{C}_Y^{[6]} \hat{Z}_{XY,B} Z_{BA}^{-1}) - \vec{C}_X^{[6]} \frac{d\hat{Z}_{XY,B}}{d\log M} \vec{C}_Y^{[6]} Z_{BA}^{-1} \right. \\ \left. - \vec{C}_W^{[6]} \tilde{\gamma}_{WX} \hat{Z}_{XY,B} \vec{C}_Y^{[6]} Z_{BA}^{-1} - \vec{C}_X^{[6]} \hat{Z}_{XY,B} \vec{C}_W^{[6]} \tilde{\gamma}_{WY} Z_{BA}^{-1} \right]$$

having defined $\gamma_{BA} \equiv -(16\pi^2) \frac{dZ_{BC}}{d\log M} Z_{CA}^{-1}$, which is the anomalous dimension matrix of dimension eight operators. At one-loop we can replace \hat{Z} with the identity and neglect the second line of the above equation, since $\tilde{\gamma}$

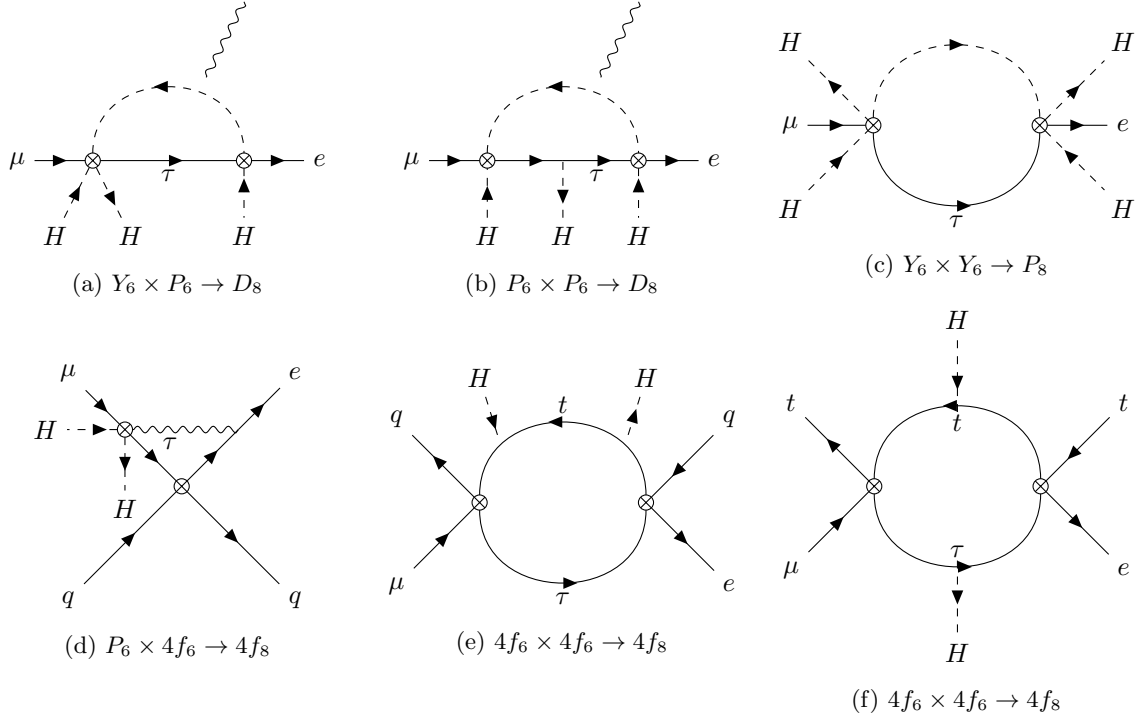


Figure 6: Classes of divergent diagrams that give observable contributions to $\mu \rightarrow e$ processes, as identified in Table 4.

and \hat{Z} both appear at one loop at leading order. The product $\epsilon \hat{Z}$ is finite, and the RGEs in $d = 4$ dimensions read

$$(16\pi^2) \frac{d\vec{C}_A^{[8]}}{d\log M} = \vec{C}_B^{[8]} \gamma_{BA} - (16\pi^2)(a_A - a_X - a_Y) \vec{C}_X^{[6]} \vec{C}_Y^{[6]} \epsilon \hat{Z}_{XY,A} - (16\pi^2) \vec{C}_X^{[6]} \frac{d\hat{Z}_{XY,A}}{d\log M} \vec{C}_Y^{[6]} \quad (57)$$

$$\equiv \vec{C}_B^{[8]} \gamma_{BA} + \vec{C}_X^{[6]} \hat{\gamma}_{XY,A} \vec{C}_Y^{[6]} \quad (58)$$

The one-loop $\hat{\gamma}$ anomalous dimension matrix that mixes two dimension six operators into dimension eight is finally

$$\hat{\gamma}_{XY,A} = (16\pi^2) \left[(a_X + a_Y - a_A) \epsilon \hat{Z}_{XY,A} - \frac{d\hat{Z}_{XY,A}}{d\log M} \right]. \quad (59)$$

The second term contribute to the mixing when renormalizable couplings appear in \hat{Z} , which carry an implicit dependence on the renormalization scale M . The beta functions of renormalized SM couplings for $\epsilon > 0$ take the form $\beta_\epsilon(\{g, g', y\}) = -\epsilon\{g, g', y\} + \beta(\{g, g', y\})$ and at one-loop

$$-\frac{d\hat{Z}_{XY,A}}{d\log M} = -\frac{d\hat{Z}_{XY,A}}{d\{g, g', y\}} \beta_\epsilon(\{g, g', y\}) = \epsilon \frac{d\hat{Z}_{XY,A}}{d\{g, g', y\}} \times \{g, g', y\} + \text{higher loops}. \quad (60)$$

3.1.1 $\mu \rightarrow \tau \times \tau \rightarrow e$ in SMEFT

We calculate the divergent part of one-loop diagrams with the product of $\mu \rightarrow \tau \times \tau \rightarrow e$ operator insertions, which, according to the estimates summarized in Table 4, give potentially detectable contributions to $\mu \rightarrow e$ observables in the dimension eight running. We work in SMEFT and unbroken SU(2), where all SM particles are taken massless, including the Higgs doublet. The diagrams have been drawn by hand and were also generated with a code based on FeynArts [42] and FeynRules [43]. In most cases⁴, the dimension eight operators to which $\mu \rightarrow e$ observables are sensitive do not contain τ external legs, so we here consider diagrams with a virtual τ line connecting two dimension six SMEFT operators. We are interested in one-particle-irreducible divergent diagrams (which restrict the number of internal propagators) that can generate the dimension eight operators of section 2.2 (which constrain the external legs), and also in some one-particle-reducible divergent diagrams that reproduce the contribution of the dimension six correction in the EOM, as discussed in section 2.4. Yukawa couplings smaller than $y_\tau \sim 10^{-2}$ are neglected, because they lead to $\mu \rightarrow e$ coefficients below experimental

⁴The exception is the $\mu e \tau \tau$ tensors, but the leading contribution to these is from tree-level matching onto the low energy EFT, which is discussed the next section.

sensitivity, assuming dimension six WC $C^{[6]} \lesssim v^2/\Lambda_{\text{NP}}^2$ and $\Lambda_{\text{NP}} = 4 \text{ TeV}$. However, the estimates of section 2.5 select diagrams that only involve top Yukawas y_t and single insertions of y_τ , while the bottom and charm Yukawas y_b, y_c do not appear.

In Figure 6 we show the “classes” of diagrams listed in Table 4, that were estimated to be within $\mu \rightarrow e$ experimental sensitivity. Each class is described below. The divergences were calculated both by hand and with an in-house developed Mathematica program, making use of the Feynman Rules listed in Appendix A.

- **Figure 6a:** $Y_6 \times P_6 \rightarrow D_8$

The penguin operators of eq.s (13)-(14) can be combined with the Yukawa operators of eq. (17). The chirality flips on the lepton line, so attaching a gauge boson potentially generates the $\mu \rightarrow e$ dipoles of eq. (25). The gauge bosons can be inserted on the internal Higgs and lepton lines or can come out of penguin operators, while the three external Higgs can be permuted in several ways among the dimension six vertices. Also, in the diagram depicted, the Yukawa operator is $\mu \rightarrow \tau$ and the penguin is $\tau \rightarrow e$, but the two vertices can be exchanged: for instance, in the case of external left-handed electrons, the possible operator combinations are: $\mathcal{O}_{He}^{\tau\mu} \times \mathcal{O}_{eH}^{e\tau}$, $\mathcal{O}_{eH}^{\tau\mu} \times \mathcal{O}_{Hl}^{(1)e\tau}$, $\mathcal{O}_{eH}^{\tau\mu} \times \mathcal{O}_{Hl}^{(3)e\tau}$. We find that these anomalous dimensions vanish. This is consistent with the dimension six version of this calculation, where neither penguin operators dressed with renormalizable Yukawa couplings, nor \mathcal{O}_{eH} dressed with a gauge loop, mix into the dimension six dipoles [28]. Note that in broken SU(2) and unitary gauge, dimension six penguins and Yukawas give Feynman rules that look like SM renormalisable interactions. By analogy with the SM, we expect them to not generate divergent non-renormalisable dipoles.

- **Figure 6b:** $P_6 \times P_6 \rightarrow D_8$

The diagrams feature double insertions of penguin operators - see eq.s (13)-(14). The two vertices couple to vector currents of leptons, so to mix into the $\mu \rightarrow e$ dipoles, the chirality flip is achieved by attaching a Higgs to the τ virtual line. The contribution is estimated to lie within experimental sensitivity, because the generated $\mu \rightarrow e$ dipole coefficient is enhanced by the ratio y_τ/y_μ due to the Yukawa couplings in the dipole operator definitions in eq. (25). The gauge bosons can be attached to the Higgs and τ in the loop, or can belong to one of the penguin vertices. Furthermore, all possible permutations of the external Higgses are taken into account. The operator pairs are $\mathcal{O}_{He} \times \mathcal{O}_{Hl}^{(1),(3)}$, where the $\tau \rightarrow e$ LFV can be mediated by either right-handed or left-handed penguins, depending on the chirality of the external legs. As the previous case, the mixing into the $\mu \rightarrow e$ dipole is found to vanish.

In addition to the 1PI diagrams of Figure 6b, dimension six terms in the EOM contribute to the mixing. Loop diagrams where the Higgs leg of a penguin operator closes into the τ line via a Yukawa interaction renormalize the redundant operator $(D^2\bar{\ell}_\tau)He_i$ (see Figure 4b). When the divergence is projected onto the on-shell basis, the penguin correction to the EOM gives additional $P_6 \times P_6 \rightarrow D_8$ mixing. However, the combination of SMEFT $\mu \rightarrow e$ dipoles that is generated is orthogonal to the γ dipole and does not contribute to low energy $\mu \rightarrow e$ observables. This is also apparent in considering non-1PI diagrams (see section 2.4) where a penguin operator is inserted in the τ line of $D^2\bar{\ell}_\tau He_i$; the amplitude is local and reproduces the EOM result when the external gauge boson belongs to the penguin vertex. In broken SU(2), penguins give flavour changing (and correct the flavour diagonal) couplings with the Z , but leave QED interactions untarnished.

- **Figure 6c:** $Y_6 \times Y_6 \rightarrow P_8$

In this class of diagrams the loop is closed with Higgs exchange between two Yukawa operators. The superficial degree of divergence is 1, and the divergence is linear in momentum. With four external Higgses, it mixes into the dimension eight $\mu \rightarrow e$ penguin operators of eq. (32). For right-handed leptons the inserted operators are $\mathcal{O}_{eH}^{\tau\mu} \times \mathcal{O}_{eH}^{*\tau e}$, while $\mathcal{O}_{eH}^{*\mu\tau} \times \mathcal{O}_{eH}^{e\tau}$ gives mixing into left-handed penguins.

- **Figure 6d:** $4f_6 \times P_6 \rightarrow 4f_8$

Two-lepton two-quark $\tau \rightarrow l$ operators can mix into $\mu \rightarrow e$ dimension eight four fermion operators by inserting a penguin in the tau line and closing the loop with a gauge boson. Only two-lepton two quark operators are considered because they contribute to $\mu \rightarrow e$ conversion (while tensors with heavy quarks contribute to $\mu \rightarrow e\gamma$), which is the process with the best upcoming sensitivity to operator coefficients. The gauge boson is attached to the other fermion lines in every possible way, and the diagram shows just one example. As discussed in section 2.4, we also include dimension six corrections to the EOM or, equivalently, non-1PI diagrams where the loop of Figure 4 dresses one of the lepton lines. These diagrams are analogous to fermion wave function renormalization and are pure-gauge, i.e $\propto \xi$ in the R_ξ gauge; to avoid calculating wave function-like diagrams, the calculation is done for $\xi = 0$, commonly known as Landau gauge. In Table 7 we summarize the $\mu \rightarrow e$ dimension eight operators generated by the product of $\tau \rightarrow l$ penguins with four fermion operators.

- **Figure 6e-6f:** $4f_6 \times 4f_6 \rightarrow 4f_8$ In the last two diagrams, pairs of two-lepton two-quark dimension six operators are connected through a fermion loop, where two Higgs legs are inserted. With the exception of dimension eight tensor with tops, $\mu \rightarrow e$ observables are sensitive to the resulting dimension eight coefficients only if the Higgs are attached to a top internal line. In the case of tensors with tops, the better sensitivity allows for the topology of Figure 6f, where a τ Yukawa is present. In Table 6 we list the dimension eight operators that are generated for every pair of dimension six four fermion operators.

	$C_{\ell q}^{(1)}$	$C_{\ell q}^{(3)}$	$C_{\ell u}$	C_{eq}	C_{eu}	C_{ledq}, C_{ledq}^*	$C_{lequ}^{(1)}, C_{lequ}^{*(1)}$	$C_{lequ}^{(3)}, C_{lequ}^{*(3)}$
$C_{\ell q}^{(1)}$	$C_{\ell^2 q^2 H^2}^{(1),(4)}$	$C_{\ell^2 q^2 H^2}^{(2),(3),(5)}$	\times	\times	$C_{lequ H^2}^{(3),(4)}$	$C_{ledq H^2}^{(1),(2)}$ $C_{ledq H^2}^{*(1),(2)}$	$C_{lequ H^2}^{(1),(2),(3),(4)}$ $C_{lequ H^2}^{*(1),(2),(3),(4)}$	$C_{lequ H^2}^{(1),(2),(3),(4)}$ $C_{lequ H^2}^{*(1),(2),(3),(4)}$
$C_{\ell q}^{(3)}$		$C_{\ell^2 q^2 H^2}^{(1),(2)}$	\times	\times	$C_{lequ H^2}^{(3),(4)}$	$C_{ledq H^2}^{(1),(2)}$ $C_{ledq H^2}^{*(1),(2)}$	$C_{lequ H^2}^{(1),(2),(3),(4)}$ $C_{lequ H^2}^{*(1),(2),(3),(4)}$	$C_{lequ H^2}^{(1),(2),(3),(4)}$ $C_{lequ H^2}^{*(1),(2),(3),(4)}$
$C_{\ell u}$			$C_{\ell^2 u^2 H^2}^{(1)}$	$C_{lequ H^2}^{(3),(4)}$	\times	\times	$C_{lequ H^2}^{(1),(3)}$ $C_{lequ H^2}^{*(1),(3)}$	$C_{lequ H^2}^{(1),(3)}$ $C_{lequ H^2}^{*(1),(3)}$
C_{eq}				$C_{e^2 q^2 H^2}^{(1),(2)}$	\times	$C_{ledq H^2}^{(1),(2)}$ $C_{ledq H^2}^{*(1),(2)}$	$C_{lequ H^2}^{(1),(2),(3),(4)}$ $C_{lequ H^2}^{*(1),(2),(3),(4)}$	$C_{lequ H^2}^{(1),(2),(3),(4)}$ $C_{lequ H^2}^{*(1),(2),(3),(4)}$
C_{eu}					$C_{e^2 u^2 H^2}$	\times	$C_{lequ H^2}^{(1),(3)}$ $C_{lequ H^2}^{*(1),(3)}$	$C_{lequ H^2}^{(1),(3)}$ $C_{lequ H^2}^{*(1),(3)}$
C_{ledq}, C_{ledq}^*						$C_{e^2 d^2 H^2}$ $C_{\ell^2 d^2 H^2}^{(1),(2)}$	\times	\times
$C_{lequ}^{(1)}, C_{lequ}^{*(1)}$							$C_{e^2 u^2 H^2}$ $C_{e^2 q^2 H^2}^{(1)}$ $C_{\ell^2 u^2 H^2}^{(1),(2)}$ $C_{\ell^2 q^2 H^2}^{(1),(3)}$	$C_{e^2 u^2 H^2}$ $C_{e^2 q^2 H^2}^{(1)}$ $C_{\ell^2 u^2 H^2}^{(1),(2)}$ $C_{\ell^2 q^2 H^2}^{(1),(3)}$
$C_{lequ}^{(3)}, C_{lequ}^{*(3)}$								$C_{e^2 u^2 H^2}$ $C_{e^2 q^2 H^2}^{(1)}$ $C_{\ell^2 u^2 H^2}^{(1),(2)}$ $C_{\ell^2 q^2 H^2}^{(1),(3)}$

Table 6: Dimension eight operators generated through the diagrams of Figure 6e and 6f with pairs of two-lepton two-quark operators, $4f_6 \times 4f_6$. Most of dimension eight coefficients are proportional to y_t^2 , with the exception of $\mathcal{O}_{\ell u} \times \mathcal{O}_{eq}$, $\mathcal{O}_{\ell q} \times \mathcal{O}_{eu}$ mixing into the tensors $\mathcal{O}_{lequ H^2}^{(3),(4)}$, where the Yukawa couplings $y_\tau y_t$ multiply the coefficient.

The complete anomalous dimensions for the above classes of diagrams can be found in Appendix B.

We discuss the example of a pair of dimension six $\tau \leftrightarrow l$ Yukawa operators mixing into the $\mu \rightarrow e$ dimension eight penguins, depicted in the representative diagram of Figure 6c. The counterterms that renormalize the divergences are the following

$$\begin{aligned}
\left(C_{eH}^{\tau\mu} \hat{Z} C_{eH}^{*\tau e}\right)_{e^2 H^4 D}^{e\mu} &= -\frac{C_{eH}^{\tau\mu} C_{eH}^{*\tau e}}{32\pi^2 \epsilon} & \left(C_{eH}^{\tau\mu} \hat{Z} C_{eH}^{*\tau e}\right)_{ve^2 H^4 D}^{e\mu} &= -\frac{3C_{eH}^{\tau\mu} C_{eH}^{*\tau e}}{32\pi^2 \epsilon} \\
\left(C_{eH}^{*\mu\tau} \hat{Z} C_{eH}^{e\tau}\right)_{\ell^2 H^4 D}^{(1)e\mu} &= \frac{C_{eH}^{*\mu\tau} C_{eH}^{e\tau}}{64\pi^2 \epsilon} & \left(C_{eH}^{*\mu\tau} \hat{Z} C_{eH}^{e\tau}\right)_{v\ell^2 H^4 D}^{(1)e\mu} &= -\frac{C_{eH}^{*\mu\tau} C_{eH}^{e\tau}}{64\pi^2 \epsilon} \\
\left(C_{eH}^{*\mu\tau} \hat{Z} C_{eH}^{e\tau}\right)_{\ell^2 H^4 D}^{(2)e\mu} &= \frac{C_{eH}^{*\mu\tau} C_{eH}^{e\tau}}{128\pi^2 \epsilon} & \left(C_{eH}^{*\mu\tau} \hat{Z} C_{eH}^{e\tau}\right)_{v\ell^2 H^4 D}^{(2)e\mu} &= -\frac{C_{eH}^{*\mu\tau} C_{eH}^{e\tau}}{16\pi^2 \epsilon} \\
\left(C_{eH}^{*\mu\tau} \hat{Z} C_{eH}^{e\tau}\right)_{\ell^2 H^4 D}^{(4)e\mu} &= \frac{C_{eH}^{*\mu\tau} C_{eH}^{e\tau}}{128\pi^2 \epsilon} & &
\end{aligned} \tag{61}$$

where the subscript in the brackets label the corresponding dimension eight operators. The operator $\mathcal{O}_{\ell^2 H^4 D}^{(4)e\mu} = \epsilon^{IJK} (\bar{\ell}_e \tau^I \gamma^\alpha \ell_\mu) (H^\dagger \tau^J H) D_\alpha (H^\dagger \tau^K H)$ is not in the list of section 2.2 because it does not contribute to low energy $\mu \rightarrow e$ observables, although it appears as a counterterm. Furthermore, the following redundant operators are radiatively generated in our off-shell calculation

$$\mathcal{O}_{ve^2 H^4 D}^{e\mu} = i(\bar{e} \overleftrightarrow{D} \mu) (H^\dagger H)^2 \equiv i(\bar{e} \not{D} \mu) (H^\dagger H)^2 - i(\not{D} \bar{e} \mu) (H^\dagger H)^2 \tag{62}$$

$$\mathcal{O}_{v\ell^2 H^4 D}^{(1)e\mu} = i(\bar{\ell}_e \overleftrightarrow{D} \ell_\mu) (H^\dagger H)^2 \tag{63}$$

	$C_{\ell q}^{(1)}$	$C_{\ell q}^{(3)}$	$C_{\ell u}$	$C_{\ell d}$	$C_{\ell edq}, C_{\ell edq}^*$	$C_{\ell equ}^{(1)}, C_{\ell equ}^{*(1)}$	$C_{\ell equ}^{(3)}, C_{\ell equ}^{*(3)}$
$C_{H\ell(1)}$	$C_{\ell^2 q^2 H^2}^{(1),(4)}$	$C_{\ell^2 q^2 H^2}^{(2),(3),(5)}$	$C_{\ell^2 u^2 H^2}^{(1)}$	$C_{\ell^2 d^2 H^2}^{(1)}$	$C_{\ell edq H^2}^{(1)}$ $C_{\ell edq H^2}^{*(1)}$	$C_{\ell equ H^2}^{(1),(3),(4)}$ $C_{\ell equ H^2}^{*(1),(3),(4)}$	$C_{\ell equ H^2}^{(1),(2),(3),(4)}$ $C_{\ell equ H^2}^{*(1),(2),(3),(4)}$
$C_{H\ell(3)}$	$C_{\ell^2 q^2 H^2}^{(2),(3)}$	$C_{\ell^2 q^2 H^2}^{(1),(4),(5)}$	$C_{\ell^2 u^2 H^2}^{(2)}$	$C_{\ell^2 d^2 H^2}^{(2)}$	$C_{\ell edq H^2}^{(2)}$ $C_{\ell edq H^2}^{*(2)}$	$C_{\ell equ H^2}^{(2),(3),(4)}$ $C_{\ell equ H^2}^{*(2),(3),(4)}$	$C_{\ell equ H^2}^{(1),(2),(3),(4)}$ $C_{\ell equ H^2}^{*(1),(2),(3),(4)}$

	C_{eq}	C_{eu}	C_{ed}	$C_{\ell edq}, C_{\ell edq}^*$	$C_{\ell equ}^{(1)}, C_{\ell equ}^{*(1)}$	$C_{\ell equ}^{(3)}, C_{\ell equ}^{*(3)}$
C_{He}	$C_{e^2 q^2 H^2}^{(1),(2)}$	$C_{e^2 u^2 H^2}$	$C_{e^2 d^2 H^2}$	$C_{\ell edq H^2}^{(1),(2)}$ $C_{\ell edq H^2}^{*(1),(2)}$	$C_{\ell equ H^2}^{(1),(2),(3),(4)}$ $C_{\ell equ H^2}^{*(1),(2),(3),(4)}$	$C_{\ell equ H^2}^{(1),(2),(3),(4)}$ $C_{\ell equ H^2}^{*(1),(2),(3),(4)}$

Table 7: Dimension eight operators generated via the diagrams of Figure 6d with pairs of two-lepton two-quark $4f_6$ and penguins P_6

$$\mathcal{O}_{v\ell^2 H^4 D}^{(2)e\mu} = i(\bar{\ell}_e \overleftrightarrow{D} \ell_{\mu J})(H_I H_J^\dagger)(H^\dagger H). \quad (64)$$

These are related to the physical/on-shell basis as follows

$$\mathcal{O}_{ve^2 H^4 D}^{e\mu} = \mathcal{O}_v^{e\mu} + [y_e^*]_{i\mu} \mathcal{O}_{\ell e H^5}^{*ie} + [y_e]_{ie} \mathcal{O}_{\ell e H^5}^{i\mu} \quad (65)$$

$$\mathcal{O}_{v\ell^2 H^4 D}^{(1)e\mu} = \mathcal{O}_v^{(1)e\mu} + [y_e]_{\mu i} \mathcal{O}_{\ell e H^5}^{ei} + [y_e^*]_{ei} \mathcal{O}_{\ell e H^5}^{* \mu i} \quad (66)$$

$$\mathcal{O}_{v\ell^2 H^4 D}^{(2)e\mu} = \mathcal{O}_v^{(2)e\mu} + [y_e]_{\mu i} \mathcal{O}_{\ell e H^5}^{ei} + [y_e^*]_{ei} \mathcal{O}_{\ell e H^5}^{* \mu i} \quad (67)$$

where $\mathcal{O}_{\ell e H^5}^{ij} = (\bar{\ell}_i H e_j)(H^\dagger H)^2$, and each of $\mathcal{O}_v^{e\mu}$, $\mathcal{O}_v^{(1)e\mu}$, $\mathcal{O}_v^{(2)e\mu}$ vanishes, when the renormalizable EOM on singlet and doublet leptons $i(\bar{\ell} \overleftrightarrow{D} \mu) - [y_e^*]_{i\mu}(H^\dagger \ell_i) = 0$, $i(\bar{\ell} \overleftrightarrow{D} \mu) - [y_e]_{\mu i}(H e_i) = 0$ are satisfied. The off-shell counterterms are on-shell equivalent to $[y_e^*]_{i\mu} \mathcal{O}_{\ell e H^5}^{*ie} + [y_e]_{ie} \mathcal{O}_{\ell e H^5}^{i\mu}$, which is beyond $\mu \rightarrow e$ experimental reach. The resulting RGEs are obtained from eq. (61) and (58), and read

$$16\pi^2 \dot{C}_{e^2 H^4 D}^{e\mu} = -C_{eH}^{\tau\mu} C_{eH}^{*\tau e} \quad (68)$$

$$16\pi^2 \dot{C}_{\ell^2 H^4 D}^{(1)e\mu} = \frac{1}{2} C_{eH}^{*\mu\tau} C_{eH}^{e\tau} \quad 16\pi^2 \dot{C}_{\ell^2 H^4 D}^{(2)e\mu} = \frac{1}{4} C_{eH}^{*\mu\tau} C_{eH}^{e\tau} \quad (69)$$

where the dot on the dimension eight coefficients corresponds to $d/d \log M$.

3.2 Matching SMEFT onto the low energy EFT

In Table 5 of Section 2.3, we identified the relevant matching contributions to low energy $\mu \leftrightarrow e$ interactions from the double insertion of $\mu \rightarrow \tau \times \tau \rightarrow e$ dimension six SMEFT operators. At the matching scale m_W , the electroweak symmetry is spontaneously broken by the Higgs VEV, and the h, Z, W and t are removed from the low energy EFT. The matching is performed by identifying the matrix elements of a $\mu \rightarrow e$ process calculated in the theories above and below the matching scale, with the electroweak symmetry broken in both theories. As a result, products of $\tau \leftrightarrow l$ SMEFT operators can match onto $\mu \rightarrow e$ three and four point functions. The interesting diagrams are illustrated in Figure 7. When the Higgs doublet acquires a VEV, Yukawa operators contribute to the mass matrix

$$m_{e_i} \delta_{ij} = v \left([y_e]_{ij} - C_{eH}^{ij} \right) \quad (70)$$

and the h couplings

$$-\frac{h}{\sqrt{2}} \bar{e}_i P_R e_j \left([y_e]_{ij} - 3C_{eH}^{ij} \right) + \text{h.c.} = -\frac{h}{\sqrt{2}} \bar{e}_i P_R e_j \left(\frac{m_{e_i} \delta_{ij}}{v} - 2C_{eH}^{ij} \right) + \text{h.c.} \quad (71)$$

of charged leptons with a different prefactor, such that h acquires LFV couplings in the lepton mass eigenstate basis.

The two-loop Barr-Zee diagrams (Figure 7c-7d) match to the dipole at tree level in the low energy EFT. The lepton line is connected via Z and h exchange to a top or W loop, where the Z and h respectively couple to the lepton line via a penguin and an off-diagonal Yukawa operator. Such diagrams can be significant [44] (despite the two-loop suppression), because they are not suppressed by small Yukawa couplings. We estimate these diagrams from the results of [45], who calculated the Barr-Zee diagrams in the two Higgs Doublet Model

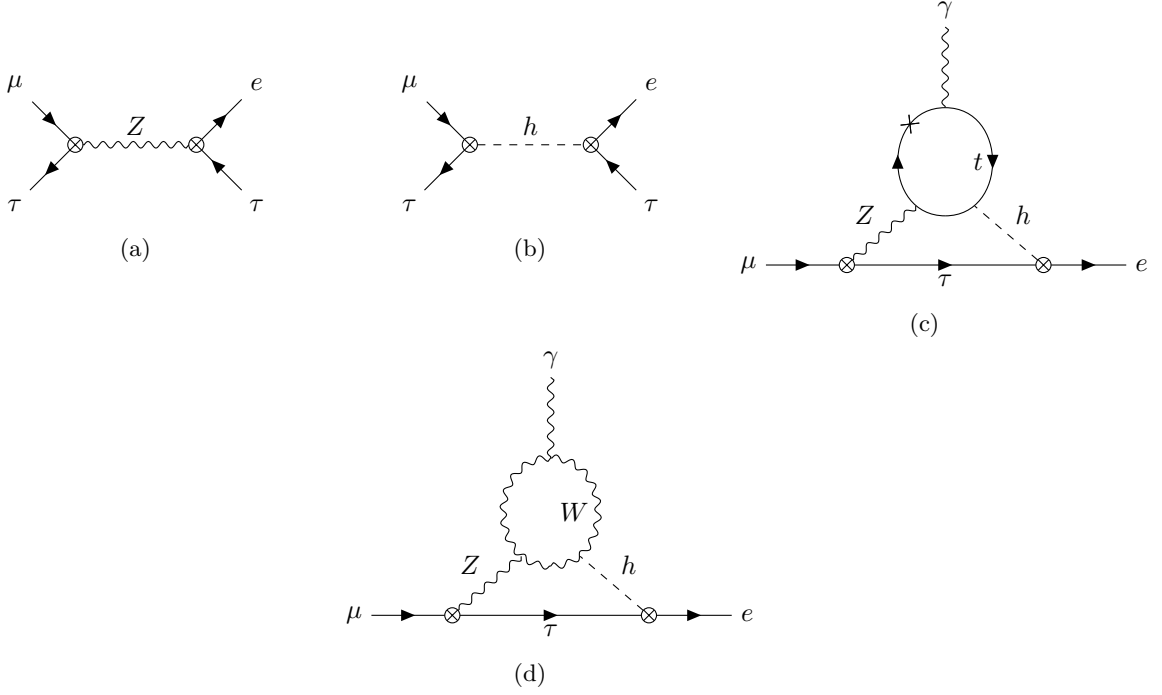


Figure 7: Diagrams matching pairs of dimension six $\tau \rightarrow l$ SMEFT operators onto low energy $\mu \rightarrow e$ operators.

(2HDM) with LFV couplings, where they provide the leading contribution to $\mu \rightarrow e\gamma$ (because the diagrams are not suppressed by y_μ). In the 2HDM results of [45], the Z -diagrams are suppressed (relative to γ diagrams) because the C -even dipole moment only couples the Z to the vector current of leptons, so there is a suppression of $(1 - 4\sin^2\theta_W) \lesssim 0.03$. However in our case, the Z -lepton vertex is a penguin operator with a flavour-changing coefficient that we wish to constrain, and so does not suffer from such SM factors. The estimated contributions to the dipole coefficients are [45] :

$$C_{D,R} \simeq \frac{9e\alpha_e}{64\pi^3} \frac{v}{m_\mu} \left[C_{He}^{\tau\mu} C_{eH}^{e\tau} + \left(C_{H\ell}^{(1)e\tau} + C_{H\ell}^{(3)e\tau} \right) C_{eH}^{\tau\mu} \right] \quad (72)$$

$$C_{D,L} \simeq \frac{9e\alpha_e}{64\pi^3} \frac{v}{m_\mu} \left[C_{eH}^{*\tau e} \left(C_{H\ell}^{(1)\tau\mu} + C_{H\ell}^{(3)\tau\mu} \right) + C_{eH}^{*\mu\tau} C_{He}^{e\tau} \right] \quad (73)$$

A dipole is also generated at one-loop with a pair of penguin operators, which look like the flavor changing version of the electroweak correction to $(g - 2)_\mu$ with a Z exchange. However, assuming the future limits on penguin coefficients shown in Table 2, the contribution is below $\mu \rightarrow e\gamma$ upcoming experimental sensitivity.

Four lepton $e\mu\tau\tau$ operators get matching contribution from tree-level diagrams with a Z, h exchange between penguin vertices or LFV Higgs boson couplings, as illustrated in the diagrams of Figure 7a and 7b. SMEFT τ -LFV penguins and Yukawa corrections are matched at m_W onto low energy four lepton operator coefficients

as follows

$$C_{T,RR}^{e\mu\tau\tau} = -\frac{1}{4}C_{eH}^{e\tau}C_{eH}^{\tau\mu}\frac{v^2}{m_h^2} \quad (74)$$

$$C_{T,LL}^{e\mu\tau\tau} = -\frac{1}{4}C_{eH}^{*\tau e}C_{eH}^{*\mu\tau}\frac{v^2}{m_h^2} \quad (75)$$

$$C_{S,RR}^{e\mu\tau\tau} = -C_{eH}^{e\tau}C_{eH}^{\tau\mu}\frac{v^2}{m_h^2} \quad (76)$$

$$C_{S,LL}^{e\mu\tau\tau} = -C_{eH}^{*\tau e}C_{eH}^{*\mu\tau}\frac{v^2}{m_h^2} \quad (77)$$

$$C_{S,RL}^{e\mu\tau\tau} = \frac{2g^2}{\cos^2\theta_W}\left(C_{He}^{\tau\mu}C_{H\ell}^{(1)e\tau} + C_{He}^{\tau\mu}C_{H\ell}^{(3)e\tau}\right)\frac{v^2}{M_Z^2} \quad (78)$$

$$C_{S,LR}^{e\mu\tau\tau} = \frac{2g^2}{\cos^2\theta_W}\left(C_{He}^{e\tau}C_{H\ell}^{(1)\tau\mu} + C_{He}^{e\tau}C_{H\ell}^{(3)\tau\mu}\right)\frac{v^2}{M_Z^2} \quad (79)$$

$$C_{V,LL}^{e\mu\tau\tau} = -\frac{g^2}{\cos^2\theta_W}\left(C_{H\ell}^{(1)e\tau}C_{H\ell}^{(1)\tau\mu} + C_{H\ell}^{(3)e\tau}C_{H\ell}^{(3)\tau\mu} + C_{H\ell}^{(1)e\tau}C_{H\ell}^{(3)\tau\mu} + C_{H\ell}^{(1)\tau\mu}C_{H\ell}^{(3)e\tau}\right)\frac{v^2}{M_Z^2} \quad (80)$$

$$C_{V,RR}^{e\mu\tau\tau} = -\frac{g^2}{\cos^2\theta_W}C_{He}^{e\tau}C_{He}^{\tau\mu}\frac{v^2}{M_Z^2} \quad (81)$$

where the low energy EFT basis is in the notation of [46]. We report for completeness the matching conditions for $e\mu\tau\tau$ vector coefficients, although $\mu \rightarrow e$ observables are not sensitive to them.

4 Phenomenological implications

This section gives limits on pairs of $\tau \leftrightarrow l$ coefficients from their contribution to $\mu \rightarrow e$ processes, and we discuss some examples where the upcoming sensitivity of $\mu \rightarrow e$ observables is complementary to the future direct limits from $\tau \rightarrow l$ processes. Section 4.1 considers $\mu \leftrightarrow e$ amplitudes generated by the fish diagrams of Figure 6e-6f, and compares with the limits arising from $B \rightarrow \tau$ LFV decays (summarised in Appendix C). An example of $\mu \leftrightarrow e$ from matching out the Higgs is given in Section 4.2, where we compare the sensitivity of $\mu \rightarrow e$ processes to $h \rightarrow \tau^\pm l^\mp$ decays. Appendix D gives results for the cases where the $\mu \leftrightarrow e$ sensitivity is marginal or uninteresting.

The limits we quote apply to pairs of $\tau \leftrightarrow l$ coefficients at a New Physics scale $\Lambda_{\text{NP}} = 4$ TeV. We assume that dimension six $\tau \leftrightarrow l$ operators are generated at $\Lambda_{\text{NP}} = 4$ TeV and contribute to $\mu \rightarrow e$ observables in two ways: first, as discussed in section 3.1, via Renormalisation Group mixing into dimension eight $\mu \rightarrow e$ operators in SMEFT between Λ_{NP} and m_W , and second via the matching at m_W of combined dimension six $\tau \leftrightarrow l$ operators onto $\mu \rightarrow e$ operators as calculated in section 3.2. The running is described with the solution of the RGEs given in eq. (11), then the dimension eight $\mu \rightarrow e$ operators are matched onto the low energy EFT as given in [23]. The sensitivity of current $\mu \leftrightarrow e$ experiments to coefficients at m_W is tabulated in [46]; we extrapolate these limits to the future experimental reaches given in table 1, in order to determine the experimental sensitivities of $\mu \rightarrow e$ processes to the product of $\tau \rightarrow l$ operator coefficients. In most cases, we just rescale the sensitivities of [46]. But for the limits from $\mu A \rightarrow e A$ on vector operators with quarks, we recalculate the sensitivities on an Aluminium target, as will be used by upcoming experiments. The current bounds are from Gold targets, which have more neutrons than protons, whereas Aluminium contains equal numbers of protons and neutrons (u and d quarks). So Gold has comparable sensitivity to $(\bar{e}\gamma\mu)(\bar{u}\gamma u + \bar{d}\gamma d)$ and $(\bar{e}\gamma\mu)(\bar{u}\gamma u - \bar{d}\gamma d)$, whereas the sensitivity of Aluminium to $(\bar{e}\gamma\mu)(\bar{u}\gamma u - \bar{d}\gamma d)$ is suppressed by a loop.

Note that we distinguish *sensitivities* from *constraints* or *bounds*. But we use *limits* to mean either. A constraint identifies the region of parameter space where the coefficients must sit, while a sensitivity represents the smallest absolute value that can be experimentally detected. The notion of sensitivity is particularly useful when the number of parameters is larger than the number of observables, so that exclusion bounds on single coefficients cannot be inferred. A coefficient smaller than the sensitivity escapes experimental detection but larger values can also escape detection if accidental cancellations occur. In practise, in this manuscript we obtain sensitivities, because we consider one non-zero pair of $\tau \leftrightarrow l$ operators at a time and compute the contribution to $\mu \rightarrow e$ observables.

Our results are interesting, because they show that upcoming $\mu \leftrightarrow e$ experiments could be sensitive to $\tau \leftrightarrow l$ coefficients beyond the reach of $\tau \leftrightarrow l$ searches. We obtain experimental sensitivities $B_{\mu \leftrightarrow e}$ to the product of coefficients

$$\left|C^{[6]\tau\mu}C^{[6]e\tau}\right| \lesssim B_{\mu \leftrightarrow e}. \quad (82)$$

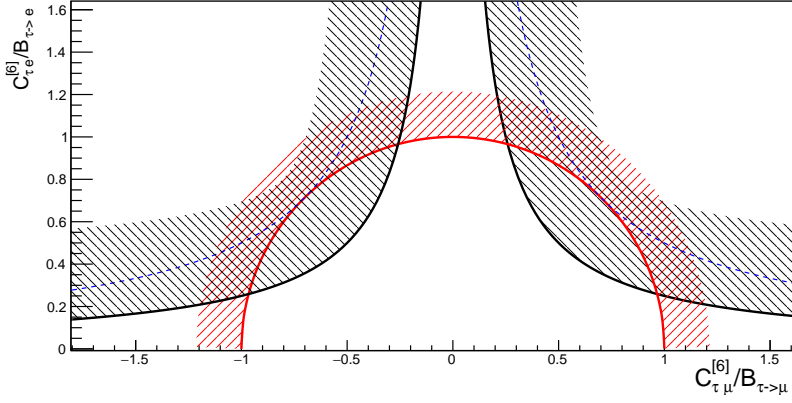


Figure 8: The plot shows the parameter space probed by direct $\tau \leftrightarrow l$ searches and by $\mu \rightarrow e$ observables, in the $C_{\tau\mu} - C_{\tau e}$ plane. The direct searches can probe the region outside the ellipse of eq. (83) (which correspond to the red circle when the Wilson coefficients are normalized by the sensitivities $B_{\tau \leftrightarrow l}$ of the $\tau \leftrightarrow l$ processes), while $\mu \rightarrow e$ is sensitive to the area above the hyperbolae, as defined in eq. (82). The blue dashed hyperbolae correspond to the boundary condition $B_{\mu \leftrightarrow e}/(B_{\tau \leftrightarrow e} B_{\tau \leftrightarrow \mu}) = 1/2$, while the black ones satisfies $B_{\mu \leftrightarrow e}/(B_{\tau \leftrightarrow e} B_{\tau \leftrightarrow \mu}) < 1/2$. In this second case $\mu \rightarrow e$ searches are able to probe parameter space missed by $\tau \leftrightarrow l$ observables.

The same coefficients $C^{[6]\tau\mu}$, $C^{[6]e\tau}$ might contribute to constrained $\tau \leftrightarrow l$ processes and be respectively subjected to the sensitivity “limits” $B_{\tau \rightarrow \mu}$, $B_{\tau \rightarrow e}$ imposed by direct τ LFV searches. In the $C^{[6]\tau\mu} - C^{[6]e\tau}$ plane, this identifies an ellipse

$$\frac{|C^{[6]\tau\mu}|^2}{B_{\tau \leftrightarrow \mu}^2} + \frac{|C^{[6]e\tau}|^2}{B_{\tau \leftrightarrow e}^2} \lesssim 1 \quad (83)$$

that encloses the coefficient space to which $\tau \leftrightarrow l$ observables are not sensitive. On the other hand, $\mu \rightarrow e$ searches can detect coefficients in the region bounded by the hyperbola in eq. (82). If the following inequality is satisfied

$$B_{\mu \leftrightarrow e} < \frac{B_{\tau \leftrightarrow e} B_{\tau \leftrightarrow \mu}}{2} \quad (84)$$

the hyperbola enters the ellipse and $\mu \rightarrow e$ processes are able to probe a region of parameter space that eludes the direct $\tau \leftrightarrow l$ searches. This is illustrated in Figure 8. In the subsequent sections we discuss examples where eq. (84) is satisfied considering the upcoming experimental sensitivities on $\mu \rightarrow e$ and $\tau \rightarrow l$ processes.

4.1 Fish diagrams with internal top quarks

In this section, we discuss some examples where the sensitivity of $\mu \rightarrow e$ conversion to some $\tau \leftrightarrow l$ coefficients is complementary to B decays. The “fish” diagrams that mix four fermion $\tau \leftrightarrow l$ interactions into dimension eight $\mu \rightarrow e$ operators are illustrated in Figure 6e-6f of section 3.1. In these diagrams, one or two Higgs are attached to a heavy top internal line, so the $\tau \leftrightarrow l$ operators that our calculation can probe contain one quark doublet or up-type singlet in the third generation. In the former case, the operator can contribute to the LFV decays of the B mesons with a τ (ν_τ) in the final state. The following subsections are organized by the different $\mu \rightarrow e$ interactions that the $\tau \leftrightarrow l$ operators mix into.

4.1.1 $\mu \rightarrow e$ scalars

Consider, for example, the operators $\mathcal{O}_{eq}^{\tau\mu 13} = (\bar{\tau}\gamma\mu)(\bar{q}_1\gamma q_3)$ and $\mathcal{O}_{lequ}^{(3)e\tau 31} = (\bar{\ell}_e\sigma\tau)(\bar{q}_3\sigma u)$, which mix into the $\mu \rightarrow e$ scalar and tensor dimension eight operators $\mathcal{O}_{lequH^2}^{(1),(2),(3),(4)}$ of eq.s (34)-(35) (with up quarks) via the diagram of Figure 9. These match at m_W onto scalar and tensor operators in the low energy EFT, with the following coefficients⁵

$$C_{S,RR}^{uu}(m_W) = \frac{3}{2\pi^2} \frac{m_t^2}{v^2} C_{eq}^{\tau\mu 13}(\Lambda_{\text{NP}}) \times C_{lequ}^{(3)e\tau 3u}(\Lambda_{\text{NP}}) \log\left(\frac{m_W}{\Lambda_{\text{NP}}}\right) \quad (85)$$

$$C_{T,RR}^{uu}(m_W) = \frac{3}{8\pi^2} \frac{m_t^2}{v^2} C_{eq}^{\tau\mu 13}(\Lambda_{\text{NP}}) \times C_{lequ}^{(3)e\tau 3u}(\Lambda_{\text{NP}}) \log\left(\frac{m_W}{\Lambda_{\text{NP}}}\right) \quad (86)$$

⁵ This simple solution does not include the QCD running of tensors and scalars from $\Lambda_{\text{NP}} \rightarrow m_W$. Since QCD does not renormalize vector coefficients, this QCD running is analogous to the rescaling of QED tensor \leftrightarrow scalar mixing below m_W [46], and can be estimated to be a $\lesssim 10\%$ effect. It is therefore neglected.

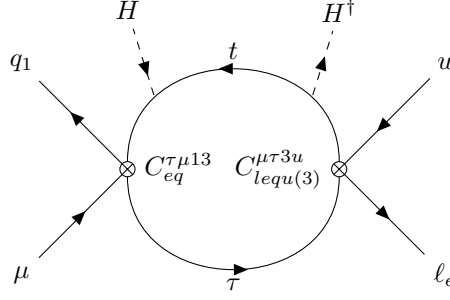


Figure 9: The operators $C_{eq}^{e\tau 31}, C_{lequ}^{(3)e\tau 31}$ are inserted in the left diagram and mix into the dimension eight $\mu \rightarrow e$ scalar/tensor operators $\mathcal{O}_{lequH^2}^{(1),(2),(3),(4)}$ of eq.s (34)-(35).

where $m_t \sim v$ is the top quark mass.

Scalar operators with up quarks contribute at tree-level to $\mu \rightarrow e$ conversion in nuclei (see eg [38]), where a muon is stopped in a target, captured by a nucleus, and converts into an electron in the presence of LFV interaction with nucleons. Scalar interactions of first generation quarks match onto nucleon operators with large matching coefficients, and the rate for spin-independent conversion is enhanced by the atomic number of the target, giving a good current sensitivity to scalar coefficients $C_S^{uu} \lesssim 10^{-8}$ [46]. Including the impressive improvement in sensitivity promised by upcoming experiments, $Br(\mu Au \rightarrow e Au) \lesssim 10^{-12} \rightarrow Br(\mu Al \rightarrow e Al) \sim 10^{-16}$, $\mu \rightarrow e$ conversion will be able to probe scalar coefficients as small as $C_S^{uu} \sim 10^{-10}$.

Tensors with light-quarks contribute to the spin-independent rate via their QED mixing into scalars, which introduces a $\sim 1/10$ suppression. For this reason, the tensor of eq. (86) contribute to the $\mu \rightarrow e$ conversion rate as $C_T \sim C_S/40$ and is therefore neglected. So the upcoming $\mu \rightarrow e$ conversion experiments can set the following limit (sensitivity) on the product of the coefficients at $\Lambda_{NP} = 4$ TeV

$$C_{eq}^{\tau\mu 13} \times C_{lequ}^{(3)e\tau 31} \lesssim 1.5 \times 10^{-10} \quad (87)$$

The two $\tau \leftrightarrow l$ operators could also induce the leptonic decays of B mesons $B_d^0 \rightarrow \mu^\pm \tau^\mp$ and $B^+ \rightarrow \bar{\tau} \nu$. The current 95%C.L. experimental constraints on these processes lead to the following limits on the coefficients

$$\begin{aligned} Br(B_d^0 \rightarrow \mu^\pm \tau^\mp) &< 1.4 \times 10^{-5} & \rightarrow & C_{eq}^{\tau\mu 13} \lesssim 1.4 \times 10^{-3} \\ Br(B^+ \rightarrow \bar{\tau} \nu) &= 1.6 \times 10^{-4} & \rightarrow & C_{lequ}^{(3)e\tau 31} \lesssim 2.2 \times 10^{-3}. \end{aligned} \quad (88)$$

These limits were obtained with the public code Flavio [47] and analytically, and are discussed in more detail in Appendix C, which reviews the sensitivity of B decays to interesting operator coefficients.

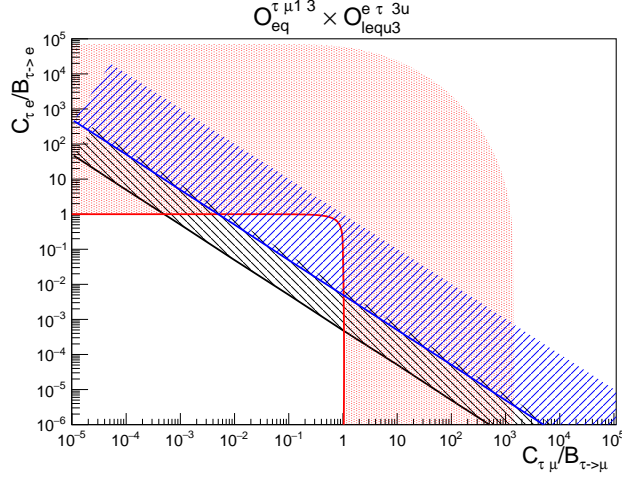
In order to compare future B decay sensitivities to the future reach of $\mu \rightarrow e$ conversion, we suppose that Belle II could improve the sensitivities to B decays by an order of magnitude, so the limits of eq. (88) on the Wilson coefficients will get $\sim \sqrt{10}$ better. Comparing the product of the upcoming B sensitivities with the limit in eq. (87) that arise from future $\mu \rightarrow e$ conversion gives (the (f) superscript stands for “future”)

$$B_{\mu \leftrightarrow e}^{(f)} = (B_{\tau \leftrightarrow e}^{(f)} B_{\tau \leftrightarrow \mu}^{(f)}) \times (5 \times 10^{-4}) \quad (89)$$

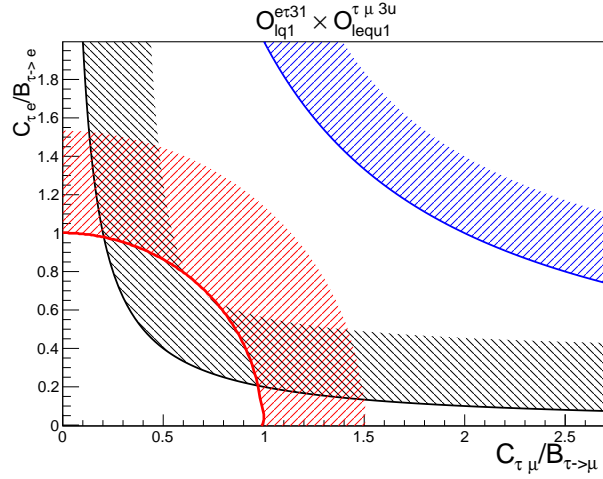
which satisfies the condition of eq. (84). We fall in the scenario depicted in Figure 10a, where $\mu \rightarrow e$ probes a region inside the ellipse, beyond the reach of $B \rightarrow \tau$ direct searches. Notice that the hyperbola of the current $\mu \rightarrow e$ conversion results already enters the ellipse of the $B \rightarrow \tau$ LFV decays (with the current sensitivities $B_{\mu \leftrightarrow e}^{(c)} / (B_{\tau \leftrightarrow e}^{(c)} B_{\tau \leftrightarrow \mu}^{(c)}) \sim 5 \times 10^{-3}$). This is because tensors contribute to the B decays rate via the one-loop QED mixing to scalars, while the (dimension six)² \rightarrow (dimension eight) mixing benefits from a large anomalous dimension.

The pair of $\tau \leftrightarrow l$ dimension six operators $C_{eq}^{(1)e\tau 13} C_{lequ}^{(1)\tau\mu 3u}$ similarly mixes into the dimension eight $\mu \rightarrow e$ scalars with a singlet u . In this case, B decays are currently more sensitive than $\mu \rightarrow e$ processes to the product of the coefficients ($B_{\mu \leftrightarrow e}^{(c)} / (B_{\tau \leftrightarrow e}^{(c)} B_{\tau \leftrightarrow \mu}^{(c)}) \sim 2$). However, in the next generation of experiments, the sensitivity ratio will be reduced by one order of magnitude to $B_{\mu \leftrightarrow e}^{(f)} / (B_{\tau \leftrightarrow e}^{(f)} B_{\tau \leftrightarrow \mu}^{(f)}) \sim 0.2$, allowing the $\mu \rightarrow e$ conversion hyperbola to enter the ellipse of the direct $\tau \leftrightarrow l$ searches (see Figure 10b).

In Tables 8 and 9, we compare the sensitivities of $\tau \leftrightarrow l$ and $\mu \rightarrow e$ processes to the product of several operators that mix into scalars with first generation quarks, via diagrams similar to Figure 9. Note that the pairs in the table feature an electron doublet and a singlet muon, but opposite chiralities are also possible. For instance, $C_{eq}^{\tau\mu 13} C_{lequ}^{(1)e\tau 3u}$ mix into $C_{lequH^2}^{(1),(2)e\mu 1u}$ while $C_{eq}^{e\tau 31} C_{lequ}^{*(1)\mu\tau 3u}$ contributes to the RGEs of $C_{lequH^2}^{*(1),(2)\mu e 1u}$. Although the anomalous dimensions are the same (and so are the $\mu \rightarrow e$ sensitivities), the dimension six operator



(a) Parameter space probed by $\mu \rightarrow e$ conversion (straight lines) and LFV B decays (box), in the $C_{eq}^{\tau\mu 13} - C_{\ell equ}^{(3)e\tau 3u}$ plane. The blue line correspond to the current experimental reach, while in the black one we assume $Br(\mu Al \rightarrow e Al) \sim 10^{-16}$. In both cases, the $\mu \rightarrow e$ hyperbole enter the ellipse beyond the reach of B decays.



(b) Similar to Figure 10a, in the $C_{\ell q}^{(1)e\tau 13} - C_{\ell equ}^{(1)\tau\mu 3u}$ plane. For this pair of operators, $\mu \rightarrow e$ will have a better sensitivity to the coefficient product than B decays with the upcoming experimental improvement.

Figure 10

that was $\tau \leftrightarrow e$ is now $\tau \leftrightarrow \mu$ and vice-versa, which might lead to slightly different direct limits on the $\tau \leftrightarrow l$ interactions. In the above-example, the branching ratios sensitivities of the B_d^0 decay into $\tau e, \tau \mu$ differ by a factor ~ 3 , and as a result the limits on the vector coefficients $C_{eq}^{e\tau 13}, C_{eq}^{\tau\mu 31}$ is $\sim \sqrt{3}$ different. We do not present the tables for the pairs with exchanged $\mu \leftrightarrow e$, as the marginally different numbers do not modify our conclusions.

4.1.2 $\mu \rightarrow e$ tensors with heavy quarks

The fish diagrams that generated scalar and tensor $\mu \rightarrow e$ operators on u quarks, arise also with external c quarks. Although the sensitivity of $\mu \rightarrow e$ conversion to charm scalars is insufficient for our purposes, $\mu \rightarrow e\gamma$ has interesting sensitivity to the charm tensors, because their mixing to the dipole is enhanced $\propto m_c/m_\mu$. The pairs of $\tau \leftrightarrow l$ operators that mix to $\mu \leftrightarrow e$ tensors with external charms, and the sensitivities of B decays and $Br(\mu \rightarrow e\gamma) < 10^{-14}$ are summarized in Table 10.

Leptonic and semi-leptonic B decays have recently attracted attention due to several anomalies with respect to SM expectations, see e.g. Ref. [48]. Our LFV operators could potentially address the anomalies in “charged current” b transitions (such as $B^+ \rightarrow \tau^+ \nu$), however the observed rates are often below the SM expectations, so cannot be explained by lepton-flavour-changing interactions that necessarily increase the rates (because they cannot interfere destructively with the SM). An exception is the SM expectation for $R_{D^{*\tau/l}}^{\text{SM}} \equiv Br(B \rightarrow D^* \tau \bar{\nu})/Br(B \rightarrow D^* l \bar{\nu}) \sim 0.24$ [47] which is smaller than the observed value $R_{D^{*\tau/l}}^{\text{exp}} \sim 0.3$ [49]. We can fit the difference by enhancing the branching fraction in the numerator with the tensor operator $C_{\ell equ}^{(3)l\tau 3c}$. The latter can be paired with the vector $C_{eq}^{\tau\mu 23}$ to mix into a dimension eight tensor with external

coefficients	$B_{\tau \leftrightarrow e}^{(c)} B_{\tau \leftrightarrow \mu}^{(c)}$	$B_{\mu \rightarrow e}^{(f)}$
$C_{\ell u}^{\tau e \tau u} C_{\ell e q u}^{(1) \tau \mu 1 t}$	— × —	2×10^{-9}
$C_{\ell u}^{\tau e \tau u} C_{\ell e q u}^{(3) \tau \mu 1 t}$	— × —	1.5×10^{-10}
$C_{e q}^{\tau \mu 13} C_{\ell e q u}^{(1) e \tau 3 u}$	$1.5 \times 10^{-3}(c) \times 4.3 \times 10^{-4}(c)$	2×10^{-9}
$C_{e q}^{\tau \mu 13} C_{\ell e q u}^{(3) e \tau 3 u}$	$1.5 \times 10^{-3}(c) \times 2.4 \times 10^{-3}(c)$	1.5×10^{-10}
$C_{e u}^{\tau \mu t u} C_{\ell e q u}^{(1) e \tau 1 t}$	— × —	-2×10^{-9}
$C_{e u}^{\tau \mu t u} C_{\ell e q u}^{(3) e \tau 1 t}$	— × —	1.5×10^{-10}
$C_{\ell q}^{(1) e \tau 13} C_{\ell e q u}^{(1) \tau \mu 3 u}$	$2.3 \times 10^{-3}(c) \times 4.3 \times 10^{-5}(c)$	2×10^{-9}
$C_{\ell q}^{(3) e \tau 13} C_{\ell e q u}^{(1) \tau \mu 3 u}$	$2.3 \times 10^{-3}(c) \times 4.3 \times 10^{-5}(c)$	2×10^{-9}
$C_{\ell q}^{(1) e \tau 13} C_{\ell e q u}^{(3) \tau \mu 3 u}$	$2.3 \times 10^{-3}(c) \times 1.8 \times 10^{-4}(c)$	1.5×10^{-10}
$C_{\ell q}^{(3) e \tau 13} C_{\ell e q u}^{(3) \tau \mu 3 u}$	$2.3 \times 10^{-3}(c) \times 1.8 \times 10^{-4}(c)$	1.5×10^{-10}

Table 8: The product of current (c) direct limits $B_{\tau \leftrightarrow e}^{(c)} B_{\tau \leftrightarrow \mu}^{(c)}$ on pairs of coefficients that mix to a $\mu \rightarrow e$ dimension eight scalar operator with a singlet u quark (see eq. (34)), upon which applies the limit $B_{\mu \rightarrow e}^{(f)}$ arising from future $\mu \rightarrow e$ conversion ($Br(\mu Al \rightarrow e Al) \sim 10^{-16}$). The “limits” are on coefficients at $\Lambda_{\text{NP}} \sim 4$ TeV. Details on the limits that apply to operators with permuted indices are given in the text below eq. (89). To compare $B_{\mu \rightarrow e}^{(f)}$ with the future sensitivity of direct $\tau \leftrightarrow l$ searches, the product $B_{\tau \leftrightarrow e}^{(c)} B_{\tau \leftrightarrow \mu}^{(c)}$ should be divided by 10: $B_{\tau \leftrightarrow e}^{(f)} B_{\tau \leftrightarrow \mu}^{(f)} \sim B_{\tau \leftrightarrow e}^{(c)} B_{\tau \leftrightarrow \mu}^{(c)} / 10$.

coefficients	$B_{\tau \leftrightarrow e}^{(c)} B_{\tau \leftrightarrow \mu}^{(c)}$	$B_{\mu \rightarrow e}^{(f)}$
$C_{\ell q}^{(3) e \tau 31} C_{\ell e d q}^{\tau \mu d 3}$	$2.3 \times 10^{-3}(c) \times 2.2 \times 10^{-4}(c)$	1×10^{-9}
$C_{\ell q}^{(3) \tau \mu 13} (C_{\ell e d q}^{\tau e d 3})^*$	$1.5 \times 10^{-3}(c) \times 3.4 \times 10^{-4}(c)$	1×10^{-9}

Table 9: Similar to table 8, for dimension eight scalar $\mu \rightarrow e$ operators involving a singlet d quark (see eq. (33)). The limit $B_{\mu \rightarrow e}^{(f)}$ arises from $\mu \rightarrow e$ conversion ($Br(\mu Al \rightarrow e Al) \sim 10^{-16}$).

charms, to which $Br(\mu \rightarrow e \gamma) \sim 10^{-14}$ has the sensitivity $B_{\mu \rightarrow e}$ reported in Table 10. In the $C_{\ell e q u}^{(3) e \tau 3 c} - C_{e q}^{\tau \mu 23}$ plane, the ellipse is now shifted to the right and centered on the best-fit value of $C_{\ell e q u}^{(3) e \tau 3 c}$ (see Figure 11). In the simplified scenario where the discrepancy $|R_{D^{* \tau / e}}^{\text{SM}} - R_{D^{* \tau / e}}^{\text{exp}}|$ is fully explained by the presence of the $\tau \leftrightarrow e$ tensor, non-observation $\mu \rightarrow e \gamma$ signal in future experiments would make it unlikely for the coefficients to occupy the portion of the red ellipse overlapping the blue region.

Table 11 summarises the case of $\mu \leftrightarrow e$ operator with external top quarks. The mixing of tensors with a top bilinear into the dipole is enhanced by the ratio m_t/m_μ , so the upcoming $\mu \rightarrow e \gamma$ experiments can probe dimension 6 coefficients $C_T^{[6] e \mu t t} \gtrsim 5 \times 10^{-12}$. We suppose that the SMEFT mixing of dimension eight tensors into the dimension eight dipoles is comparable to the dimension six mixing [28]. This impressive sensitivity explains why the diagrams of Figure 6f with external top legs are interesting regardless of the y_τ Yukawa suppression.

The SMEFT $\tau \leftrightarrow l$ operators that are inserted in those diagrams contain a flavour diagonal quark pair in the third generation. Vectors with tops contribute to the rate of $\tau \rightarrow 3l$ via one-loop penguin diagrams, while the dimension six tensors contribute to $\tau \rightarrow l \gamma$ via the above-discussed mixing into the $\tau \leftrightarrow l$ dipole. Tensors are not considered in our tables, because $\tau \rightarrow l \gamma$ has already an excellent sensitivity to the operator coefficients. In Table 11 the direct “limits” on the product of $\tau \leftrightarrow l$ dimension six vectors arising from $\tau \rightarrow 3l$ searches are compared with the sensitivity of $Br(\mu \rightarrow e \gamma) < 10^{-14}$.

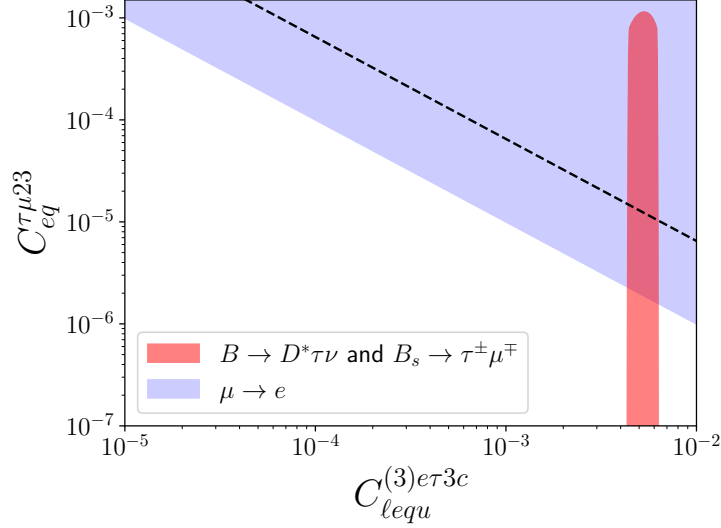


Figure 11: The plot shows the parameter space probed by B LFV decays and by future $\mu \rightarrow e\gamma$, in the $C_{\ell equ}^{(3)e\tau 3c} - C_{eq}^{\tau\mu 23}$ plane. The ellipse is centered to the best-fit value of $C_{\ell equ}^{(3)e\tau 3c}$ that can explain the R_{D^*} anomaly (see text for details). Non-observation of $\mu \rightarrow e\gamma$ can give a limit on $C_{eq}^{\tau\mu 23}$ (assuming only this pair to be non-zero). The dashed line correspond to the current MEG upper bound $Br(\mu \rightarrow e\gamma) < 4 \times 10^{-13}$.

coefficients	$B_{\tau \leftrightarrow e}^{(c)} B_{\tau \leftrightarrow \mu}^{(c)}$	$B_{\mu \rightarrow e}^{(f)}$
$C_{\ell u}^{e\tau tc} C_{\ell equ}^{(1)\tau\mu 2t}$	— × —	1.2×10^{-7}
$C_{\ell u}^{e\tau tc} C_{\ell equ}^{(3)\tau\mu 2t}$	— × —	1×10^{-8}
$C_{eq}^{\tau\mu 23} C_{\ell equ}^{(1)e\tau 3c}$	$2.3 \times 10^{-3}(c) \times 1.0 \times 10^{-2}(c)$	1.2×10^{-7}
$C_{eq}^{\tau\mu 23} C_{\ell equ}^{(3)e\tau 3c}$	$2.3 \times 10^{-3}(c) \times 5.0 \times 10^{-3}(c)$	1×10^{-8}
$C_{eu}^{\tau\mu tc} C_{\ell equ}^{(1)e\tau 2t}$	— × —	1.2×10^{-7}
$C_{eu}^{\tau\mu tc} C_{\ell equ}^{(3)e\tau 2t}$	— × —	1×10^{-8}
$C_{\ell q}^{(1)e\tau 23} C_{\ell equ}^{(1)\tau\mu 3c}$	$2.3 \times 10^{-3}(c) \times 9.0 \times 10^{-3}(c)$	1.2×10^{-7}
$C_{\ell q}^{(3)e\tau 23} C_{\ell equ}^{(1)\tau\mu 3c}$	$2.3 \times 10^{-3}(c) \times 9.0 \times 10^{-3}(c)$	1×10^{-7}
$C_{\ell q}^{(1)e\tau 23} C_{\ell equ}^{(3)\tau\mu 3c}$	$2.3 \times 10^{-3}(c) \times 6.4 \times 10^{-3}(c)$	1.2×10^{-7}
$C_{\ell q}^{(3)e\tau 23} C_{\ell equ}^{(3)\tau\mu 3c}$	$2.3 \times 10^{-3}(c) \times 6.4 \times 10^{-3}(c)$	1×10^{-9}

Table 10: Similar to table 8, for $\mu \rightarrow e$ dimension eight tensor operators (see eq. (35)) with a c quark bilinear. The sensitivity $B_{\mu \rightarrow e}^{(f)}$ arises from $\mu \rightarrow e\gamma$ with a branching ratio $Br(\mu \rightarrow e\gamma) \sim 10^{-14}$. The “limits” are on coefficients at $\Lambda_{\text{NP}} \sim 4$ TeV.

coefficients	$B_{\tau \leftrightarrow e}^{(c)} B_{\tau \leftrightarrow \mu}^{(c)}$	$B_{\mu \rightarrow e}^{(f)}$
$C_{\ell u}^{e\tau tt} C_{eq}^{\tau\mu 33}$	$1.0 \times 10^{-2}(c) \times 2.0 \times 10^{-2}(c)$	1.0×10^{-6}
$C_{\ell q}^{(3)e\tau 33} C_{eu}^{\tau\mu tt}$	$4.5 \times 10^{-3}(c) \times 1.0 \times 10^{-2}(c)$	1.0×10^{-6}
$C_{\ell q}^{(1)e\tau 33} C_{eu}^{\tau\mu tt}$	$4.0 \times 10^{-2}(c) \times 1.0 \times 10^{-2}(c)$	-1.0×10^{-6}

Table 11: Similar to table 8, with the product of (current) direct limits $B_{\tau \leftrightarrow e}^{(c)} B_{\tau \leftrightarrow \mu}^{(c)}$ on pairs of $\tau \leftrightarrow l$ coefficients that mix to a $\mu \rightarrow e$ dimension eight tensor operator (see eq. (35)) with two top quarks, upon which applies the limit $B_{\mu \rightarrow e}$. All the limits apply to the coefficients at $\Lambda_{\text{NP}} \sim 4$ TeV. The limit $B_{\mu \rightarrow e}^{(f)}$ arises from $\mu \rightarrow e\gamma$ ($Br(\mu \rightarrow e\gamma) < 10^{-14}$), due to the large mixing of the top-tensor to the dipole, while the limits $B_{\tau \leftrightarrow l}^{(c)}$ are from the current upper limits on $Br(\tau \rightarrow 3l)$ given in Table 1. Future limits $B_{\tau \leftrightarrow e}^{(f)} B_{\tau \leftrightarrow \mu}^{(f)}$ are $\sim B_{\tau \leftrightarrow e}^{(c)} B_{\tau \leftrightarrow \mu}^{(c)} / 10$.

4.1.3 $\mu \rightarrow e$ vectors

The remaining fish diagrams give mixing of two dimension six $\tau \leftrightarrow l$ SMEFT operators into dimension eight $\mu \rightarrow e$ vectors with first generation quarks. The sensitivities of $\mu \rightarrow e$ conversion and B decays on the product of the operator coefficients are summarized in Table 12 for lepton singlets and in Table 13 for lepton doublets. (The $\mu \rightarrow e$ conversion estimates assume an Aluminium target — see the beginning of Section 4.)

coefficients	$B_{\tau \leftrightarrow e}^{(c)} B_{\tau \leftrightarrow \mu}^{(c)}$	$B_{\mu \rightarrow e}^{(f)}$
$C_{eq}^{e\tau 31} C_{eq}^{\tau\mu 13}$	$2.3 \times 10^{-3}(c) \times 1.5 \times 10^{-3}(c)$	2.5×10^{-9}
$C_{eq}^{e\tau 13} C_{eq}^{\tau\mu 31}$	$2.3 \times 10^{-3}(c) \times 1.5 \times 10^{-3}(c)$	1×10^{-8}
$C_{eu}^{e\tau tu} C_{eu}^{\tau\mu ut}$	— \times —	2.5×10^{-9}
$C_{eu}^{e\tau ut} C_{eu}^{\tau\mu tu}$	— \times —	2.5×10^{-9}
$(C_{ledq}^{\tau ed 3})^* C_{ledq}^{\tau\mu d 3}$	$3.4 \times 10^{-4}(c) \times 2.2 \times 10^{-4}(c)$	4×10^{-8}
$(C_{lequ}^{(1)\tau e 1t})^* C_{lequ}^{(1)\tau\mu 1t}$	— \times —	2×10^{-8}
$(C_{lequ}^{(1)\tau e 3u})^* C_{lequ}^{(1)\tau\mu 3u}$	$5.8 \times 10^{-5}(c) \times 4.3 \times 10^{-5}(c)$	4×10^{-8}
$(C_{lequ}^{(3)\tau e 1t})^* C_{lequ}^{(3)\tau\mu 1t}$	— \times —	1×10^{-10}
$(C_{lequ}^{(3)\tau e 3u})^* C_{lequ}^{(3)\tau\mu 3u}$	$2.4 \times 10^{-4}(c) \times 2.4 \times 10^{-4}(c)$	2.5×10^{-10}
$(C_{lequ}^{(1)\tau e 1t})^* C_{lequ}^{(3)\tau\mu 1t}$	— \times —	2×10^{-9}
$(C_{lequ}^{(3)\tau e 1t})^* C_{lequ}^{(1)\tau\mu 1t}$	— \times —	2×10^{-9}
$(C_{lequ}^{(1)\tau e 3u})^* C_{lequ}^{(3)\tau\mu 3u}$	$5.8 \times 10^{-5}(c) \times 2.4 \times 10^{-4}(c)$	4×10^{-9}
$(C_{lequ}^{(3)\tau e 3u})^* C_{lequ}^{(1)\tau\mu 3u}$	$2.4 \times 10^{-4}(c) \times 4.3 \times 10^{-5}(c)$	4×10^{-9}

Table 12: Similar to tables 8, for dimension eight $\mu \rightarrow e$ vector operators with SU(2) singlet leptons (see eq.s (30)-(31)). .

coefficients	$B_{\tau \leftrightarrow e}^{(c)} B_{\tau \leftrightarrow \mu}^{(c)}$	$B_{\mu \rightarrow e}^{(f)}$
$C_{\ell q}^{(1)e\tau 31} C_{\ell q}^{(1)\tau\mu 13}$	$2.3 \times 10^{-3}(c) \times 1.5 \times 10^{-3}(c)$	1×10^{-8}
$C_{\ell q}^{(1)e\tau 13} C_{\ell q}^{(1)\tau\mu 31}$	$2.3 \times 10^{-3}(c) \times 1.5 \times 10^{-3}(c)$	2.5×10^{-9}
$C_{\ell q}^{(3)e\tau 31} C_{\ell q}^{(3)\tau\mu 13}$	$2.3 \times 10^{-3}(c) \times 1.5 \times 10^{-3}(c)$	2×10^{-9}
$C_{\ell q}^{(3)e\tau 13} C_{\ell q}^{(3)\tau\mu 31}$	$2.3 \times 10^{-3}(c) \times 1.5 \times 10^{-3}(c)$	2.5×10^{-9}
$C_{\ell q}^{(3)e\tau 13} C_{\ell q}^{(1)\tau\mu 31}$	$2.3 \times 10^{-3}(c) \times 1.5 \times 10^{-3}(c)$	2.5×10^{-9}
$C_{\ell q}^{(1)e\tau 13} C_{\ell q}^{(3)\tau\mu 31}$	$2.3 \times 10^{-3}(c) \times 1.5 \times 10^{-3}(c)$	2.5×10^{-9}
$C_{\ell q}^{(3)e\tau 31} C_{\ell q}^{(1)\tau\mu 13}$	$2.3 \times 10^{-3}(c) \times 1.5 \times 10^{-3}(c)$	1×10^{-8}
$C_{\ell q}^{(1)e\tau 31} C_{\ell q}^{(3)\tau\mu 13}$	$2.3 \times 10^{-3}(c) \times 1.5 \times 10^{-3}(c)$	1×10^{-8}
$C_{\ell u}^{e\tau ut} C_{\ell u}^{\tau\mu tu}$	— \times —	1×10^{-8}
$C_{\ell u}^{e\tau tu} C_{\ell u}^{\tau\mu ut}$	— \times —	2.5×10^{-9}
$(C_{\ell equ}^{(1)e\tau 3u})^* C_{\ell equ}^{(1)\mu\tau 3u}$	$4.5 \times 10^{-4}(c) \times 4.5 \times 10^{-4}(c)$	4×10^{-8}
$(C_{\ell equ}^{(1)e\tau 1t})^* C_{\ell equ}^{(1)\mu\tau 1t}$	— \times —	4×10^{-8}
$(C_{\ell equ}^{(3)e\tau 3u})^* C_{\ell equ}^{(3)\mu\tau 3u}$	$1.8 \times 10^{-3}(c) \times 1.8 \times 10^{-3}(c)$	1.25×10^{-10}
$(C_{\ell equ}^{(3)e\tau 1t})^* C_{\ell equ}^{(3)\mu\tau 1t}$	— \times —	1.25×10^{-10}
$(C_{\ell equ}^{(1)e\tau 1t})^* C_{\ell equ}^{(3)\mu\tau 1t}$	— \times —	3×10^{-9}
$(C_{\ell equ}^{(1)e\tau 3u})^* C_{\ell equ}^{(3)\mu\tau 3u}$	$4.5 \times 10^{-5}(c) \times 1.8 \times 10^{-3}(c)$	1.6×10^{-9}
$(C_{\ell equ}^{(3)e\tau 1t})^* C_{\ell equ}^{(1)\mu\tau 1t}$	— \times —	3×10^{-9}
$(C_{\ell equ}^{(3)e\tau 3u})^* C_{\ell equ}^{(1)\mu\tau 3u}$	$1.8 \times 10^{-3}(c) \times 4.5 \times 10^{-5}(c)$	1.6×10^{-9}

Table 13: Similar to tables 8, to generate $\mu \rightarrow e$ vector operators with a doublet lepton bilinear (see eq.s (26)-(29)).

4.2 Higgs LFV couplings

In this section we discuss the sensitivities of $\mu \rightarrow e$ observables to dimension six Yukawa operators \mathcal{O}_{eH} (eq. (17)), and compare them with the upcoming direct limits imposed by $h \rightarrow \tau l$ decays. Pairs of Yukawa $\tau \leftrightarrow l$ operators contribute to various $\mu \rightarrow e$ interactions at dimension eight. They mix into penguins via the divergent diagrams of Figure 6c, which match onto the vector operators involved at tree-level in the $\mu \rightarrow e$ conversion and $\mu \rightarrow \bar{e}ee$ rates. In addition, dimension six Yukawas are inserted in the diagrams of Figures 7b-??, that give matching contributions to the $\mu e \tau \tau$ tensor and dipole respectively. The matching conditions are written in eq.s (??) and (74)-(75). $\mu \rightarrow e\gamma$ is marginally more sensitive to the $\mu e \tau \tau$ tensor than on the dipole; this is due to the large tensor-to-dipole mixing and the built-in y_μ Yukawa suppression in the dipole definition, which lead to the already discussed enhancement m_τ/m_μ . As a result, $\mu \rightarrow e\gamma$ is the most sensitive process, and an upcoming experimental reach of $Br(\mu \rightarrow e\gamma) \lesssim 10^{-14}$ gives :

$$|C_{eH}^{e\tau} C_{eH}^{\tau\mu}|, |C_{eH}^{\tau e} C_{eH}^{\mu\tau}| \lesssim 6 \times 10^{-9}. \quad (90)$$

In the charged lepton mass-eigenstate basis, the dimension six Yukawas induce flavour-changing interactions of 125 GeV-Higgs (see eq. 71), so $h \rightarrow \tau l$ decays probe the off-diagonal coefficients $C_{eH}^{\tau l, l\tau}$. The most stringent upper limits on the rates are currently set by CMS [50], and ILC is expected to improve them by one order of magnitude [16]. The projected sensitivities to the branching ratios lead to the bounds

$$\begin{aligned} Br(h \rightarrow \tau e) < 2.3 \times 10^{-4} & \quad \rightarrow \quad \sqrt{|C_{eH}^{e\tau}|^2 + |C_{eH}^{\tau e}|^2} < 3.2 \times 10^{-4} \\ Br(h \rightarrow \tau \mu) < 2.4 \times 10^{-4} & \quad \rightarrow \quad \sqrt{|C_{eH}^{\tau\mu}|^2 + |C_{eH}^{\mu\tau}|^2} < 3 \times 10^{-4}. \end{aligned} \quad (91)$$

The product of the direct limits is larger than $2 \times$ the sensitivity of eq. (89), so that $\mu \rightarrow e$ probe a region of parameter space that is beyond the reach of future LFV Higgs decays (see Figure 8).

5 Summary

The $\mu \rightarrow e$ experiments under construction are expected to improve the current branching ratio sensitivities by several orders of magnitude. In some cases the improvement is such that the upcoming experiments will be able to probe contributions to $\mu \rightarrow e$ observables that are the result of combined $\mu \rightarrow \tau$ and $\tau \rightarrow e$ interactions in loop diagrams, beyond the reach of direct $\tau \leftrightarrow l$ searches (where $l \in \{e, \mu\}$). However, the relationship between $\tau \leftrightarrow l$ and $\mu \leftrightarrow e$ observables is generically model-dependent, as we discussed in Section 2.1. The goal of this paper is to retain the model-independent contributions to $\mu \rightarrow e$ processes from $\tau \leftrightarrow l$ lepton flavour change, although these may be subdominant. To do so, we assume that the New Physics responsible for $\tau \leftrightarrow l$ LFV is heavy ($\Lambda_{\text{NP}} \gtrsim 4 \text{ TeV}$) and we parameterise it with $\tau \leftrightarrow l$ dimension six operators in the “on-shell” operator basis of SMEFT. We briefly introduce our EFT formalism in section 2.2.

We insert $\mu \rightarrow \tau$ and $\tau \rightarrow e$ dimension six interactions $\mathcal{O}(1/\Lambda_{\text{NP}}^2)$ in diagrams that generates $\mu \rightarrow e$ amplitudes at dimension eight $\mathcal{O}(1/\Lambda_{\text{NP}}^4)$. We only compute the contributions that are phenomenologically relevant, i.e within the reach of future experiments. Firstly, we focus on a subspace of dimension eight operators to which $\mu \rightarrow e$ observables are sensitive, as given in [23] and presented in Section 2.3. Secondly, in Section 2.5 we draw and estimate diagrams with two $\tau \leftrightarrow l$ dimension six interactions generating the above-mentioned dimension eight operators, and we disregard the contributions smaller than the upcoming experimental sensitivity.

Log-enhanced corrections to $\mu \rightarrow e$ dimension eight coefficients are the result of the $(\text{dimension } 6)^2 \rightarrow (\text{dimension } 8)$ mixing which appear in the Renormalization Group evolution, that we review in Section 2.2. Calculating this mixing present some technical challenges. The “on-shell” operator bases we use at dimension six and eight are reduced using the Equation of Motion (EOM), i.e do not contain operators that are related by applying the classical EOM on some field. In order to include the dimension 8 contributions that arise from using the EOM up to dimension 6 in reducing to the on-shell basis at dimension 6, we include some not-1PI diagrams in our calculations. This is more carefully discussed in Section 2.4.

In Section 3 we describe the calculation of the interesting contributions to $\mu \rightarrow e$ processes from $\tau \leftrightarrow l$ interactions, depicted in the diagrams of Figure 6 and Figure 7. Pairs of $\tau \leftrightarrow l$ operators are assumed to be generated at a New Physics scale $\Lambda_{\text{NP}} = 4 \text{ TeV}$ and mix into dimension eight $\mu \rightarrow e$ interactions when evolved down to the experimental scale of $\mu \rightarrow e$ observables. Between Λ_{NP} and m_W , the running is performed in SMEFT as described in section 3.1 and employing the RGEs solution of eq. (11). The complete list of the $(\text{dimension } 6)^2 \rightarrow (\text{dimension } 8)$ anomalous dimensions that we obtained is given in Appendix B.

The dimension eight SMEFT operators that are generated in running are matched onto low energy interactions at m_W as described in [23]. We also include the contribution from pairs of $\tau \leftrightarrow l$ operators which generate $\mu \leftrightarrow e$ operators at tree level in matching, as discussed in section 3.2. Between m_W and the experimental scale Λ_{exp} , the running of low energy Wilson Coefficients is taken from [46], while we find that $\mu \rightarrow \tau \times \tau \rightarrow e$ RGEs mixing is negligible in the EFT below m_W , as discussed at the end of section 2.2.

We thus determined the sensitivity of $\mu \rightarrow e$ processes to products of $\tau \leftrightarrow l$ operator coefficients. Sensitivities represent the largest absolute value that is experimentally detectable and are obtained by considering one non-zero pair of $\tau \leftrightarrow l$ operators at a time. They give a hyperbola in the $C^{[6]\tau\mu}$ - $C^{[6]e\tau}$ plane of the dimension six coefficients (see Figure 8), outside which $\mu \rightarrow e$ observables can probe. In the same plane, direct $\tau \leftrightarrow l$ searches are sensitive to the region outside an ellipse. In Section 4 we discuss two examples where the hyperbola passes inside the ellipse: Section 4.1 shows that the contributions of fish diagrams (see Figure 6e-6f) to $\mu \rightarrow e$ observables allow to probe products of $\tau \leftrightarrow l$ coefficients involving third generation quarks. These same interactions contribute to the rate of LFV $B \rightarrow \tau(\nu_\tau)$ meson decays, which can directly probe the size of the Wilson Coefficients (The “limits” arising from the upper bounds on $B \rightarrow \tau(\nu_\tau) + \dots$ are summarized in Appendix C). In most cases, we find that upcoming $\mu \rightarrow e$ experiments are sensitive to coefficients beyond the reach of future $B \rightarrow \tau(\nu_\tau) + \dots$ searches. In Section 4.2, we study the sensitivity of upcoming $\mu \rightarrow e$ searches to products of LFV Higgs couplings, which overcomes the projected reach of the ILC to $h \rightarrow \tau^\pm l^\mp$.

In this paper, we computed in SMEFT the contributions to $\mu \rightarrow e$ observables arising from $(\mu \rightarrow \tau) \times (\tau \rightarrow e)$ interactions. This required calculating a subset of the RGEs for dimension eight operators, so far missing in the literature. As a result, we obtained limits on products of $\tau \leftrightarrow l$ SMEFT coefficients assuming non-observation of $\mu \rightarrow e$ in future experiments. This can give model-independent relations among $\mu \leftrightarrow e$, $\tau \leftrightarrow e$ and $\tau \leftrightarrow \mu$ LFV: in the event of a detected $\tau \leftrightarrow \mu$ signal, the non-observation of $\mu \leftrightarrow e$ would suggest that some $\tau \leftrightarrow e$ interactions are unlikely (if they occur, additional $\mu \leftrightarrow e$ interactions are required to obtain a cancellation in the $\mu \leftrightarrow e$ amplitude). This could provide theoretical guidance on where to search, or not, for $\tau \leftrightarrow e$.

We find that $\mu \rightarrow e$ processes have a good sensitivity to products of $\tau \leftrightarrow l$ operators that involve b quarks. These mediate leptonic flavour changing B decays, which are a promising avenue for New Physics in light of the recent anomalies. In most cases the anomalous rates are below the SM expectations, requiring destructive interference with the SM that cannot be addressed by our LFV operators. An exception is the R_{D^*} anomaly, where the experimental value is larger than the SM prediction and, as discussed in Section 4.1.2 (see Figure 11), can be fitted by increasing the rate of $B \rightarrow D^* \tau \nu$ with $\tau \leftrightarrow e$ operators. This is an example of the above-discussed relations that we can extrapolate from our calculation; the non-observation of $\mu \rightarrow e$ processes

can identify values where $\tau \leftrightarrow \mu$ is unlikely to be seen.

Acknowledgements

The work of MG has been supported by STFC under the Consolidated Grant ST/T000988/1. MA is supported by a doctoral fellowship from the IN2P3.

A Feynman Rules

In this section we list the Feynman Rules for the interactions involved in the diagrams of section 3.1. Capital letters $I, J, L, K \dots$ are used to label SU(2) indices, while lower-case letters i, j, l, k are generation indices. τ^a are the Pauli matrices and $\epsilon_{12} = -\epsilon_{21} = 1, \epsilon_{11} = \epsilon_{22} = 0$ is the anti-symmetric SU(2) tensor. The Feynman rules are obtained calculating by hand the iM amplitude of the tree-level processes.

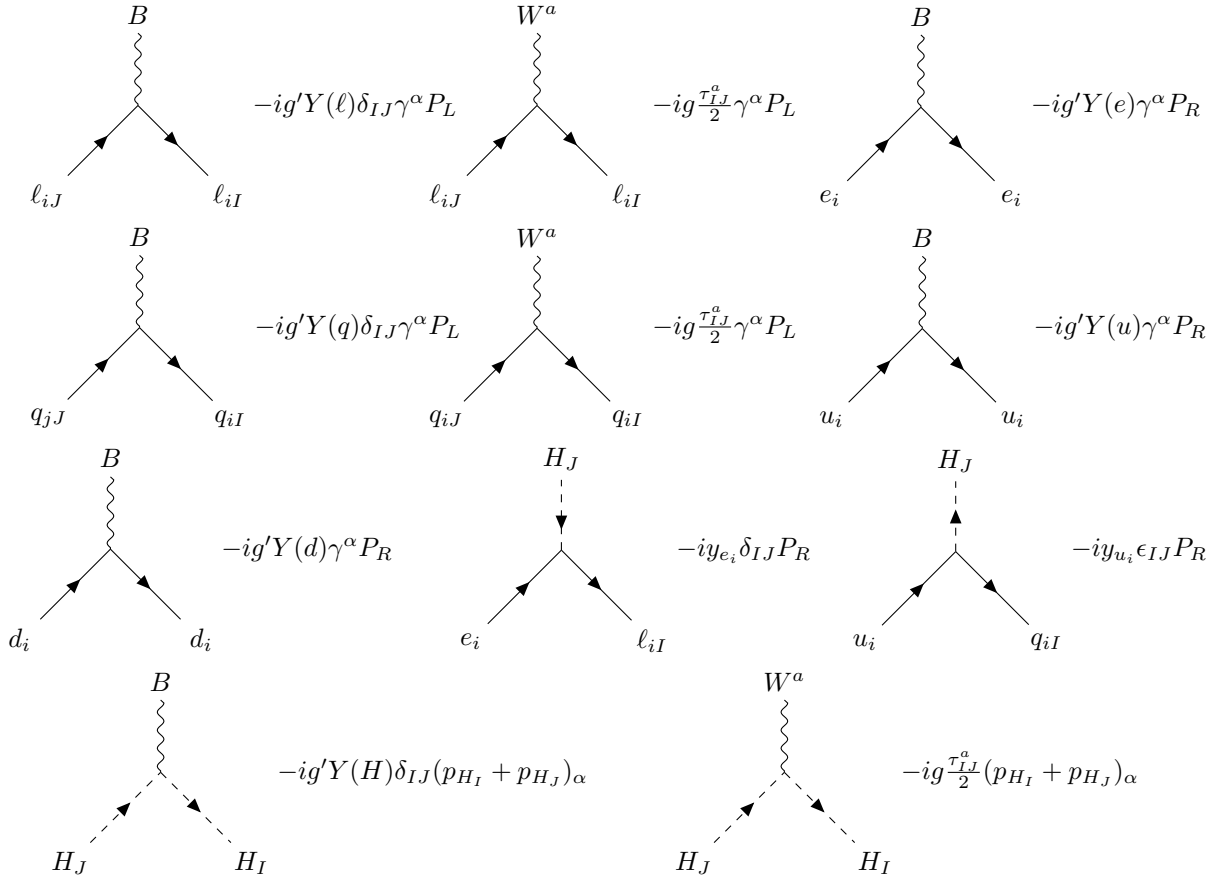


Figure 12: Feynman rules for the dimension four interaction. The Higgs momenta follow the hypercharge arrow.

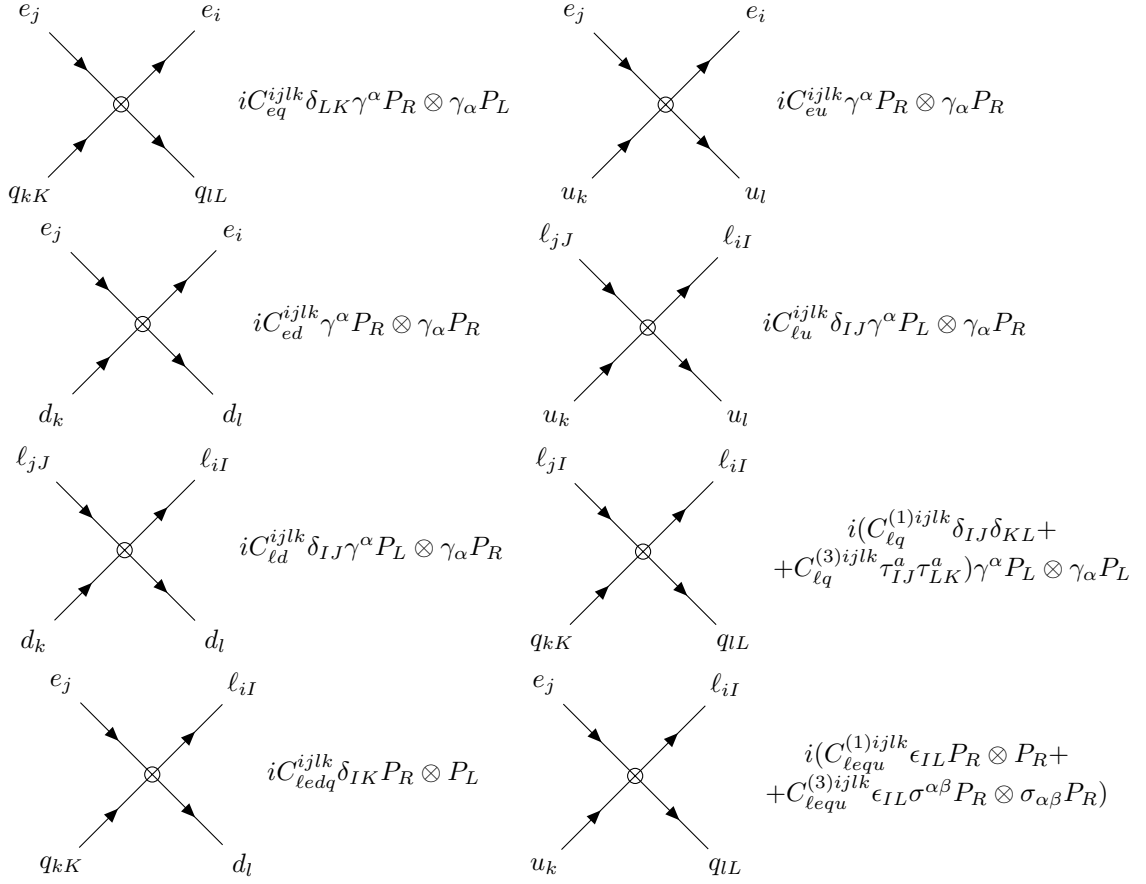


Figure 13: Feynman rules for the dimension six SMEFT four-fermion interaction $4f_6$ of section 2.3. In the product $\Gamma_1 \otimes \Gamma_2$ the left matrix Γ_1 multiplies the lepton bilinear. Scalar and tensor with opposite chiralities have the same Feynman rules with conjugate coefficients and exchanged flavour indices within lepton and quark bilinears.

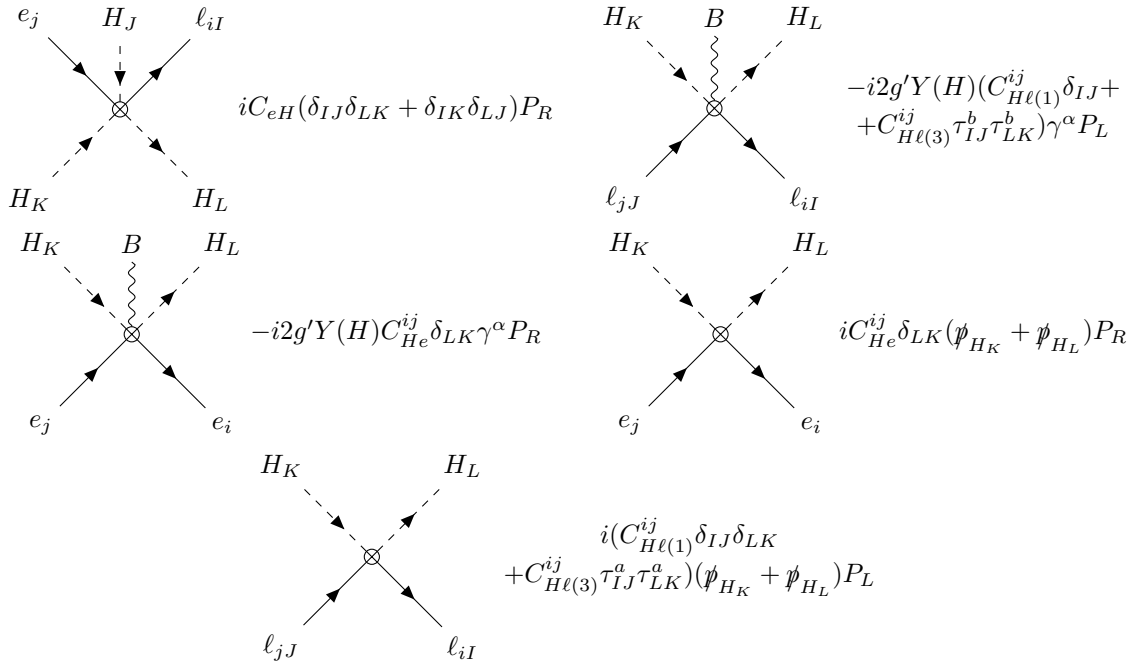


Figure 14: Feynman rules for the dimension six SMEFT two fermion operators Y_6, P_6 of section 2.3. The Higgs momenta follow the hypercharge arrows.

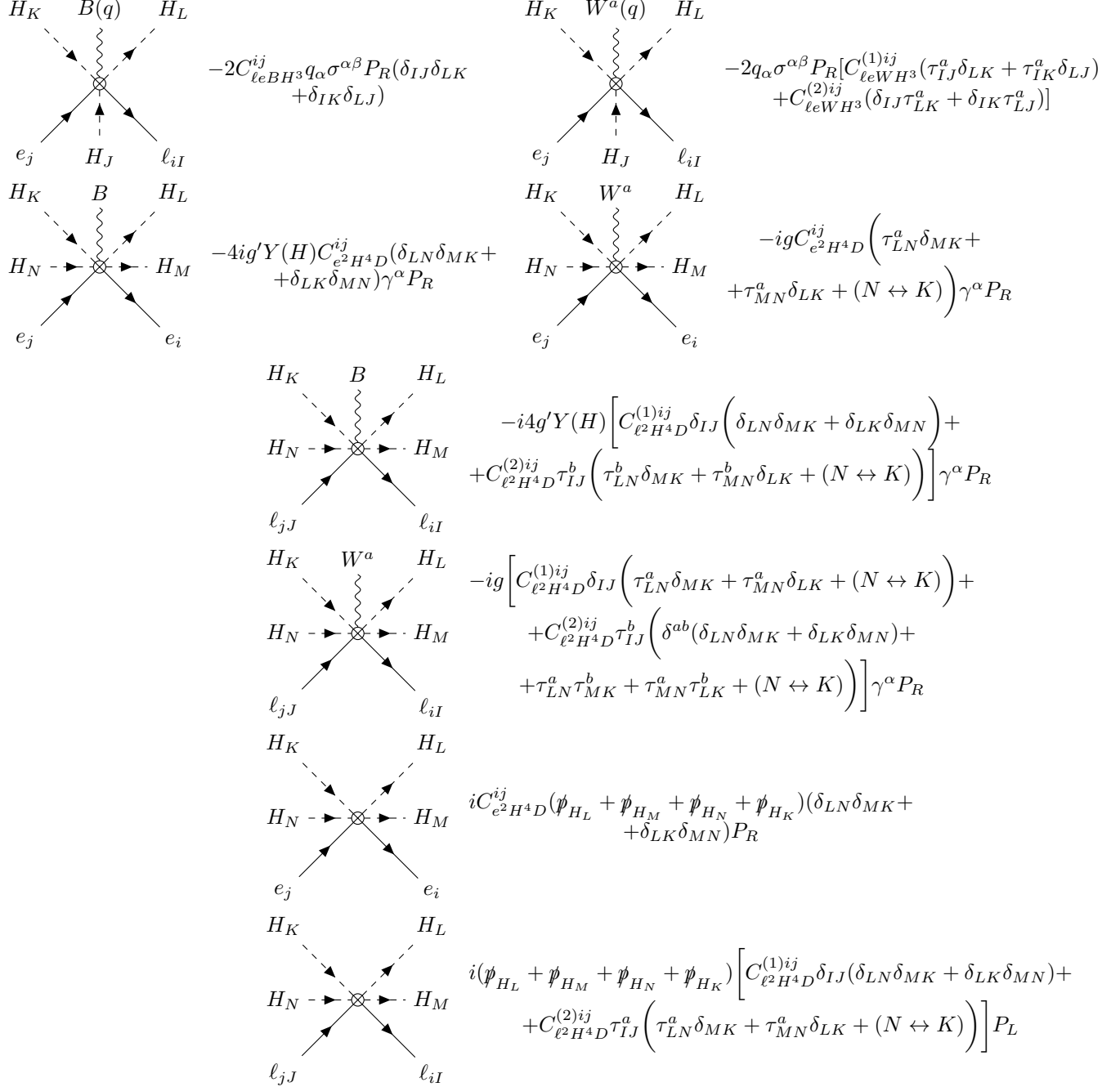


Figure 15: Feynman rules for the dimension eight SMEFT two fermion operators D_8, P_8 of section 2.3. The Higgs momenta directions follow the hypercharge arrow, while the bosons momentum q is outgoing

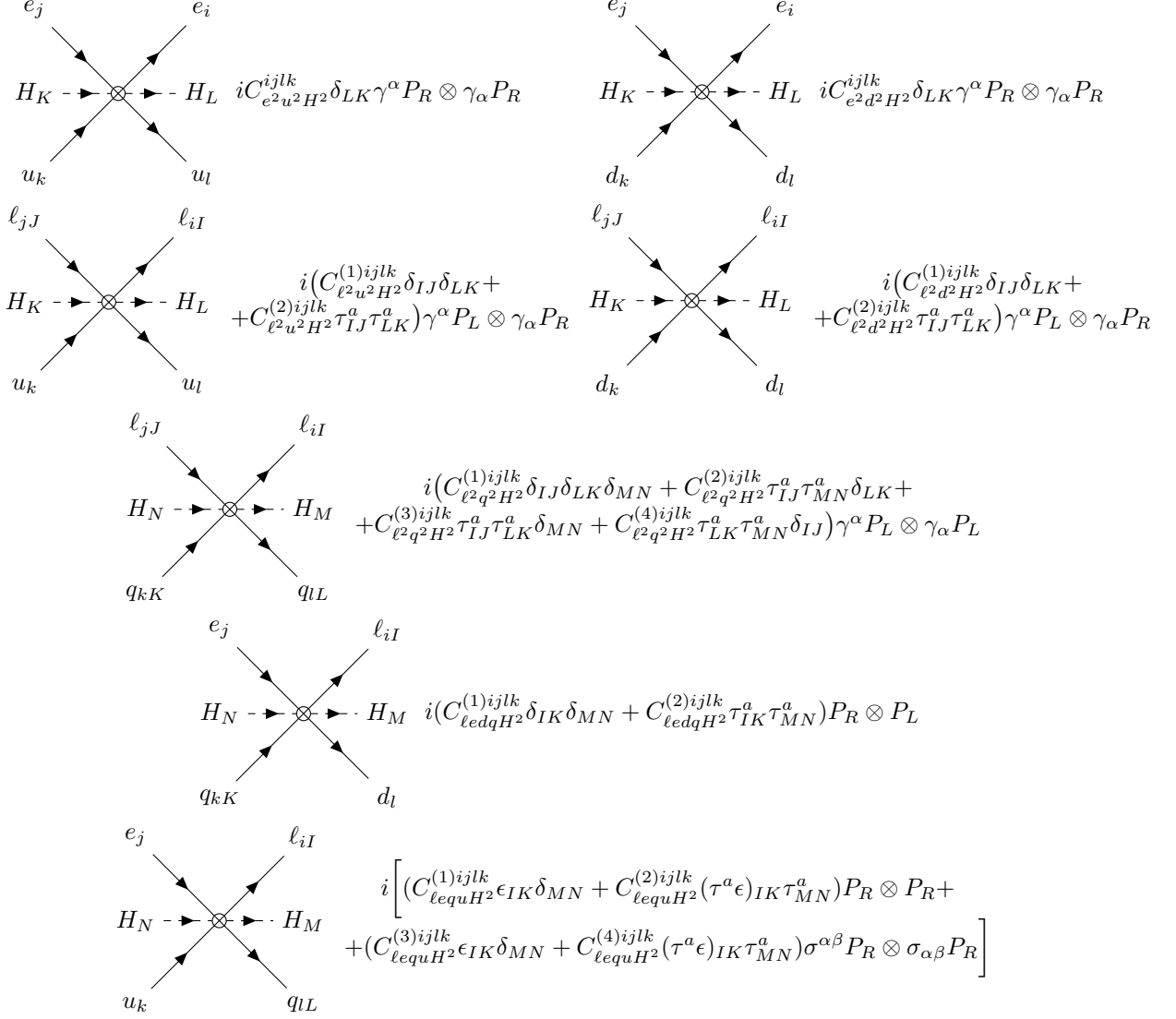


Figure 16: Feynman rules for the dimension eight SMEFT four-fermion interactions $4f_8$ of section 2.3. We consider only the dimension eight operators involved in the diagrams of section 3.1.1. In the product $\Gamma_1 \otimes \Gamma_2$ the left matrix Γ_1 multiplies the lepton bilinear. Scalar and tensor with opposite chiralities have the same Feynman rules with conjugate coefficients and exchanged flavour indices within lepton and quark bilinears.

B Anomalous Dimensions

In this section we write the renormalization group equations for the mixing of a $\mu \rightarrow \tau$ dimension six operator, multiplied by a $\tau \rightarrow e$ dimension six operator, into a dimension eight $\mu \rightarrow e$ operator. These anomalous dimensions are generated by the diagrams of section 3.1.1. We conveniently present the RGEs divided in the “classes” introduced in the same section. The operator definitions can be found in section 2.3. The upper dot \dot{C} on the Wilson coefficient indicate the logarithmic derivative with respect to the renormalization scale M . The anomalous dimensions are written for the dimension eight operators of Section 2.3, which are relevant for $\mu \rightarrow e$ processes that are otherwise flavour diagonal, although more general flavour structures can be obtained with the appropriate substitutions. For non-Hermitian operators such as $\mathcal{O}_{lequH^2}^{(1)}$, we write the RGEs for the $\mu \rightarrow e$ operators $\mathcal{O}_{lequH^2}^{(1)e\mu ii}, \mathcal{O}_{lequH^2}^{*(1)\mu e ii}$. This is to more explicitly show the $\tau \leftrightarrow l$ operator pairs upon which we obtain limits in section 4.

B.1 $4f_6 \times 4f_6 \rightarrow 4f_8$

Figure 6f shows the mixing $\propto y_t y_\tau$ of pairs of dimension six $\tau \rightarrow l$ operators into the dimension eight $\mu \rightarrow e$ tensor with top legs. We align $\tau \leftrightarrow e, \tau \leftrightarrow \mu$ Wilson coefficients respectively in row and column vectors to write the following anomalous dimensions, relevant for the $B_{\mu \rightarrow e}$ sensitivity of Table 11.

$$16\pi^2 \dot{C}_{lequH^2}^{(3)e\mu 3t} = \begin{pmatrix} C_{lu}^{e\tau tt} & C_{\ell q}^{(1)e\tau 33} & C_{\ell q}^{(3)e\tau 33} & C_{lequ}^{(1)e\tau 3t} & C_{lequ}^{(3)e\tau 3t} \\ y_\tau y_t & 0 & 0 & 0 & \\ 0 & -y_\tau y_t & 0 & 0 & \\ 0 & y_\tau y_t & 0 & 0 & \\ 0 & 0 & 0 & 3y_\tau y_t & \\ 0 & 0 & 3y_\tau y_t & -8y_\tau y_t & \end{pmatrix} \begin{pmatrix} C_{eq}^{\tau\mu 33} \\ C_{eu}^{\tau\mu tt} \\ C_{(1)\tau\mu 3t}^{lequ} \\ C_{lequ}^{\tau\mu 3t} \end{pmatrix} \quad (92)$$

$$16\pi^2 \dot{C}_{lequH^2}^{*(3)\mu e 3t} = \begin{pmatrix} C_{lu}^{\tau\mu tt} & C_{\ell q}^{(1)\tau\mu 33} & C_{\ell q}^{(3)\tau\mu 33} & C_{lequ}^{*(1)\mu\tau 3t} & C_{lequ}^{*(3)\mu\tau 3t} \\ y_\tau y_t & 0 & 0 & 0 & \\ 0 & -y_\tau y_t & 0 & 0 & \\ 0 & y_\tau y_t & 0 & 0 & \\ 0 & 0 & 0 & 3y_\tau y_t & \\ 0 & 0 & 3y_\tau y_t & -8y_\tau y_t & \end{pmatrix} \begin{pmatrix} C_{eq}^{e\tau 33} \\ C_{eu}^{e\tau tt} \\ C_{(1)\tau e 3t}^{*lequ} \\ C_{lequ}^{*(3)\tau e 3t} \end{pmatrix} \quad (93)$$

$$16\pi^2 \dot{C}_{lequH^2}^{(4)e\mu 3t} = \begin{pmatrix} C_{lu}^{e\tau tt} & C_{\ell q}^{(1)e\tau 33} & C_{\ell q}^{(3)e\tau 33} & C_{lequ}^{(1)e\tau 3t} & C_{lequ}^{(3)e\tau 3t} \\ y_\tau y_t & 0 & 0 & 0 & \\ 0 & -y_\tau y_t & 0 & 0 & \\ 0 & -y_\tau y_t & 0 & 0 & \\ 0 & 0 & 0 & y_\tau y_t & \\ 0 & 0 & y_\tau y_t & 8y_\tau y_t & \end{pmatrix} \begin{pmatrix} C_{eq}^{\tau\mu 33} \\ C_{eu}^{\tau\mu tt} \\ C_{(1)\tau\mu 3t}^{lequ} \\ C_{lequ}^{\tau\mu 3t} \end{pmatrix} \quad (94)$$

$$16\pi^2 \dot{C}_{lequH^2}^{*(4)\mu e 3t} = \begin{pmatrix} C_{lu}^{\tau\mu tt} & C_{\ell q}^{(1)\tau\mu 33} & C_{\ell q}^{(3)\tau\mu 33} & C_{lequ}^{*(1)\mu\tau 3t} & C_{lequ}^{*(3)\mu\tau 3t} \\ y_\tau y_t & 0 & 0 & 0 & \\ 0 & -y_\tau y_t & 0 & 0 & \\ 0 & -y_\tau y_t & 0 & 0 & \\ 0 & 0 & 0 & y_\tau y_t & \\ 0 & 0 & y_\tau y_t & 8y_\tau y_t & \end{pmatrix} \begin{pmatrix} C_{eq}^{e\tau 33} \\ C_{eu}^{e\tau tt} \\ C_{(1)\tau e 3t}^{*lequ} \\ C_{lequ}^{*(3)\tau e 3t} \end{pmatrix} \quad (95)$$

In Figure 6e we show a representative diagram with the double insertion of two-lepton two-quark $\tau \rightarrow l$ operators of dimension six, which renormalizes the coefficient of $\mu \rightarrow e$ dimension eight four fermion operators. The mixing is proportional to the square of the top Yukawa y_t^2 . The RGEs for scalar and tensor with a up-singlet quark

(the sensitivities of $\mu \rightarrow e$ processes that we obtain from this mixing are summarized in Tables 8 and 10) read

$$16\pi^2 \dot{C}_{lequH^2}^{(1)e\mu ii} = \begin{pmatrix} C_{\ell u}^{e\tau i} & C_{lequ}^{(1)e\tau i} & C_{lequ}^{(3)e\tau 3i} & C_{lequ}^{(1)e\tau it} & C_{lequ}^{(3)e\tau it} & C_{\ell q}^{(1)e\tau i3} & C_{\ell q}^{(3)e\tau i3} \end{pmatrix} \begin{pmatrix} -2y_t^2 & -24y_t^2 & 0 & 0 & 0 & 0 \\ 0 & 0 & -y_t^2 & 0 & 0 & 0 \\ 0 & 0 & -12y_t^2 & 0 & 0 & 0 \\ 0 & 0 & 0 & 2y_t^2 & 0 & 0 \\ 0 & 0 & 0 & -24y_t^2 & 0 & 0 \\ 0 & 0 & 0 & 0 & y_t^2 & -12y_t^2 \\ 0 & 0 & 0 & 0 & -3y_t^2 & 36y_t^2 \end{pmatrix} \begin{pmatrix} C_{lequ}^{(1)\tau\mu it} \\ C_{lequ}^{(3)\tau\mu it} \\ C_{lequ}^{e\tau\mu i3} \\ C_{eq}^{\tau\mu i3} \\ C_{eu}^{\tau\mu ti} \\ C_{lequ}^{(1)\tau\mu 3i} \\ C_{lequ}^{(3)\tau\mu 3i} \end{pmatrix} \quad (96)$$

$$16\pi^2 \dot{C}_{lequH^2}^{*(1)\mu e ii} = \begin{pmatrix} C_{\ell u}^{\tau\mu it} & C_{lequ}^{*(1)\mu\tau 3i} & C_{lequ}^{*(3)\mu\tau 3i} & C_{lequ}^{*(1)\mu\tau it} & C_{lequ}^{*(3)\mu\tau it} & C_{\ell q}^{(1)\tau\mu 3i} & C_{\ell q}^{(3)\tau\mu 3i} \end{pmatrix} \begin{pmatrix} -2y_t^2 & -24y_t^2 & 0 & 0 & 0 & 0 \\ 0 & 0 & -y_t^2 & 0 & 0 & 0 \\ 0 & 0 & -12y_t^2 & 0 & 0 & 0 \\ 0 & 0 & 0 & 2y_t^2 & 0 & 0 \\ 0 & 0 & 0 & -24y_t^2 & 0 & 0 \\ 0 & 0 & 0 & 0 & y_t^2 & -12y_t^2 \\ 0 & 0 & 0 & 0 & -3y_t^2 & 36y_t^2 \end{pmatrix} \begin{pmatrix} C_{lequ}^{*(1)\tau e it} \\ C_{lequ}^{*(3)\tau e it} \\ C_{lequ}^{e\tau 3i} \\ C_{eq}^{\tau e 3i} \\ C_{eu}^{\tau e it} \\ C_{lequ}^{*(1)\tau e 3i} \\ C_{lequ}^{*(3)\tau e 3i} \end{pmatrix} \quad (97)$$

$$16\pi^2 \dot{C}_{lequH^2}^{(2)e\mu ii} = \begin{pmatrix} C_{lequ}^{(1)e\tau 3i} & C_{lequ}^{(3)e\tau 3i} & C_{\ell q}^{(1)e\tau i3} & C_{\ell q}^{(3)e\tau i3} \end{pmatrix} \begin{pmatrix} -y_t^2 & 0 & 0 \\ -12y_t^2 & 0 & 0 \\ 0 & y_t^2 & -12y_t^2 \\ 0 & y_t^2 & -12y_t^2 \end{pmatrix} \begin{pmatrix} C_{eq}^{\tau\mu i3} \\ C_{lequ}^{(1)\tau\mu 3i} \\ C_{lequ}^{(3)\tau\mu 3i} \end{pmatrix} \quad (98)$$

$$16\pi^2 \dot{C}_{lequH^2}^{*(2)\mu e ii} = \begin{pmatrix} C_{lequ}^{*(1)\mu\tau 3i} & C_{lequ}^{*(3)\mu\tau 3i} & C_{\ell q}^{(1)\tau\mu 3i} & C_{\ell q}^{(3)\tau\mu 3i} \end{pmatrix} \begin{pmatrix} -y_t^2 & 0 & 0 \\ -12y_t^2 & 0 & 0 \\ 0 & y_t^2 & -12y_t^2 \\ 0 & y_t^2 & -12y_t^2 \end{pmatrix} \begin{pmatrix} C_{eq}^{\tau e 3i} \\ C_{lequ}^{*(1)\tau e 3i} \\ C_{lequ}^{*(3)\tau e 3i} \end{pmatrix} \quad (99)$$

$$16\pi^2 \dot{C}_{lequH^2}^{(3)e\mu ii} = \begin{pmatrix} C_{\ell u}^{e\tau i} & C_{lequ}^{(1)e\tau 3i} & C_{lequ}^{(3)e\tau 3i} & C_{lequ}^{(1)e\tau it} & C_{lequ}^{(3)e\tau it} & C_{\ell q}^{(1)e\tau i3} & C_{\ell q}^{(3)e\tau i3} \end{pmatrix} \begin{pmatrix} -y_t^2/2 & -6y_t^2 & 0 & 0 & 0 & 0 \\ 0 & 0 & -y_t^2/4 & 0 & 0 & 0 \\ 0 & 0 & -3y_t^2 & 0 & 0 & 0 \\ 0 & 0 & 0 & -y_t^2/2 & 0 & 0 \\ 0 & 0 & 0 & 6y_t^2 & 0 & 0 \\ 0 & 0 & 0 & 0 & -y_t^2/4 & 3y_t^2 \\ 0 & 0 & 0 & 0 & 3y_t^2/4 & -9y_t^2 \end{pmatrix} \begin{pmatrix} C_{lequ}^{(1)\tau\mu it} \\ C_{lequ}^{(3)\tau\mu it} \\ C_{lequ}^{e\tau\mu i3} \\ C_{eq}^{\tau\mu i3} \\ C_{eu}^{\tau\mu ti} \\ C_{lequ}^{(1)\tau\mu 3i} \\ C_{lequ}^{(3)\tau\mu 3i} \end{pmatrix} \quad (100)$$

$$16\pi^2 \dot{C}_{lequH^2}^{*(3)\mu e ii} = \begin{pmatrix} C_{\ell u}^{\tau\mu it} & C_{lequ}^{*(1)\mu\tau 3i} & C_{lequ}^{*(3)\mu\tau 3i} & C_{lequ}^{*(1)\mu\tau it} & C_{lequ}^{*(3)\mu\tau it} & C_{\ell q}^{(1)\tau\mu 3i} & C_{\ell q}^{(3)\tau\mu 3i} \end{pmatrix} \begin{pmatrix} -y_t^2/2 & -6y_t^2 & 0 & 0 & 0 & 0 \\ 0 & 0 & -y_t^2/4 & 0 & 0 & 0 \\ 0 & 0 & -3y_t^2 & 0 & 0 & 0 \\ 0 & 0 & 0 & -y_t^2/2 & 0 & 0 \\ 0 & 0 & 0 & 6y_t^2 & 0 & 0 \\ 0 & 0 & 0 & 0 & -y_t^2/4 & 3y_t^2 \\ 0 & 0 & 0 & 0 & 3y_t^2/4 & -9y_t^2 \end{pmatrix} \begin{pmatrix} C_{lequ}^{*(1)\tau e it} \\ C_{lequ}^{*(3)\tau e it} \\ C_{lequ}^{e\tau 3i} \\ C_{eq}^{\tau e 3i} \\ C_{eu}^{\tau e it} \\ C_{lequ}^{*(1)\tau e 3i} \\ C_{lequ}^{*(3)\tau e 3i} \end{pmatrix} \quad (101)$$

$$16\pi^2 \dot{C}_{lequH^2}^{(4)e\mu ii} = \begin{pmatrix} C_{lequ}^{(1)e\tau 3i} & C_{lequ}^{(3)e\tau 3i} & C_{\ell q}^{(1)e\tau i3} & C_{\ell q}^{(3)e\tau i3} \end{pmatrix} \begin{pmatrix} -y_t^2/4 & 0 & 0 \\ -3y_t^2 & 0 & 0 \\ 0 & -y_t^2/4 & 3y_t^2 \\ 0 & -y_t^2/4 & 3y_t^2 \end{pmatrix} \begin{pmatrix} C_{eq}^{\tau\mu i3} \\ C_{lequ}^{(1)\tau\mu 3i} \\ C_{lequ}^{(3)\tau\mu 3i} \end{pmatrix} \quad (102)$$

$$16\pi^2 \dot{C}_{\ell equ H^2}^{*(4)\mu e ii} = \begin{pmatrix} C_{\ell equ}^{*(1)\mu\tau 3i} & C_{\ell equ}^{*(3)\mu\tau 3i} & C_{\ell q}^{(1)\tau\mu 3i} & C_{\ell q}^{(3)\tau\mu 3i} \\ \begin{pmatrix} -y_t^2/4 & 0 & 0 \\ -3y_t^2 & 0 & 0 \\ 0 & -y_t^2/4 & 3y_t^2 \\ 0 & -y_t^2/4 & 3y_t^2 \end{pmatrix} & \begin{pmatrix} C_{eq}^{e\tau 3i} \\ C_{\ell equ}^{*(1)\tau e 3i} \\ C_{\ell equ}^{*(3)\tau e 3i} \end{pmatrix} \end{pmatrix}. \quad (103)$$

For scalars with a singlet down-quark (sensitivities in Table 9), the mixing is

$$16\pi^2 \dot{C}_{\ell edq H^2}^{(1)e\mu ii} = \begin{pmatrix} C_{\ell q}^{(1)e\tau i3} & C_{\ell q}^{(3)e\tau i3} & C_{\ell edq}^{e\tau i3} \\ \begin{pmatrix} -y_t^2 & 0 \\ -3y_t^2 & 0 \\ 0 & y_t^2 \end{pmatrix} & \begin{pmatrix} C_{\ell edq}^{\tau\mu i3} \\ C_{eq}^{\tau\mu 3i} \end{pmatrix} \end{pmatrix} \quad (104)$$

$$16\pi^2 \dot{C}_{\ell edq H^2}^{*(1)\mu e ii} = \begin{pmatrix} C_{\ell q}^{(1)\tau\mu 3i} & C_{\ell q}^{(3)\tau\mu 3i} & C_{\ell edq}^{*\mu\tau i3} \\ \begin{pmatrix} -y_t^2 & 0 \\ -3y_t^2 & 0 \\ 0 & y_t^2 \end{pmatrix} & \begin{pmatrix} C_{\ell edq}^{*\tau e i3} \\ C_{eq}^{e\tau i3} \end{pmatrix} \end{pmatrix} \quad (105)$$

$$16\pi^2 \dot{C}_{\ell edq H^2}^{(2)e\mu ii} = \begin{pmatrix} C_{\ell q}^{(1)e\tau i3} & C_{\ell q}^{(3)e\tau i3} & C_{\ell edq}^{e\tau i3} \\ \begin{pmatrix} y_t^2 & 0 \\ -y_t^2 & 0 \\ 0 & -y_t^2 \end{pmatrix} & \begin{pmatrix} C_{\ell edq}^{\tau\mu i3} \\ C_{eq}^{\tau\mu 3i} \end{pmatrix} \end{pmatrix} \quad (106)$$

$$16\pi^2 \dot{C}_{\ell edq H^2}^{*(2)\mu e ii} = \begin{pmatrix} C_{\ell q}^{(1)\tau\mu 3i} & C_{\ell q}^{(3)\tau\mu 3i} & C_{\ell edq}^{*\mu\tau i3} \\ \begin{pmatrix} y_t^2 & 0 \\ -y_t^2 & 0 \\ 0 & -y_t^2 \end{pmatrix} & \begin{pmatrix} C_{\ell edq}^{*\tau e i3} \\ C_{eq}^{e\tau i3} \end{pmatrix} \end{pmatrix} \quad (107)$$

The anomalous dimensions for the mixing into $\mu \rightarrow e$ vectors with SU(2) lepton singlets are (sensitivities in Table 12)

$$16\pi^2 \dot{C}_{e^2 q^2 H^2}^{(1)e\mu ii} = \begin{pmatrix} C_{eq}^{e\tau 3i} & C_{eq}^{e\tau i3} & C_{\ell equ}^{*(1)\tau e it} & C_{\ell equ}^{*(3)\tau e it} \\ \begin{pmatrix} -4y_t^2 & 0 & 0 & 0 \\ 0 & y_t^2 & 0 & 0 \\ 0 & 0 & -y_t^2/2 & -6y_t^2 \\ 0 & 0 & -6y_t^2 & -72y_t^2 \end{pmatrix} & \begin{pmatrix} C_{eq}^{\tau\mu i3} \\ C_{eq}^{\tau\mu 3i} \\ C_{\ell equ}^{(1)\tau\mu it} \\ C_{\ell equ}^{(3)\tau\mu it} \end{pmatrix} \end{pmatrix} \quad (108)$$

$$16\pi^2 \dot{C}_{e^2 q^2 H^2}^{(2)e\mu ii} = \begin{pmatrix} C_{eq}^{e\tau 3i} & C_{eq}^{e\tau i3} \\ \begin{pmatrix} 4y_t^2 & 0 \\ 0 & -y_t^2 \end{pmatrix} & \begin{pmatrix} C_{eq}^{\tau\mu i3} \\ C_{eq}^{\tau\mu 3i} \end{pmatrix} \end{pmatrix} \quad (109)$$

$$16\pi^2 \dot{C}_{e^2 u^2 H^2}^{e\mu ii} = \begin{pmatrix} C_{eu}^{e\tau ti} & C_{eu}^{e\tau it} & C_{\ell equ}^{*(1)\tau e 3i} & C_{\ell equ}^{*(3)\tau e 3i} \\ \begin{pmatrix} -2y_t^2 & 0 & 0 & 0 \\ 0 & 8y_t^2 & 0 & 0 \\ 0 & 0 & y_t^2/2 & -6y_t^2 \\ 0 & 0 & -6y_t^2 & 72y_t^2 \end{pmatrix} & \begin{pmatrix} C_{eu}^{\tau\mu it} \\ C_{eu}^{\tau\mu ti} \\ C_{\ell equ}^{(1)\tau\mu 3i} \\ C_{\ell equ}^{(3)\tau\mu 3i} \end{pmatrix} \end{pmatrix} \quad (110)$$

$$16\pi^2 \dot{C}_{e^2 d^2 H^2}^{e\mu ii} = -\frac{y_t^2}{2} C_{\ell edq}^{*\tau e i3} C_{\ell edq}^{\tau\mu i3} \quad (111)$$

while for vectors with lepton doublets (sensitivities in Table 13) these are

$$16\pi^2 \dot{C}_{\ell^2 q^2 H^2}^{(1)e\mu ii} = \begin{pmatrix} C_{\ell q}^{(1)e\tau 3i} & C_{\ell q}^{(3)e\tau 3i} & C_{\ell q}^{(1)e\tau i3} & C_{\ell q}^{(3)e\tau i3} & C_{\ell equ}^{(1)e\tau it} & C_{\ell equ}^{(3)e\tau it} \end{pmatrix} \begin{pmatrix} -y_t^2 & 0 & 0 & 0 & 0 & 0 \\ 0 & -3y_t^2 & 0 & 0 & 0 & 0 \\ 0 & 0 & 4y_t^2 & 0 & 0 & 0 \\ 0 & 0 & 0 & 12y_t^2 & 0 & 0 \\ 0 & 0 & 0 & 0 & y_t^2/4 & -3y_t^2 \\ 0 & 0 & 0 & 0 & -3y_t^2 & 36y_t^2 \end{pmatrix} \begin{pmatrix} C_{\ell q}^{(1)\tau\mu i3} \\ C_{\ell q}^{(3)\tau\mu i3} \\ C_{\ell q}^{(1)\tau\mu 3i} \\ C_{\ell q}^{(3)\tau\mu 3i} \\ C_{\ell equ}^{*(1)\mu\tau it} \\ C_{\ell equ}^{*(3)\mu\tau it} \end{pmatrix} \quad (112)$$

$$16\pi^2 \dot{C}_{\ell^2 q^2 H^2}^{(2)e\mu ii} = \begin{pmatrix} C_{\ell q}^{(1)e\tau ti} & C_{\ell q}^{(3)e\tau ti} & C_{\ell q}^{(1)e\tau it} & C_{\ell q}^{(3)e\tau it} \end{pmatrix} \begin{pmatrix} 0 & y_t^2 & 0 & 0 \\ y_t^2 & -2y_t^2 & 0 & 0 \\ 0 & 0 & 0 & -4y_t^2 \\ 0 & 0 & -4y_t^2 & -8y_t^2 \end{pmatrix} \begin{pmatrix} C_{\ell q}^{(1)\tau\mu i3} \\ C_{\ell q}^{(3)\tau\mu i3} \\ C_{\ell q}^{(1)\tau\mu 3i} \\ C_{\ell q}^{(3)\tau\mu 3i} \end{pmatrix} \quad (113)$$

$$16\pi^2 \dot{C}_{\ell^2 q^2 H^2}^{(3)e\mu ii} = \begin{pmatrix} C_{\ell q}^{(1)e\tau 3i} & C_{\ell q}^{(3)e\tau 3i} & C_{\ell q}^{(1)e\tau i3} & C_{\ell q}^{(3)e\tau i3} & C_{\ell equ}^{(1)e\tau it} & C_{\ell equ}^{(3)e\tau it} \end{pmatrix} \begin{pmatrix} 0 & -y_t^2 & 0 & 0 & 0 & 0 \\ -y_t^2 & -2y_t^2 & 0 & 0 & 0 & 0 \\ 0 & 0 & 0 & 4y_t^2 & 0 & 0 \\ 0 & 0 & 4y_t^2 & -8y_t^2 & 0 & 0 \\ 0 & 0 & 0 & 0 & -y_t^2/4 & 3y_t^2 \\ 0 & 0 & 0 & 0 & 3y_t^2 & -36y_t^2 \end{pmatrix} \begin{pmatrix} C_{\ell q}^{(1)\tau\mu i3} \\ C_{\ell q}^{(3)\tau\mu i3} \\ C_{\ell q}^{(1)\tau\mu 3i} \\ C_{\ell q}^{(3)\tau\mu 3i} \\ C_{\ell equ}^{*(1)\mu\tau it} \\ C_{\ell equ}^{*(3)\mu\tau it} \end{pmatrix} \quad (114)$$

$$16\pi^2 \dot{C}_{\ell^2 q^2 H^2}^{(4)e\mu ii} = \begin{pmatrix} C_{\ell q}^{(1)e\tau 3i} & C_{\ell q}^{(3)e\tau 3i} & C_{\ell q}^{(1)e\tau i3} & C_{\ell q}^{(3)e\tau i3} \end{pmatrix} \begin{pmatrix} y_t^2 & 0 & 0 & 0 \\ 0 & -y_t^2 & 0 & 0 \\ 0 & 0 & -4y_t^2 & 0 \\ 0 & 0 & 0 & 4y_t^2 \end{pmatrix} \begin{pmatrix} C_{\ell q}^{(1)\tau\mu i3} \\ C_{\ell q}^{(3)\tau\mu i3} \\ C_{\ell q}^{(1)\tau\mu 3i} \\ C_{\ell q}^{(3)\tau\mu 3i} \end{pmatrix} \quad (115)$$

$$16\pi^2 \dot{C}_{\ell^2 u^2 H^2}^{(1)e\mu ii} = \begin{pmatrix} C_{\ell u}^{e\tau ti} & C_{\ell u}^{e\tau it} & C_{\ell equ}^{(1)e\tau 3i} & C_{\ell equ}^{(3)e\tau 3i} \end{pmatrix} \begin{pmatrix} -8y_t^2 & 0 & 0 & 0 \\ 0 & 2y_t^2 & 0 & 0 \\ 0 & 0 & -y_t^2/4 & -3y_t^2 \\ 0 & 0 & -3y_t^2 & -36y_t^2 \end{pmatrix} \begin{pmatrix} C_{\ell u}^{\tau\mu it} \\ C_{\ell u}^{\tau\mu ti} \\ C_{\ell equ}^{*(1)\mu\tau 3i} \\ C_{\ell equ}^{*(3)\mu\tau 3i} \end{pmatrix} \quad (116)$$

$$16\pi^2 \dot{C}_{\ell^2 u^2 H^2}^{(2)e\mu ii} = \begin{pmatrix} C_{\ell equ}^{(1)e\tau 3i} & C_{\ell equ}^{(3)e\tau 3i} \end{pmatrix} \begin{pmatrix} -y_t^2/4 & -3y_t^2 \\ -3y_t^2 & -36y_t^2 \end{pmatrix} \begin{pmatrix} C_{\ell equ}^{*(1)\mu\tau 3i} \\ C_{\ell equ}^{*(3)\mu\tau 3i} \end{pmatrix} \quad (117)$$

$$16\pi^2 \dot{C}_{\ell^2 d^2 H^2}^{(1)e\mu ii} = \frac{y_t^2}{4} C_{\ell edq}^{e\tau i3} C_{\ell edq}^{*\mu\tau i3} \quad 16\pi^2 \dot{C}_{\ell^2 d^2 H^2}^{(2)e\mu ii} = -\frac{y_t^2}{4} C_{\ell edq}^{e\tau i3} C_{\ell edq}^{*\mu\tau i3} \quad (118)$$

B.2 $P_6 \times 4f_6 \rightarrow 4f_8$

Dimension six $\tau \rightarrow l$ four fermion interactions renormalise $\mu \rightarrow e$ dimension eight operators via gauge loops where one vertex is a flavour changing penguin (eq. (13)-(14)), as depicted in Figure 6d. One-particle-irreducible

vertex corrections and “wavefunction-like” contributions (see section 2.4 for a discussion) give the following gauge invariant anomalous dimensions, where we align four-fermion interactions and penguins respectively in row and column vectors:

$$16\pi^2 \dot{C}_{lequH^2}^{(1)e\mu ii} = \begin{pmatrix} C_{lequ}^{(1)e\tau ii} & C_{lequ}^{(3)e\tau ii} & C_{lequ}^{(1)\tau\mu ii} & C_{lequ}^{(3)\tau\mu ii} \\ \begin{pmatrix} 3g'^2 & 0 & 0 \\ -20g'^2 & 0 & 0 \\ 0 & 6g'^2 & 0 \\ 0 & -20g'^2 & 36g'^2 \end{pmatrix} & \begin{pmatrix} C_{He}^{\tau\mu} \\ C_{H^e}^{(1)e\tau} \\ C_{H^\ell}^\ell \\ C_{H^\ell}^{(3)e\tau} \end{pmatrix} \end{pmatrix} \quad (119)$$

$$16\pi^2 \dot{C}_{lequH^2}^{*(1)\mu\tau ii} = \begin{pmatrix} C_{lequ}^{*(1)\mu\tau ii} & C_{lequ}^{*(3)\mu\tau ii} & C_{lequ}^{*(1)\tau e ii} & C_{lequ}^{*(3)\tau e ii} \\ \begin{pmatrix} 3g'^2 & 0 & 0 \\ -20g'^2 & 0 & 0 \\ 0 & 6g'^2 & 0 \\ 0 & -20g'^2 & 36g'^2 \end{pmatrix} & \begin{pmatrix} C_{He}^{e\tau} \\ C_{H^e}^{(1)\tau\mu} \\ C_{H^\ell}^\ell \\ C_{H^\ell}^{(3)\tau\mu} \end{pmatrix} \end{pmatrix} \quad (120)$$

$$16\pi^2 \dot{C}_{lequH^2}^{(2)e\mu ii} = \begin{pmatrix} C_{lequ}^{(1)e\tau ii} & C_{lequ}^{(3)e\tau ii} & C_{lequ}^{(1)\tau\mu ii} & C_{lequ}^{(3)\tau\mu ii} \\ \begin{pmatrix} -3g'^2 & 0 & 0 \\ 12g'^2 & 0 & 0 \\ 0 & 0 & 6g'^2 \\ 0 & 12g'^2 & -20g'^2 \end{pmatrix} & \begin{pmatrix} C_{He}^{\tau\mu} \\ C_{H^e}^{(1)e\tau} \\ C_{H^\ell}^\ell \\ C_{H^\ell}^{(3)e\tau} \end{pmatrix} \end{pmatrix} \quad (121)$$

$$16\pi^2 \dot{C}_{lequH^2}^{*(2)\mu\tau ii} = \begin{pmatrix} C_{lequ}^{*(1)\mu\tau ii} & C_{lequ}^{*(3)\mu\tau ii} & C_{lequ}^{*(1)\tau e ii} & C_{lequ}^{*(3)\tau e ii} \\ \begin{pmatrix} -3g'^2 & 0 & 0 \\ 12g'^2 & 0 & 0 \\ 0 & 0 & 6g'^2 \\ 0 & 12g'^2 & -20g'^2 \end{pmatrix} & \begin{pmatrix} C_{He}^{e\tau} \\ C_{H^e}^{(1)\tau\mu} \\ C_{H^\ell}^\ell \\ C_{H^\ell}^{(3)\tau\mu} \end{pmatrix} \end{pmatrix} \quad (122)$$

$$16\pi^2 \dot{C}_{lequH^2}^{(3)e\mu ii} = \begin{pmatrix} C_{lequ}^{(1)e\tau ii} & C_{lequ}^{(3)e\tau ii} & C_{lequ}^{(1)\tau\mu ii} & C_{lequ}^{(3)\tau\mu ii} \\ \begin{pmatrix} -5g'^2/12 & 0 & 0 \\ g'^2 & 0 & 0 \\ 0 & -5g'^2/12 & 3g^2/4 \\ 0 & -4g'^2 & -6g^2 \end{pmatrix} & \begin{pmatrix} C_{He}^{\tau\mu} \\ C_{H^e}^{(1)e\tau} \\ C_{H^\ell}^\ell \\ C_{H^\ell}^{(3)e\tau} \end{pmatrix} \end{pmatrix} \quad (123)$$

$$16\pi^2 \dot{C}_{lequH^2}^{*(3)\mu\tau ii} = \begin{pmatrix} C_{lequ}^{*(1)\mu\tau ii} & C_{lequ}^{*(3)\mu\tau ii} & C_{lequ}^{*(1)\tau e ii} & C_{lequ}^{*(3)\tau e ii} \\ \begin{pmatrix} -5g'^2/12 & 0 & 0 \\ g'^2 & 0 & 0 \\ 0 & -5g'^2/12 & 3g^2/4 \\ 0 & -4g'^2 & -6g^2 \end{pmatrix} & \begin{pmatrix} C_{He}^{e\tau} \\ C_{H^e}^{(1)\tau\mu} \\ C_{H^\ell}^\ell \\ C_{H^\ell}^{(3)\tau\mu} \end{pmatrix} \end{pmatrix} \quad (124)$$

$$16\pi^2 \dot{C}_{lequH^2}^{(4)e\mu ii} = \begin{pmatrix} C_{lequ}^{(1)e\tau ii} & C_{lequ}^{(3)e\tau ii} & C_{lequ}^{(1)\tau\mu ii} & C_{lequ}^{(3)\tau\mu ii} \\ \begin{pmatrix} g^2/4 & 0 & 0 \\ 3g^2 & 0 & 0 \\ 0 & g^2/4 & -5g'^2/12 \\ 0 & -2g^2 & -4g'^2 \end{pmatrix} & \begin{pmatrix} C_{He}^{\tau\mu} \\ C_{H^e}^{(1)e\tau} \\ C_{H^\ell}^\ell \\ C_{H^\ell}^{(3)e\tau} \end{pmatrix} \end{pmatrix} \quad (125)$$

$$16\pi^2 \dot{C}_{lequH^2}^{*(4)\mu\tau ii} = \begin{pmatrix} C_{lequ}^{*(1)\mu\tau ii} & C_{lequ}^{*(3)\mu\tau ii} & C_{lequ}^{*(1)\tau e ii} & C_{lequ}^{*(3)\tau e ii} \\ \begin{pmatrix} g^2/4 & 0 & 0 \\ 3g^2 & 0 & 0 \\ 0 & g^2/4 & -5g'^2/12 \\ 0 & -2g^2 & -4g'^2 \end{pmatrix} & \begin{pmatrix} C_{He}^{e\tau} \\ C_{H^e}^{(1)\tau\mu} \\ C_{H^\ell}^\ell \\ C_{H^\ell}^{(3)\tau\mu} \end{pmatrix} \end{pmatrix} \quad (126)$$

$$16\pi^2 \dot{C}_{\ell edq H^2}^{(1)e\mu ii} = \begin{pmatrix} C_{\ell edq}^{e\tau ii} & C_{\ell edq}^{\tau\mu ii} \\ 3g'^2 & 0 \\ 0 & 6g'^2 \end{pmatrix} \begin{pmatrix} C_{He}^{\tau\mu} \\ C_{H\ell}^{(1)e\tau} \end{pmatrix} \quad (127)$$

$$16\pi^2 \dot{C}_{\ell edq H^2}^{*(1)\mu e ii} = \begin{pmatrix} C_{\ell edq}^{*\mu\tau ii} & C_{\ell edq}^{*\tau e ii} \\ 3g'^2 & 0 \\ 0 & 6g'^2 \end{pmatrix} \begin{pmatrix} C_{He}^{e\tau} \\ C_{H\ell}^{(1)\tau\mu} \end{pmatrix} \quad (128)$$

$$16\pi^2 \dot{C}_{\ell edq H^2}^{(2)e\mu ii} = \begin{pmatrix} C_{\ell edq}^{e\tau ii} & C_{\ell edq}^{\tau\mu ii} \\ -3g^2 & 0 \\ 0 & 6g'^2 \end{pmatrix} \begin{pmatrix} C_{He}^{\tau\mu} \\ C_{H\ell}^{(3)e\tau} \end{pmatrix} \quad (129)$$

$$16\pi^2 \dot{C}_{\ell edq H^2}^{*(2)\mu e ii} = \begin{pmatrix} C_{\ell edq}^{*\mu\tau ii} & C_{\ell edq}^{*\tau e ii} \\ -3g^2 & 0 \\ 0 & 6g'^2 \end{pmatrix} \begin{pmatrix} C_{He}^{e\tau} \\ C_{H\ell}^{(3)\tau\mu} \end{pmatrix} \quad (130)$$

$$16\pi^2 \dot{C}_{\ell^2 q^2 H^2}^{(1)e\mu ii} = \begin{pmatrix} C_{\ell q}^{(1)e\tau ii} & C_{\ell q}^{(3)e\tau ii} & C_{\ell q}^{(1)\tau\mu ii} & C_{\ell q}^{(3)\tau\mu ii} \\ g'^2 & 0 & 0 & 0 \\ 0 & 9g^2 & 0 & 0 \\ 0 & 0 & g'^2 & 0 \\ 0 & 0 & 0 & 9g^2 \end{pmatrix} \begin{pmatrix} C_{H\ell}^{(1)\tau\mu} \\ C_{H\ell}^{(3)\tau\mu} \\ C_{H\ell}^{(1)e\tau} \\ C_{H\ell}^{(3)e\tau} \end{pmatrix} \quad (131)$$

$$16\pi^2 \dot{C}_{\ell^2 q^2 H^2}^{(2)e\mu ii} = \begin{pmatrix} C_{\ell q}^{(1)e\tau ii} & C_{\ell q}^{(3)e\tau ii} & C_{\ell q}^{(1)\tau\mu ii} & C_{\ell q}^{(3)\tau\mu ii} \\ 0 & g'^2 & 0 & 0 \\ 3g^2 & 0 & 0 & 0 \\ 0 & 0 & 0 & g'^2 \\ 0 & 0 & 3g^2 & 0 \end{pmatrix} \begin{pmatrix} C_{H\ell}^{(1)\tau\mu} \\ C_{H\ell}^{(3)\tau\mu} \\ C_{H\ell}^{(1)e\tau} \\ C_{H\ell}^{(3)e\tau} \end{pmatrix} \quad (132)$$

$$16\pi^2 \dot{C}_{\ell^2 q^2 H^2}^{(3)e\mu ii} = \begin{pmatrix} C_{\ell q}^{(1)e\tau ii} & C_{\ell q}^{(3)e\tau ii} & C_{\ell q}^{(1)\tau\mu ii} & C_{\ell q}^{(3)\tau\mu ii} \\ 0 & 3g^2 & 0 & 0 \\ g'^2 & -10g^2 & 0 & 0 \\ 0 & 0 & 0 & 3g^2 \\ 0 & 0 & g'^2 & -10g^2 \end{pmatrix} \begin{pmatrix} C_{H\ell}^{(1)\tau\mu} \\ C_{H\ell}^{(3)\tau\mu} \\ C_{H\ell}^{(1)e\tau} \\ C_{H\ell}^{(3)e\tau} \end{pmatrix} \quad (133)$$

$$16\pi^2 \dot{C}_{\ell^2 q^2 H^2}^{(4)e\mu ii} = \begin{pmatrix} C_{\ell q}^{(1)e\tau ii} & C_{\ell q}^{(3)e\tau ii} & C_{\ell q}^{(1)\tau\mu ii} & C_{\ell q}^{(3)\tau\mu ii} \\ 3g^2 & 0 & 0 & 0 \\ 0 & g'^2 & 0 & 0 \\ 0 & 0 & 3g^2 & 0 \\ 0 & 0 & 0 & g'^2 \end{pmatrix} \begin{pmatrix} C_{H\ell}^{(1)\tau\mu} \\ C_{H\ell}^{(3)\tau\mu} \\ C_{H\ell}^{(1)e\tau} \\ C_{H\ell}^{(3)e\tau} \end{pmatrix} \quad (134)$$

$$16\pi^2 \dot{C}_{e^2 u^2 H^2}^{e\mu ii} = \begin{pmatrix} C_{eu}^{e\tau ii} & C_{eu}^{\tau\mu ii} \\ 4g'^2 & 0 \\ 0 & 4g'^2 \end{pmatrix} \begin{pmatrix} C_{He}^{\tau\mu} \\ C_{He}^{e\tau} \end{pmatrix} \quad (135)$$

$$16\pi^2 \dot{C}_{e^2 d^2 H^2}^{e\mu ii} = \begin{pmatrix} C_{ed}^{e\tau ii} & C_{ed}^{\tau\mu ii} \\ -2g'^2 & 0 \\ 0 & -2g'^2 \end{pmatrix} \begin{pmatrix} C_{He}^{\tau\mu} \\ C_{He}^{e\tau} \end{pmatrix} \quad (136)$$

$$16\pi^2 \dot{C}_{e^2 q^2 H^2}^{(1)e\mu ii} = \begin{pmatrix} C_{eq}^{e\tau ii} & C_{eq}^{\tau\mu ii} \\ -g'^2 & 0 \\ 0 & -g'^2 \end{pmatrix} \begin{pmatrix} C_{He}^{\tau\mu} \\ C_{He}^{e\tau} \end{pmatrix} \quad (137)$$

$$16\pi^2 \dot{C}_{e^2 q^2 H^2}^{(2)e\mu ii} = \begin{pmatrix} C_{eq}^{e\tau ii} & C_{eq}^{\tau\mu ii} \\ -3g^2 & 0 \\ 0 & -3g^2 \end{pmatrix} \begin{pmatrix} C_{He}^{\tau\mu} \\ C_{He}^{e\tau} \end{pmatrix} \quad (138)$$

$$16\pi^2 \dot{C}_{\ell^2 u^2 H^2}^{(1)e\mu ii} = \begin{pmatrix} C_{\ell u}^{e\tau ii} & C_{\ell u}^{\tau\mu ii} \\ -4g'^2 & 0 \\ 0 & -4g'^2 \end{pmatrix} \begin{pmatrix} C_{H\ell}^{(1)\tau\mu} \\ C_{H\ell}^{(1)e\tau} \end{pmatrix} \quad (139)$$

$$16\pi^2 \dot{C}_{\ell^2 u^2 H^2}^{(2)e\mu ii} = \begin{pmatrix} C_{\ell u}^{e\tau ii} & C_{\ell u}^{\tau\mu ii} \\ -4g'^2 & 0 \\ 0 & -4g'^2 \end{pmatrix} \begin{pmatrix} C_{H\ell}^{(3)\tau\mu} \\ C_{H\ell}^{(3)e\tau} \end{pmatrix} \quad (140)$$

$$16\pi^2 \dot{C}_{\ell^2 d^2 H^2}^{(1)e\mu ii} = \begin{pmatrix} C_{\ell d}^{e\tau ii} & C_{\ell d}^{\tau\mu ii} \\ 2g'^2 & 0 \\ 0 & 2g'^2 \end{pmatrix} \begin{pmatrix} C_{H\ell}^{(1)\tau\mu} \\ C_{H\ell}^{(1)e\tau} \end{pmatrix} \quad (141)$$

$$16\pi^2 \dot{C}_{\ell^2 d^2 H^2}^{(2)e\mu ii} = \begin{pmatrix} C_{\ell d}^{e\tau ii} & C_{\ell d}^{\tau\mu ii} \\ 2g'^2 & 0 \\ 0 & 2g'^2 \end{pmatrix} \begin{pmatrix} C_{H\ell}^{(3)\tau\mu} \\ C_{H\ell}^{(3)e\tau} \end{pmatrix} \quad (142)$$

B.3 $Y_6 \times Y_6 \rightarrow P_8$

We here write the RGEs for the mixing of two dimension six $\tau \rightarrow l$ Yukawa (eq. (17)) into the dimension eight $\mu \rightarrow e$ penguins (eq. (32)). More details can be found in section 3.1.1 of the text.

$$16\pi^2 \dot{C}_{e^2 H^4 D}^{e\mu} = -C_{eH}^{\tau\mu} C_{eH}^{*\tau e} \quad (143)$$

$$16\pi^2 \dot{C}_{\ell^2 H^4 D}^{(1)e\mu} = \frac{1}{2} C_{eH}^{*\mu\tau} C_{eH}^{e\tau} \quad 16\pi^2 \dot{C}_{\ell^2 H^4 D}^{(2)e\mu} = \frac{1}{4} C_{eH}^{*\mu\tau} C_{eH}^{e\tau} \quad (144)$$

C Limits from B Decays

In the body of the paper, we saw that $\mu \leftrightarrow e$ processes have a good sensitivity to products of $\tau \leftrightarrow l$ coefficients which both involve a top quark, via the fish diagram of Figure 6 e). When the top quark is in an doublet, these same $\tau \leftrightarrow l$ coefficients mediate B decays, which is discussed in this section.

We set limits on the $\tau \leftrightarrow l$ coefficients from their contributions to leptonic and semi-leptonic B decays. They can induce “neutral current” processes, such as $B_d \rightarrow \tau^\pm l^\mp$, which are absent in the SM, and also contribute to “charged current” decays such as $B^+ \rightarrow \bar{\tau} \nu$, to which the SM does contribute but with a different-flavoured neutrino. Since our coefficients are lepton-flavour-changing, they cannot interfere with the Standard Model, so necessarily increase the Branching Ratios with respect to their SM expectation. This makes it difficult to fit the current B anomalies with LFV operators, because many of the anomalies are experimental deficits with respect to the SM predictions.

The list of decays that are included is given in table 14, along with the value of the Branching Ratio (BR) which we use to extract limits (A coefficient at its upper limit gives this BR). For processes where the SM contribution is negligible, this value is the experimental 95% C.L. upper bound on the BR. In the case of SM processes where prediction \approx observation, this value is the SM prediction + theory uncertainty + 2σ experimental uncertainty. This definition is used because we would like to remove the SM part and require that the flavour-changing interactions contribute less than the remainder. However, it can occur that the SM prediction exceeds the experimental observation (as in some “B anomalies”).

To extrapolate the limits we obtain from current experimental constraints into the future, we suppose a factor of 10 improvement in the experimental sensitivity (and in the theoretical precision), such that the future limits will be a factor of ~ 3 better.

Our limits are obtained using Flavio [47]. The limits obtained from two-body leptonic decays were checked analytically, using the well-known formula for the rate as a function of operator coefficients at the experimental scale m_b :

$$\Gamma(B_0 \rightarrow \bar{\tau}\mu) = \frac{E_\mu^2 f_B^2}{16\pi v^4} \left\{ (|C_{V,LX}^{db\mu\tau}|^2 + |C_{V,RX}^{db\mu\tau}|^2)(E_\tau - E_\mu) + (|C_{S,RX}^{db\mu\tau}|^2 + |C_{S,LX}^{db\mu\tau}|^2) \frac{m_B^2}{m_b^2} (E_\tau + E_\mu) + \dots \right\} \quad (145)$$

where “...” are cross-terms and m_μ is neglected. A numerical limit can be obtained by, for instance, comparing to the experimental rate for $B^+ \rightarrow \bar{\tau}\nu$.

The coefficients are run from $m_b \rightarrow \Lambda_{\text{NP}} = 4$ TeV with the one-loop RGEs of QCD (which shrinks scalar coefficients by a factor $\sim 3/5$), with tree-level matching to SMEFT operators when passing m_W . Electroweak running is neglected, except in the case of tensor to scalar mixing in SMEFT⁶ (where $C_S(m_W) \sim 0.3C_T(\Lambda_{\text{NP}})$), which for instance, mixes single-top tensors $\mathcal{O}_{\text{lequ}}^{(3)\tau e 3u}$ into scalars that induce $B^+ \rightarrow \bar{e}\nu$.

coefficient	limit	process	BR
$C_{eq}^{e\tau 32}, C_{\ell q}^{(1)e\tau 32} + C_{\ell q}^{(3)e\tau 32}$	$2.3 \times 10^{-3}(\text{c})$	$B^+ \rightarrow K + \tau^\pm e^\mp$	$< 4.4 \times 10^{-5}$ [51]
$C_{eq}^{e\tau 31}, C_{\ell q}^{(1)e\tau 31} + C_{\ell q}^{(3)e\tau 31}$	$2.3 \times 10^{-3}(\text{c})$	$B_d^0 \rightarrow \tau^\pm e^\mp$	$< 3.0 \times 10^{-5}$ [52]
$C_{eq}^{\mu\tau 32}, C_{\ell q}^{(1)\mu\tau 32} + C_{\ell q}^{(3)\mu\tau 32}$	$2.3 \times 10^{-3}(\text{c})$	$B_s^0 \rightarrow \tau^\pm \mu^\mp$	$< 4.3 \times 10^{-5}$ [53]
$C_{eq}^{\mu\tau 31}, C_{\ell q}^{(1)\mu\tau 31} + C_{\ell q}^{(3)\mu\tau 31}$	$1.5 \times 10^{-3}(\text{c})$	$B_d^0 \rightarrow \tau^\pm \mu^\mp$	$< 1.2 \times 10^{-5}$ [53]
$C_{\ell edq}^{e\tau d3}, C_{\ell edq}^{\tau e d3}$	$3.4 \times 10^{-4}(\text{c})$	$B_d^0 \rightarrow e^\pm \tau^\mp$	$< 3.0 \times 10^{-5}$ [52]
$C_{\ell edq}^{\mu\tau d3}, C_{\ell edq}^{\tau\mu d3}$	$2.2 \times 10^{-4}(\text{c})$	$B_d^0 \rightarrow \mu^\pm \tau^\mp$	$< 1.2 \times 10^{-5}$ [53]
$C_{\ell edq}^{\mu\tau s3}, C_{\ell edq}^{\tau\mu s3}$	$3.3 \times 10^{-4}(\text{c})$	$B_s^0 \rightarrow \mu^\pm \tau^\mp$	$< 4.3 \times 10^{-5}$ [53]
$C_{\text{lequ}}^{(1)l\tau 3u}$	$4.5 \times 10^{-4}(\text{c})$	$B^- \rightarrow \tau \bar{\nu}$	1.4×10^{-4} [47, 54]
$C_{\text{lequ}}^{(1)\tau e 3u}$	$5.8 \times 10^{-5}(\text{c})$	$B^- \rightarrow e \bar{\nu}$	$\leq 1.2 \times 10^{-6}$ [55]
$C_{\text{lequ}}^{(1)\tau\mu 3u}$	$4.3 \times 10^{-5}(\text{c})$	$B^- \rightarrow \mu \bar{\nu}$	$\leq 1.0 \times 10^{-6}$ [56]
$C_{\text{lequ}}^{(1)l\tau 3c}$	$1.0 \times 10^{-2}(\text{c})$	$B_c^- \rightarrow \tau \bar{\nu}$	0.1 [47]
$C_{\text{lequ}}^{(1)\tau e 3c}$	$9.0 \times 10^{-3}(\text{c})$	$B_d^0 \rightarrow D e \bar{\nu}$	$\leq 3.0 \times 10^{-2}$ [47]
$C_{\text{lequ}}^{(1)\tau\mu 3c}$	$9.0 \times 10^{-3}(\text{c})$	$B_d^0 \rightarrow D \mu \bar{\nu}$	$\leq 3.1 \times 10^{-2}$ [47]
$C_{\text{lequ}}^{(3)l\tau 3u}$	$1.8 \times 10^{-3}(\text{c})$	$B^- \rightarrow \tau \bar{\nu}$	1.4×10^{-4} [47, 54]
$C_{\text{lequ}}^{(3)\tau e 3u}$	$2.4 \times 10^{-4}(\text{c})$	$B^- \rightarrow e \bar{\nu}$	$\leq 1.2 \times 10^{-6}$ [55]
$C_{\text{lequ}}^{(3)\tau\mu 3u}$	$1.8 \times 10^{-4}(\text{c})$	$B^- \rightarrow \mu \bar{\nu}$	$\leq 1.0 \times 10^{-6}$ [56]
$C_{\text{lequ}}^{(3)l\tau 3c}$	$5.0 \times 10^{-3}(\text{c})$	$R_{\tau/l}(B \rightarrow D^* l \bar{\nu})$	0.28 [47]
$C_{\text{lequ}}^{(3)\tau e 3c}$	$5.3 \times 10^{-3}(\text{c})$	$B_d^0 \rightarrow D^* e \bar{\nu}$	$\leq 7.3 \times 10^{-2}$ [47]
$C_{\text{lequ}}^{(3)\tau\mu 3c}$	$6.4 \times 10^{-3}(\text{c})$	$B_d^0 \rightarrow D^* \mu \bar{\nu}$	$\leq 7.7 \times 10^{-2}$ [47]

Table 14: Current limits (c) on $\tau \leftrightarrow e$ and $\tau \leftrightarrow \mu$ coefficients of SMEFT operators, at 4 TeV, arising from the B decays given in the third column. The limits saturate the Branching Ratio given in the last column (which may not be the cited experimental limit, see discussion in Appendix C). Limits on vector coefficients apply for permuted lepton and quark flavour indices, scalars apply as given.

⁶The tensor to scalar mixing below m_W in QED is negligible for “charged-current” tensors involving a b and a ν .

D Table of Sensitivities

coefficients	$B_{\tau \leftrightarrow e}^{(f)} B_{\tau \leftrightarrow \mu}^{(f)}$	$B_{\mu \rightarrow e}^{(f)}$
$C_{\ell e q u}^{(1) e \tau 1 u} C_{H e}^{\tau \mu}$	$8.3 \times 10^{-5}(f) \times 1.2 \times 10^{-4}(f)$	5×10^{-9}
$C_{\ell e q u}^{(3) e \tau 1 u} C_{H e}^{\tau \mu}$	$7.7 \times 10^{-5}(f) \times 1.2 \times 10^{-4}(f)$	2×10^{-9}
$(C_{\ell e q u}^{(1) \tau e 1 u})^* C_{H \ell(1)}^{\tau \mu}$	$8.3 \times 10^{-5}(f) \times 1.0 \times 10^{-4}(f)$	1×10^{-8}
$(C_{\ell e q u}^{(3) \tau e 1 u})^* C_{H \ell(1)}^{\tau \mu}$	$7.7 \times 10^{-5}(f) \times 1.0 \times 10^{-4}(f)$	2×10^{-9}
$(C_{\ell e q u}^{(1) \tau e 1 u})^* C_{H \ell(3)}^{\tau \mu}$	$8.3 \times 10^{-5}(f) \times 1.0 \times 10^{-4}(f)$	1×10^{-8}
$(C_{\ell e q u}^{(3) \tau e 1 u})^* C_{H \ell(3)}^{\tau \mu}$	$7.7 \times 10^{-5}(f) \times 1.0 \times 10^{-4}(f)$	3×10^{-10}
$C_{\ell e d q}^{e \tau d 1} C_{H e}^{\tau \mu}$	$8.3 \times 10^{-5}(f) \times 1.2 \times 10^{-4}(f)$	5×10^{-9}
$(C_{\ell e d q}^{\tau e d 1})^* C_{H \ell(1)}^{\tau \mu}$	$8.3 \times 10^{-5}(f) \times 1.0 \times 10^{-4}(f)$	1×10^{-8}
$(C_{\ell e d q}^{\tau e d 1})^* C_{H \ell(3)}^{\tau \mu}$	$8.3 \times 10^{-5}(f) \times 1.0 \times 10^{-4}(f)$	1×10^{-8}

Table 15: Pair of $\tau \leftrightarrow l$ penguin and four fermion dimension six operators that generate $\mu \rightarrow e$ scalar/tensor dimension eight operators with a singlet u and d quark. The future (f) “limits” $B_{\tau \leftrightarrow l}^{(f)}$ on $\tau \leftrightarrow l$ vectors and scalars are from the upper bounds on the LFV decays $\tau \rightarrow l \rho(\eta)$ and $\tau \rightarrow \pi l$ respectively (adapted from [46]). The limits on penguins follow from their contribution to four-lepton vector interactions $\tau \rightarrow 3l$. The same bound applies to the dimension six operators with $\mu \leftrightarrow e$ interchanged. The sensitivities $B_{\mu \rightarrow e}^{(f)}$ arise from future $\mu \rightarrow e$ conversion. Bolded pairs indicate that the sensitivity of $\mu \rightarrow e$ is better than the one arising from direct $\tau \leftrightarrow l$ searches (see eq. (84)).

coefficients	$B_{\tau \leftrightarrow e}^{(f)} B_{\tau \leftrightarrow \mu}^{(f)}$	$B_{\mu \rightarrow e}^{(f)}$
$C_{e u}^{e \tau u u} C_{H e}^{\tau \mu}$	$2.4 \times 10^{-4}(f) \times 1.1 \times 10^{-4}(f)$	4.6×10^{-8}
$C_{e d}^{e \tau d d} C_{H e}^{\tau \mu}$	$2.4 \times 10^{-4}(f) \times 1.1 \times 10^{-4}(f)$	8.2×10^{-8}
$C_{\ell q}^{(1) e \tau 1 1} C_{H \ell(1)}^{\tau \mu}$	$7.0 \times 10^{-4}(f) \times 1. \times 10^{-4}(f)$	1×10^{-7}
$C_{\ell q}^{(1) e \tau 1 1} C_{H \ell(3)}^{\tau \mu}$	$7.0 \times 10^{-4}(f) \times 1. \times 10^{-4}(f)$	8.5×10^{-8}
$C_{\ell q}^{(3) e \tau 1 1} C_{H \ell(1)}^{\tau \mu}$	$1.2 \times 10^{-4}(f) \times 1. \times 10^{-4}(f)$	1×10^{-8}
$C_{\ell q}^{(3) e \tau 1 1} C_{H \ell(3)}^{\tau \mu}$	$1.2 \times 10^{-4}(f) \times 1. \times 10^{-4}(f)$	3.2×10^{-9}

Table 16: Similar to Table 15 but with product of penguin and four-fermion dimension six operators that mix into $\mu \rightarrow e$ vectors at dimension eight.

References

- [1] Yoshitaka Kuno and Yasuhiro Okada. Muon decay and physics beyond the standard model. *Rev. Mod. Phys.*, 73:151–202, 2001.
- [2] Lorenzo Calibbi and Giovanni Signorelli. Charged Lepton Flavour Violation: An Experimental and Theoretical Introduction. *Riv. Nuovo Cim.*, 41(2):71–174, 2018.
- [3] G. Hernández-Tomé, G. López Castro, and P. Roig. Flavor violating leptonic decays of τ and μ leptons in the Standard Model with massive neutrinos. *Eur. Phys. J. C*, 79(1):84, 2019. [Erratum: *Eur.Phys.J.C* 80, 438 (2020)].
- [4] Patrick Blackstone, Matteo Fael, and Emilie Passemar. $\tau \rightarrow \mu\mu\mu$ at a rate of one out of 10^{14} tau decays? *Eur. Phys. J. C*, 80(6):506, 2020.
- [5] A. M. Baldini et al. Search for the lepton flavour violating decay $\mu^+ \rightarrow e^+\gamma$ with the full dataset of the MEG experiment. *Eur. Phys. J. C*, 76(8):434, 2016.
- [6] A. M. Baldini et al. The design of the MEG II experiment. *Eur. Phys. J. C*, 78(5):380, 2018.
- [7] U. Bellgardt et al. Search for the Decay $\mu^+ \rightarrow e^+ e^+ e^-$. *Nucl. Phys. B*, 299:1–6, 1988.
- [8] A. Blondel et al. Research Proposal for an Experiment to Search for the Decay $\mu \rightarrow eee$. 1 2013.
- [9] Wilhelm H. Bertl et al. A Search for muon to electron conversion in muonic gold. *Eur. Phys. J. C*, 47:337–346, 2006.
- [10] Y. G. Cui et al. Conceptual design report for experimental search for lepton flavor violating mu- - e-conversion at sensitivity of $10^{*-}(-16)$ with a slow-extracted bunched proton beam (COMET). 6 2009.
- [11] Bernard Aubert et al. Searches for Lepton Flavor Violation in the Decays $\tau^+ \rightarrow e^+ \gamma$ and $\tau^+ \rightarrow \mu^+ \gamma$. *Phys. Rev. Lett.*, 104:021802, 2010.
- [12] K. Hayasaka et al. Search for Lepton Flavor Violating Tau Decays into Three Leptons with 719 Million Produced $\tau^+\tau^-$ Pairs. *Phys. Lett. B*, 687:139–143, 2010.
- [13] W. Altmannshofer et al. The Belle II Physics Book. *PTEP*, 2019(12):123C01, 2019. [Erratum: *PTEP* 2020, 029201 (2020)].
- [14] Y. Miyazaki et al. Search for lepton flavor violating tau- decays into $l^- \eta$, $l^- \eta'$ and $l^- \pi^0$. *Phys. Lett. B*, 648:341–350, 2007.
- [15] Search for the decays of the Higgs boson $H \rightarrow ee$ and $H \rightarrow e\mu$ in pp collisions at $\sqrt{s} = 13$ TeV with the ATLAS detector. 8 2019.
- [16] Qin Qin, Qiang Li, Cai-Dian Lü, Fu-Sheng Yu, and Si-Hong Zhou. Charged lepton flavor violating Higgs decays at future e^+e^- colliders. *Eur. Phys. J. C*, 78(10):835, 2018.
- [17] Albert M Sirunyan et al. Search for lepton-flavor violating decays of the Higgs boson in the $\mu\tau$ and $e\tau$ final states in proton-proton collisions at $\sqrt{s} = 13$ TeV. *Phys. Rev. D*, 104(3):032013, 2021.
- [18] H. Georgi. Effective field theory. *Ann. Rev. Nucl. Part. Sci.*, 43:209–252, 1993.
- [19] Andrzej J. Buras. Weak Hamiltonian, CP violation and rare decays. pages 281–539, 6 1998.
- [20] Aneesh V. Manohar. Introduction to Effective Field Theories. 4 2018.
- [21] Marco Ardu, Sacha Davidson, and Luca Silvestrini. work in progress.
- [22] Elizabeth E. Jenkins, Aneesh V. Manohar, and Michael Trott. Renormalization Group Evolution of the Standard Model Dimension Six Operators I: Formalism and lambda Dependence. *JHEP*, 10:087, 2013.
- [23] Marco Ardu and Sacha Davidson. What is Leading Order for LFV in SMEFT? 3 2021.
- [24] W. Buchmüller and D. Wyler. Effective lagrangian analysis of new interactions and flavour conservation. *Nuclear Physics B*, 268(3):621–653, 1986.
- [25] B. Grzadkowski, M. Iskrzynski, M. Misiak, and J. Rosiek. Dimension-Six Terms in the Standard Model Lagrangian. *JHEP*, 10:085, 2010.

- [26] Christopher W. Murphy. Dimension-8 operators in the Standard Model Effective Field Theory. *JHEP*, 10:174, 2020.
- [27] Hao-Lin Li, Zhe Ren, Jing Shu, Ming-Lei Xiao, Jiang-Hao Yu, and Yu-Hui Zheng. Complete set of dimension-eight operators in the standard model effective field theory. *Phys. Rev. D*, 104(1):015026, 2021.
- [28] Elizabeth E. Jenkins, Aneesh V. Manohar, and Michael Trott. Renormalization Group Evolution of the Standard Model Dimension Six Operators II: Yukawa Dependence. *JHEP*, 01:035, 2014.
- [29] Rodrigo Alonso, Elizabeth E. Jenkins, Aneesh V. Manohar, and Michael Trott. Renormalization Group Evolution of the Standard Model Dimension Six Operators III: Gauge Coupling Dependence and Phenomenology. *JHEP*, 04:159, 2014.
- [30] Sacha Davidson, Martin Gorbahn, and Matthew Leak. Majorana neutrino masses in the renormalization group equations for lepton flavor violation. *Phys. Rev. D*, 98(9):095014, 2018.
- [31] Mikael Chala and Arsenii Titov. Neutrino masses in the Standard Model effective field theory. *Phys. Rev. D*, 104(3):035002, 2021.
- [32] Sacha Davidson and Martin Gorbahn. Charged lepton flavor change and nonstandard neutrino interactions. *Phys. Rev. D*, 101(1):015010, 2020.
- [33] Mikael Chala, Guilherme Guedes, Maria Ramos, and Jose Santiago. Towards the renormalisation of the Standard Model effective field theory to dimension eight: Bosonic interactions I. *SciPost Phys.*, 11:065, 2021.
- [34] Luiz Vale Silva. Effects of squared four-fermion operators of the Standard Model Effective Field Theory on meson mixing. 1 2022.
- [35] Wouter Dekens and Peter Stoffer. Low-energy effective field theory below the electroweak scale: matching at one loop. *JHEP*, 10:197, 2019.
- [36] Andreas Crivellin, Sacha Davidson, Giovanni Marco Pruna, and Adrian Signer. Renormalisation-group improved analysis of $\mu \rightarrow e$ processes in a systematic effective-field-theory approach. *JHEP*, 05:117, 2017.
- [37] Marco Ciuchini, E. Franco, L. Reina, and L. Silvestrini. Leading order QCD corrections to $b \rightarrow s \gamma$ and $b \rightarrow s g$ decays in three regularization schemes. *Nucl. Phys. B*, 421:41–64, 1994.
- [38] Ryuichiro Kitano, Masafumi Koike, and Yasuhiro Okada. Detailed calculation of lepton flavor violating muon electron conversion rate for various nuclei. *Phys. Rev. D*, 66:096002, 2002. [Erratum: Phys.Rev.D 76, 059902 (2007)].
- [39] Sacha Davidson. $\mu \rightarrow e \gamma$ and matching at m_W . *Eur. Phys. J. C*, 76(7):370, 2016.
- [40] Stefan Herrlich and Ulrich Nierste. Evanescent operators, scheme dependences and double insertions. *Nucl. Phys. B*, 455:39–58, 1995.
- [41] H. Simma. Equations of motion for effective Lagrangians and penguins in rare B decays. *Z. Phys. C*, 61:67–82, 1994.
- [42] Thomas Hahn. Generating Feynman diagrams and amplitudes with FeynArts 3. *Comput. Phys. Commun.*, 140:418–431, 2001.
- [43] Adam Alloul, Neil D. Christensen, Céline Degrande, Claude Duhr, and Benjamin Fuks. FeynRules 2.0 - A complete toolbox for tree-level phenomenology. *Comput. Phys. Commun.*, 185:2250–2300, 2014.
- [44] J. D. Bjorken, Kenneth D. Lane, and Steven Weinberg. The Decay $\mu \rightarrow e + \gamma$ in Models with Neutral Heavy Leptons. *Phys. Rev. D*, 16:1474, 1977.
- [45] D. Chang, W. S. Hou, and Wai-Yee Keung. Two loop contributions of flavor changing neutral Higgs bosons to $\mu \rightarrow e \gamma$. *Phys. Rev. D*, 48:217–224, 1993.
- [46] S. Davidson. Completeness and complementarity for $\mu \rightarrow e \gamma$, $\mu \rightarrow e \bar{e} e$ and $\mu A \rightarrow e A$. *JHEP*, 02:172, 2021.
- [47] David M. Straub. flavio: a Python package for flavour and precision phenomenology in the Standard Model and beyond. 10 2018.
- [48] Rui-Xiang Shi, Li-Sheng Geng, Benjamín Grinstein, Sebastian Jäger, and Jorge Martin Camalich. Revisiting the new-physics interpretation of the $b \rightarrow c \tau \nu$ data. *JHEP*, 12:065, 2019.

- [49] Yasmine Sara Amhis et al. Averages of b-hadron, c-hadron, and τ -lepton properties as of 2018. *Eur. Phys. J. C*, 81(3):226, 2021.
- [50] A. M. Sirunyan and A. et al. Tumasyan. Search for lepton-flavor violating decays of the Higgs boson in the $\mu\tau$ and $e\tau$ final states in proton-proton collisions at $\sqrt{s} = 13$ TeV. *Phys. Rev. D*, 104:032013, Aug 2021.
- [51] J. P. Lees et al. A search for the decay modes $B^{+-} \rightarrow h^{+-}\tau^{+-}l$. *Phys. Rev. D*, 86:012004, 2012.
- [52] Bernard Aubert et al. Searches for the decays $B^0 \rightarrow \ell^\pm\tau^\mp$ and $B^+ \rightarrow \ell^+\nu$ ($\ell=e, \mu$) using hadronic tag reconstruction. *Phys. Rev. D*, 77:091104, 2008.
- [53] Roel Aaij et al. Search for the lepton-flavour-violating decays $B_s^0 \rightarrow \tau^\pm\mu^\mp$ and $B^0 \rightarrow \tau^\pm\mu^\mp$. *Phys. Rev. Lett.*, 123(21):211801, 2019.
- [54] P.A. Zyla et al. Review of Particle Physics. *PTEP*, 2020(8):083C01, 2020.
- [55] N. Satoyama et al. A Search for the rare leptonic decays $B^+ \rightarrow \mu^+ \nu(\mu)$ and $B^+ \rightarrow e^+ \nu(\mu)$. *Phys. Lett. B*, 647:67–73, 2007.
- [56] M. T. Prim et al. Search for $B^+ \rightarrow \mu^+ \nu_\mu$ and $B^+ \rightarrow \mu^+ N$ with inclusive tagging. *Phys. Rev. D*, 101(3):032007, 2020.